

UNIVERSITÀ DEGLI STUDI DI NAPOLI

FEDERICO II

Dottorato di Ricerca in Tecniche Avanzate Biomediche e
Chirurgiche

**IDENTIFICATION OF MOLECULAR MECHANISMS
INVOLVED IN THE PATHOGENESIS AND
PROGRESSION OF AORTIC VALVE STENOSIS FOR
THE DISCOVERY OF NEW DRUG TARGETS**

Tutor: Chiar.mo Prof. Giovanni DI MINNO

Co-Tutor: Dott. Paolo POGGIO

PhD Thesis:

Vincenza VALERIO

Anno Accademico 2021-2022

List of included papers

I. Aortic Valve Sclerosis Adds to Prediction of Short-Term Mortality in Patients with Documented Coronary Atherosclerosis

Poggio P., Cavallotti L., Myasoedova V.A., Bonimi A., Songia P., Gripari P., **Valerio V.**, Amato M., Barbieri S., Faggiano P., Alamanni F., Veglia F., Pepi M., Tremoli E., Baldassarre D.

Journal of Clinical Medicine, 2019 – 5;8(8):1172

II. Aortic Valve Sclerosis as an Important Predictor of Long-Term Mortality in Patients With Carotid Atheromatous Plaque Requiring Carotid Endarterectomy

Myasoedova V.A., Saccu C., Chiesa M., Songia P., Alfieri A., Massaiu I., **Valerio V.**, Moschetta D., Gripari P., Naliato M., Cavallotti L., Spirito R., Trabattoni P., Poggio P.

Frontiers in Cardiovascular Medicine, 2021 – 28;8:653991

III. Impact of Oxidative Stress and Protein S-Glutathionylation in Aortic Valve Sclerosis Patients with Overt Atherosclerosis

Valerio V.*, Myasoedova V.A.*, Moschetta D., Porro B., Perrucci L.G., Cavalca V., Cavallotti L., Songia P., Poggio P.

Journal of Clinical Medicine, 2019 – 24;8(4):522

* These Authors contributed equally to this work.

IV. MiRNA profiling revealed enhanced susceptibility to oxidative stress of endothelial cells from bicuspid aortic valve

Poggio P., Songia P., Moschetta D., **Valerio V.**, Myasoedova V.A., Perrucci L.G., Pompilio G.

Journal of Molecular and Cellular cardiology, 2019 – 131:146-154

V. Cyclophilin A inhibition as potential treatment of human aortic valve Calcification

Perrucci L.G., Songia P., Moschetta D., Barbagallo V. A., **Valerio V.**, Myasoedova V.A., Alfieri V., Massaiu I., Roberto M., Malesevic M., Pompilio G., Poggio P.

Pharmacological Research, 2020 – 158:104888

VI. Genetic and In Vitro Inhibition of PCSK9 and Calcific Aortic Valve Stenosis

Perrot N.*, **Valerio V.***, Moschetta D., Boekholdt S.M., Dina C., Chen H.Y., Abner E., Martisson A., Manikpurage H.D., Rigade S., Capuolade R., Mass E., Clavel M.A., Le Tourneau T., Messika-Zeitoun D., Wareham N.J., Engert J.C., Polvani G., Pibarot P., Esko T., Smith J.G., Mthieu P., Thanassoulis G., Scott J.J., Bossè Y., Camera M., Theriault S., Poggio P. Arsenault B.J.

JACC. Basic to Translational Science, 2020 1:5(7):649-661.

* These Authors contributed equally to this work.

Abstract

Calcific aortic valve stenosis (CAVS) is the most common heart valve pathological condition worldwide. CAVS is an age-related disease, with a prevalence of almost 3% in the general population over 65 years of age. The disease's natural history evolves from an initial asymptomatic phase characterized by a thickening of the leaflets bearing possible micro-calcifications and a preserved left ventricle (LV) outflow tract still. This condition, known as aortic valve sclerosis (AVSc), has a prevalence of about 30% in adults older than 65 years of age. About 10% of these cases morph into aortic stenosis (AS), displaying massive calcifications and overt hemodynamic impairment. The only therapeutic option available for AS patients is either surgery or transcatheter aortic valve replacement.

As the identification of new risk factors for pre- and post-operative mortality appears to be a central issue for ensuring high quality results in risk assessment systems, we first focused our attention on secondary prevention by identifying new risk factors. We have showed that the presence of AVSc, is a predictor of short- and long-term mortality in patients with overt atherosclerosis.

Moreover, a deep understanding of CAVS pathogenic mechanisms would pave the way to new treatment opportunities and reduce its socioeconomic burden. To this end, we first focused on the study of endothelial dysfunction, an unavoidable step in CAVS' onset. In particular, by studying damage to the endothelial cells that make up the aortic valve, we were able to test and apply innovative technologies by carrying out miRNA screening. This screening allowed us to classify endothelial cells isolated from bicuspid valves as more susceptible to damage due to oxidative stress. Continuing to study oxidative stress in endothelial cells, our results showed that treatment with N-acetyl-cysteine, a known antioxidant, can reduce aortic valve calcification, leading us to consider the potential use of antioxidant drugs in the primary prevention of this disease. Finally, we directed our attention on molecular mechanisms involved in valve interstitial cells calcification. In particular, our study, revealed that Cyclophilin A and PCSK9 are causally involved in the pathogenesis of CAVS, identifying them as possible new drug targets.

Index

1. Introduction	8
1.1 The Heart	9
1.1.1 <i>The Cardiac Cycle</i>	10
1.2 Aortic Valve	10
1.2.1 <i>The Cardiac Cycle</i>	11
1.2.2 <i>The Cardiac Cycle</i>	12
1.2.2.1 <i>Valve endothelial cells</i>	13
1.2.2.2 <i>Valve interstitial cells</i>	14
1.3 Calcific Aortic Valve Stenosis	15
1.3.1 <i>CAVS's associated risk factors and Bicuspid Aortic Valve</i>	16
1.3.2 <i>Clinical manifestation and Diagnosis</i>	16
1.3.3 <i>Therapeutic options</i>	18
1.3.3.1 <i>AVR and TAVI</i>	18
1.3.3.2 <i>Pharmacological treatments</i>	21
1.4 CAVS cellular and molecular mechanisms.....	23
1.4.1 <i>Endothelial dysfunction and oxidative stress</i>	23
1.4.1.1 <i>Dysregulation of glutathione system and protein Glutathionylation</i>	24
1.4.1.2 <i>MicroRNA</i>	25
1.4.2 <i>VICs phenotypic switching in osteoblastic-like cells</i>	26
1.4.2.1 <i>Potential players involved in VICs' calcification</i>	27
1.4.2.2 <i>Cyclophilin A</i>	28
1.4.2.2.2 <i>CyPA in cardiovascular diseases</i>	29
1.4.2.3 <i>Pro-protein convertase subtilisin/kexin tipe 9</i>	30
1.4.2.3.1 <i>Structure and processing</i>	31
1.4.2.3.2 <i>PCSK9 function: role in low-density lipoprotein receptor</i>	33
1.4.2.3.3 <i>PCSK9 in aortic valve calcification</i>	35
2. Material and Metods	37
2.1 Blood and Aortic Valve Collection	38
2.2 Echocardiographic Evaluation	38
2.3 Blood Sampling and Biochemical Measurement.....	39
2.3.1 <i>Glutathione Measurement</i>	39
2.3.2 <i>Asymmetric Dimethylarginine Measurement</i>	39

2.4	Electron Paramagnetic Resonance (EPR)	40
2.5	Histological Evaluation	41
2.5.1	<i>Immunohistochemistry</i>	41
2.5.2	<i>Von Kossa Staining</i>	42
2.6	Isolation of aortic valve endothelial and interstitial cell.....	42
2.7	Gene expression	42
2.7.1	<i>RNA Isolation from tissues and cells</i>	42
2.7.2	<i>Reverse Transcription and Real Time PCR</i>	43
2.7.3	<i>TaqMan human miRNA card A and B arrays</i>	43
2.7.4	<i>Functional analysis</i>	44
2.8	Protein expression	44
2.8.1	<i>Western and Dot Blot</i>	44
2.8.2	<i>Immunoprecipitation</i>	45
2.8.3	<i>ELISA assay</i>	45
2.9	In vitro model of Protein S-Glutathionylation and Oxidative Stress	46
2.10	MTT assay.....	46
2.11	Apoptosis detection	47
2.12	Intracellular ROS detection	47
2.13	In vitro osteogenic stimuli on VECs and VICs.....	48
2.14	Calcium assay	48
2.15	Human aortic valve cell transfection.....	48
2.16	Genetic association study of PCSK9 R46L variant and CAVS	49
2.17	Statistical Analys	49
3.	Results.....	51
3.1	Aortic valce sclerosis add to prediction of short-term mortality in patients with documented coronary atherosclerosis	52
3.1.1	<i>Study design</i>	52
3.1.2	<i>Presence of AVSc: independent predictor of short-term mortality</i>	53
3.2	Aortic valve sclerosis as an important predictor of long-term mortality in patients with 2 carotid atheromatous plaque requiring carotid endarterectomy (CEA).....	55
3.2.1	<i>Study design</i>	55
3.2.2	<i>High AVSc prevalence in CEA patients</i>	56
3.2.3	<i>AVSc predicts long-term all-cause mortality</i>	57
3.2.4	<i>All carotid plaque types are associated with AVSc</i>	59

3.3	Systemic and valvular oxidative stress in calcific aortic valve disease..	62
3.3.1	<i>Patient population and characteristics</i>	62
3.3.2	<i>Systemic oxidative stress and endothelial dysfunction</i>	62
3.3.3	<i>Systemic inflammation status</i>	63
3.3.4	<i>Aortic valve protein S-glutathionylation in AVSc patients.....</i>	64
3.3.5	<i>Increased ROS emission and protein S-glutathionylation mark the transition from sclerosis to stenosis in human aortic valves.</i>	65
3.4	Protein S-glutathionylation and valve endothelial cells.....	68
3.4.1	<i>In vitro model of oxidative stress and protein S-glutathionylation in HUVEC.....</i>	68
3.4.2	<i>Protein S-glutathionylation and endothelial-to-mesenchymal transition in HUVEC.....</i>	69
3.4.3	<i>Blocking glutathione reductase buids-up ROS emission and Protein S-glutathionylation in porcine valve endothelial cells</i>	71
3.4.4	<i>Human valve endothelial cells' resilience against oxidative stress during CAVS progression</i>	75
3.4.5	<i>Protein S-glutathionylation favors endothelial morphological/functional changes in hVECs</i>	80
3.4.6	<i>NAC fendf off P-SSG and consequent calcium deposition in hVECs</i>	83
3.5	Different susceptibility to oxidative stress of endothelium in aortic valve with different morphology.....	84
3.5.1	<i>BAV and TAV human valve endothelial cells characterization</i>	84
3.5.2	<i>MiRNA profile of BAV and TAV hVECs.....</i>	85
3.5.3	<i>Differentially activated signaling pathways in BAV and TAV hVECs</i>	86
3.5.4	<i>Increased apoptosis of BAV hVECs</i>	89
3.5.5	<i>miR-328-3p directly regulate oxidative stress response in aortic valve hVECs.....</i>	91
3.6	Players in aortic valve interstitial cell calcification identifiable as novel potential drug targets.....	92
3.6.1	<i>Cyclophilin A inhibition reduce valve interstitial cells calcium deposition</i>	92
3.6.1.1	<i>Gene and protein expression levels of CyPA are elevated in AS leaflets.</i>	92
3.6.1.2	<i>CyPA expression co-localizes with calcific lesions in AS specimens.....</i>	93
3.6.1.3	<i>CyPA directly correlates with the in vitro valve interstitial cell calcification potential.....</i>	94
3.6.1.4	<i>Exogenous CyPA stimulates calcium deposition in VICs isolated by AS patients.....</i>	95

3.6.1.5	<i>Exogenous CyPA inhibition reduces calcium deposition of AS patient-derived VIC</i>	96
3.6.2	<i>PCSK9 in Calcific Aortic Valve Stenosis</i>	97
3.6.2.1	<i>Meta-analysis of the association between the PCSK9 R46L variant and CAVS</i>	97
3.6.2.2	<i>PCSK9 expression and CAVS</i>	98
3.6.2.3	<i>PCSK9 secretion and VIC calcification</i>	100
4.	Discussion	103
4.1	Aortic valve sclerosis and prediction of short-term mortality in patients affected by coronary atherosclerosis	104
4.1.1	<i>Clinical Relevance</i>	105
4.2	Aortic valve sclerosis and prediction of long-term mortality in patients affected by carotid atheromatous plaque requiring carotid endarterectomy..	106
4.2.1	<i>Clinical Relevance</i>	108
4.3	Enduring ROS emission causes aberrant protein S-glutathionylation transitioning human aortic valve cells from a sclerotic to a stenotic phenotype	109
4.3.1	<i>Conclusion</i>	112
4.4	MiRNA profiling revealed enhanced susceptibility to oxidative stress of endothelial cells from bicuspid aortic valve	113
4.4.1	<i>Conclusion</i>	114
4.5	Cyclophilin A inhibition as potential treatment of human aortic valve calcification	115
4.5.1	<i>Conclusion</i>	117
4.6	Genetic and in vitro inhibition of PCSK9 and calcific aortic valve stenosis	117
4.6.1	<i>Conclusion</i>	118
5.	Bibliography	120
6.	Appendix	145

1. Introduction

1.1 The Heart

The heart is a hollow organ with a muscular structure, located within the thoracic cavity in a district know as mediastinum. It is the central organ of the cardiovascular system that, by contracting regularly, allows the blood to reach the various body's district. A septal wall divides the heart into a left and right side. Each side can in turn be subdivided into two muscular chambers know as atria and venticles (**Figure 1.1**). The right ventricle pumps deoxygenated blood into the pulmonary artery that puches it into the lung (pulmonary or small circulation), while the left ventricle, delivers blood into the systemic circulation (big or systemic circulation) via the aorta. More in detail, the systemic deoxygenated blood through the superior and inferior vena cava arrives in the right atrium and then it is conveyed to the righ ventricle. From this ventricle, blood reaches the lungs via the pulmonary artery. After being oxygenated in the lungs, the blood returns to the left venticles through four pulmonary veins and then is pushed into the left ventricle. Finally, this latter chamber pumps oxygenated blood into the systemic circulation by means of aorta.

The blood flow is maintained unidirectional within the heart by the presence of four cardiac valves. In particular, the atrioventricular valves, tricuspid and mitral, separate the atria from ventricles on the right and left sides, respectively. Insead, the two semilunar valves, the pulmonary and aortic valves have the function to separate the ventricles by the respective major ateries branching off from them.

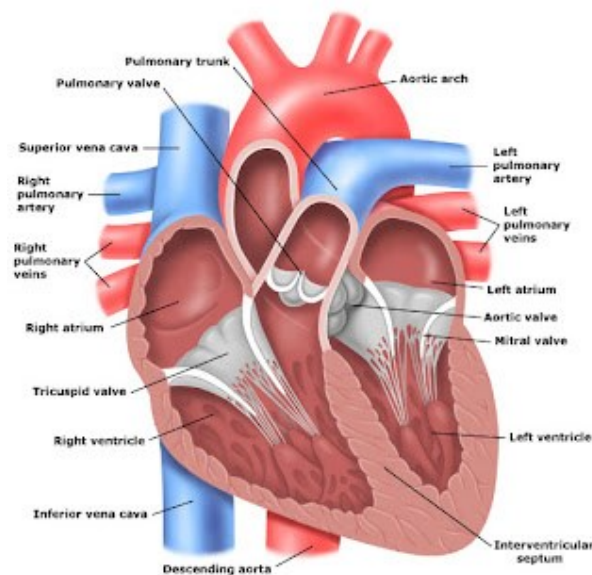


Figure 1.1. Anatomical representation of the heart.

Adapted from <http://nursingmedic.blogspot.com/2010/11/anatomy-of-heart.html>

1.1.1 The Cardiac Cycle

The blood circulation is made possible by proper coordination of the contraction and relaxation movements of the atria and ventricles. The cardiac cycle is defined as a sequence of mechanical and electrical events that consists in four phases based on ventricles and valves position. In particular there is an *inflow phase* where the inlet valve is open and the outlet valve is closed; an *isovolumetric contraction phase* in which both valves are open without blood flow; an *outflow phase* with the outlet valve open and the inlet valve closed and finally an *isovolumetric relaxation phase* in which both valves are closed without blood flow. However, these four phases are commonly divided into two main parts: the *systole* which refers to the phases of ventricular contraction, and *diastole* which instead refers to their relaxation. During the cardiac cycle, the atria receive blood returning to the heart and then thanks to diastole phase, the blood passes from the atria to the ventricles through the tricuspid and mitral valves. After that, when the systole occurs, the atrioventricular valve close and at the same time the opening of the semilunar valve results, conveying the blood from the right and left ventricles to the pulmonary and aorta arteries, respectively. The average duration of the cardiac cycle is about 800 ms and the cardiac valves open and close around 40 million times a year and more than 3 billion times during the average human lifetime¹. A typical point failure in this sophisticated system is represented by the aortic valve, since this valve manages the cardiac chamber at higher pressure in the heart².

1.2 Aortic Valve

The aortic valve is one of the heart's two semilunar valves and separates the left ventricles from the proximal part of the ascending aorta³. It has the task to maintain unidirectional blood flow from the left ventricle to the aorta and to prevent blood's regurgitation into the aorta during ventricular diastole⁴. In particular, following contraction of the ventricles, the valve opens, ensuring the passage of blood into the aorta; then when the pressure in the aorta exceeds the ventricular pressure, the valve closes, preventing the blood's return to the left ventricles.

1.2.1 The Cardiac Cycle

The aortic valve is embedded in a complex anatomical and functional structure, the aortic root, which, as a direct continuation of the left ventricle, extends from the basal leaflets' attachments to the sino-tubular junction. Forming the outflow tract from the left ventricle, the aortic root functions as the supporting structure for the aortic valve. As such, it forms a bridge between the left ventricle and the ascending aorta³. The discrete anatomic ventriculo-aortic junction is a circular locus within this root, formed where the supporting ventricular structures give way to the fibro-elastic walls of the aortic valvar sinuses⁵. In functional terms, all three sinuses of the root, and their contained leaflets, are identical. Anatomically, however, two of the valvar sinuses give rise to the coronary arteries and these can be nominated as the right, left and non-coronary aortic sinuses⁵ (**Figure 1.2**).

The aortic valve is normally composed of three leaflets, which attach to the aortic root in a semilunar fashion, ascending to the commissures (where the adjacent leaflets come together) and descending to the basal attachment of each leaflet to the aortic wall.

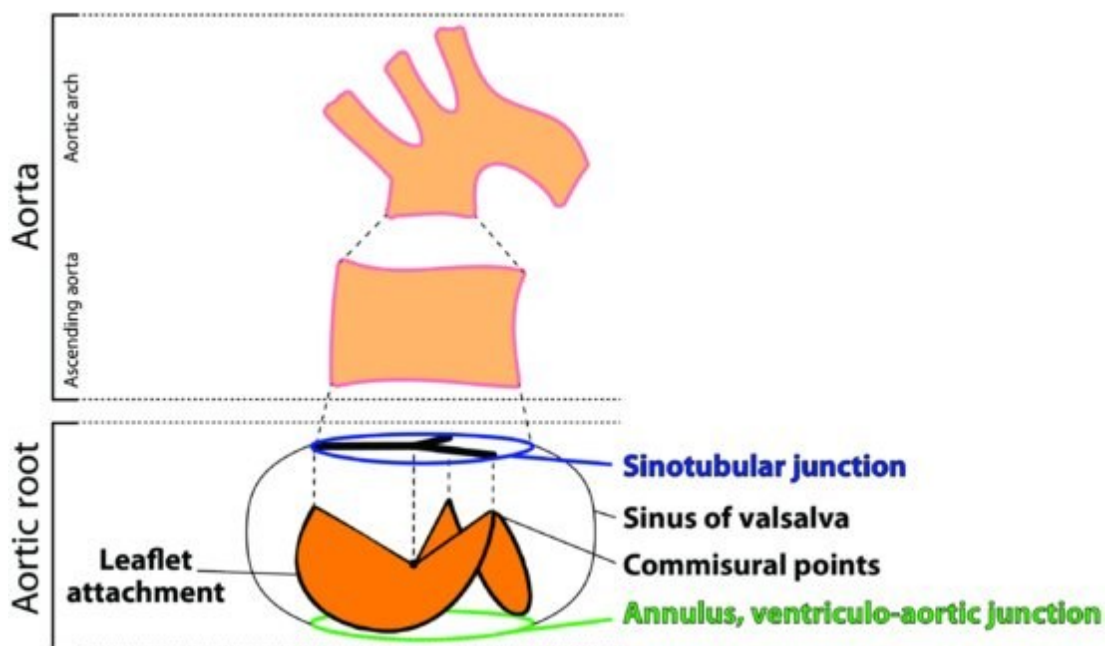


Figure 1.2. Aortic valve anatomy. Structure and nomenclature of aortic root component. The upper part of the figure represents the tracts of the thoracic aorta, with the distinctions between ascending aorta and aortic arch highlighted. The lower part of the figure summarises the detailed components of the aorta: the sinotubular junction of the aortic root with the ascending aorta; the aortic valves; the ventriculo-aortic junction of the aortic root and the left ventricle. Image from: *Perrucci et al., Comprehensive Physiology, 2017.*

1.2.2 The Cardiac Cycle

The aortic valve leaflets are flexible structure that work together to seal the valve orifice during diastole. Each leaflet is less than 1 mm thick and microscopically they have a highly specialized structure in which three different layers can be recognized⁴. The *fibrosa* layer is the most superficial layer, facing the aorta. It is composed by densely packed collagen (type I and II), disposed in circumferential direction which gives strength and stiffness to the leaflet and it is responsible for absorbing the diastolic and systolic stresses. The *ventricularis* layer, on the left ventricle side, contains largely elastin fibers radially oriented and capable of extend in diastole and recoil in systole, to minimize the leaflets area. Finally, the *spongiosa* layer, positioned between the first two, is formed mainly by glycosaminoglycans, which dampen shear forces of leaflets during the cardiac cycle and facilitate the outer layer to slide over one another during leaflets motion^{4,6}. Histological-based thickness measurements indicated that the *fibrosa*, *ventricularis* and *spongiosa* constitute 41%, 29% and 30% of the total layer thickness, respectively⁷ (**Figure 1.3**).

Two different cell types make up aortic valve leaflets: endothelial cells (VECs) that form a monolayer covering the valve surface and interstitial cells (VICs), an heterogeneous population located in the middle of the matrix forming the aortic valve (**Figure 1.3**).

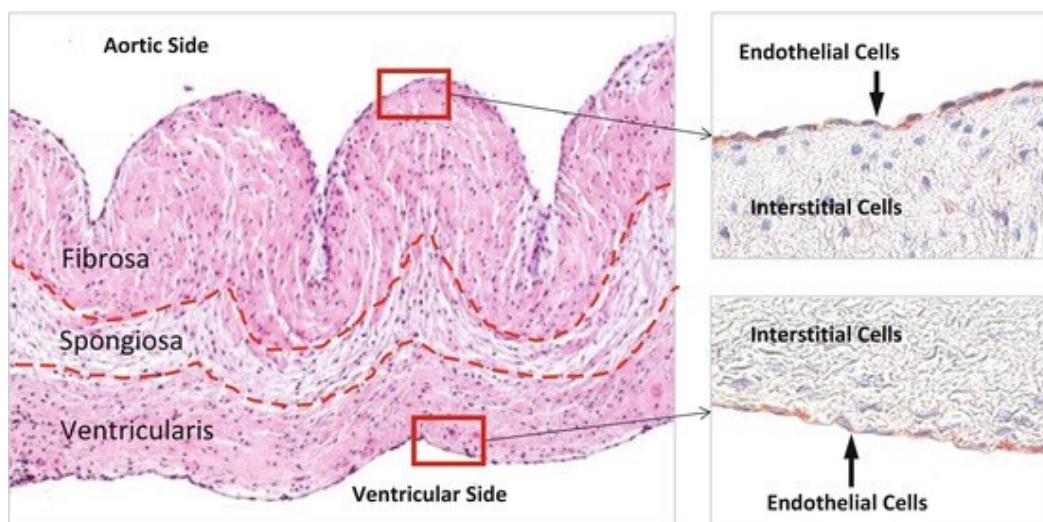


Figure 1.3. Aortic valve leaflets histological structure. The histological image shows the three layer of aortic valve leaflets: *fibrosa*, *spongiosa* e *ventricularis*. Endothelial cells line the valve on aortic and ventricular side; interstitial cells are located within the valve structure. Image from: https://link.springer.com/chapter/10.1007/978-1-4939-5617-3_12.

1.2.2.1 Valve endothelial cells

The endothelial cells, which cover both surfaces of the valve, play an essential role in ensuring that the valve function optimally, responding to the surrounding hemodynamic environment to establish and maintain valve homeostasis^{8,9}. In particular, they serve as a protective lining for the underlying tissue by regulating permeability, mediating inflammation and preventing thrombosis¹⁰. It is very interesting to observe how this cell type is highly specialized to meet the needs of the whole valve tissue. In fact, it is known that valve endothelial cells, although similar to vascular endothelial cells differ from them in several features.

From a molecular perspective, transcriptional profiling of vascular *versus* valve endothelial cells demonstrated significant differences between the two cell types *in vivo*¹¹. Anatomically, VECs are oriented circumferentially across the leaflets and perpendicular to the direction of the blood flow, in contrast to vascular endothelium, which aligns parallel to the blood flow¹². In addition, each surface of the valve is exposed to vastly different pattern of blood flow and levels of shear stress, resulting in further specialization of the VECs on the aortic and ventricular surface of the valve. Indeed, the aortic side is subjected to low velocity oscillatory and consequently low shear stress, while the ventricular side is exposed to high velocity flow resulting in high laminar shear stress⁸. Different study showing that VECs on aortic and ventricular surfaces have differential gene expression profiles and therefore, distinct phenotypes^{13,14}.

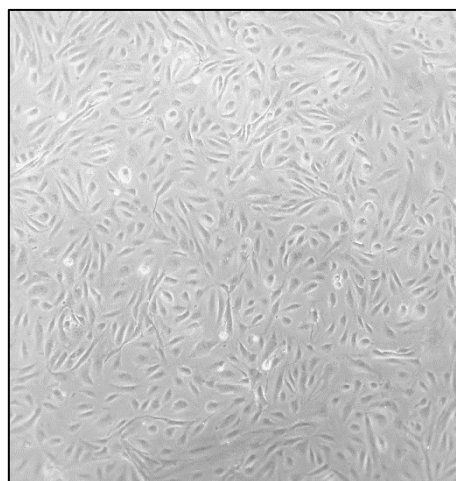


Figure 1.3. Valve endothelial cells. Phase-contrast image showing isolated valve endothelial cell at 10x Magnification.

1.2.2.2 Valve interstitial cells

Valve interstitial cells are the main cell type found in the three layers of the valve¹⁵. VICs constitute a heterogeneous population involved in the maintenance of unique valvular architecture, ensuring proper hemodynamic function but also engaged in aortic valve degeneration. They can be divided into several phenotypes, which are engaged in physiological and pathological processes. Several studies have shown that five types of VICs can be distinguished: embryonic progenitor endothelial/mesenchymal cells, quiescent VICs (qVICs), activated VICs (aVICs), progenitor VICs (pVICs), and osteoblastic VICs (obVICs)^{16,17}.

VIC phenotype is believed to be plastic and reversible. Indeed, the qVICs, fibroblast-like cells, in healthy valves represent the majority of the cells, but in response to injury or disease, these cells are able to acquire a secretory myofibroblast-like phenotype, typical of aVICs¹⁸⁻²⁰, characterized by the expression of α -smooth muscle actin (SMA)²¹.

This process allows the secretion and turnover of extracellular matrix (ECM) proteins, which repair the tissue micro-damage and enable the long-term durability of the leaflets structure²². The local environment (paracrine endothelium-derived signals)²³, the inflammatory cytokines (TGF- β 1 and BMPs)²⁹, the biochemical and biomechanical properties of the ECM^{24,25}, and mechanical stimuli induced by hemodynamic forces (normal or pathological stretching of the valve tissue) regulate the VIC phenotype and function^{26,27}.

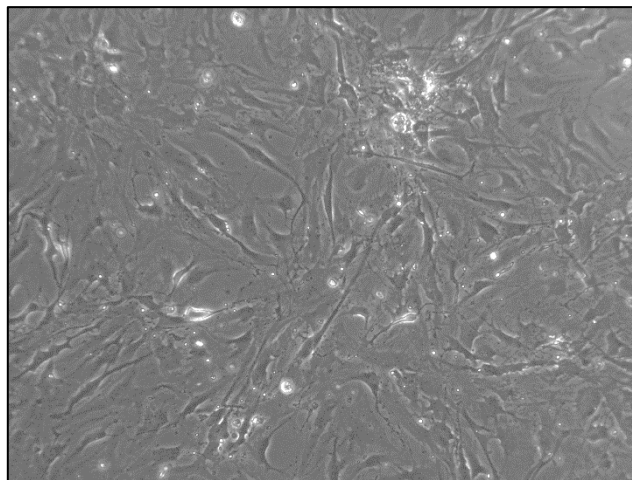


Figure 1.3. Valve interstitial cells. Phase-contrast image showing isolated valve interstitial cell at 10x Magnification.

1.3 Calcific Aortic Valve Stenosis

Calcific aortic valve stenosis (CAVS) is the most common valve disorder in the aging population of Western world^{28,29}. With a prevalence of almost 3% in the general population over 65 year of age, CAVS is destined to become a growing economic and health burden³⁰.

This disease is characterized pathologically by thickening, fibrosis and finally calcification of the aortic valve leaflets which together are able to cause left ventricular outflow tract obstruction³¹. Originally, valve calcification was considered as an inevitable consequence of ageing with clinical relevance when symptoms due to valve obstruction occur. However, our understanding of the pathophysiology of CAVS has evolved, and to date calcific aortic valve stenosis is considered as an active and multifactorial process³².

The functional evolution of CAVS consists of two different stages. The first, known as aortic valve sclerosis (AVSc), is an asymptomatic phase characterized by a thickening of the leaflets bearing possible micro-calcification but with a preserved left ventricle outflow tract^{31,33}. This condition has a prevalence of about 30% in adults older than 65 years of age. About 10% of these cases morph in the second and final phase of CAVS, aortic valve stenosis (AS), displaying massive calcifications and overt hemodynamic impairment²⁸ (**Figure 1.4**).

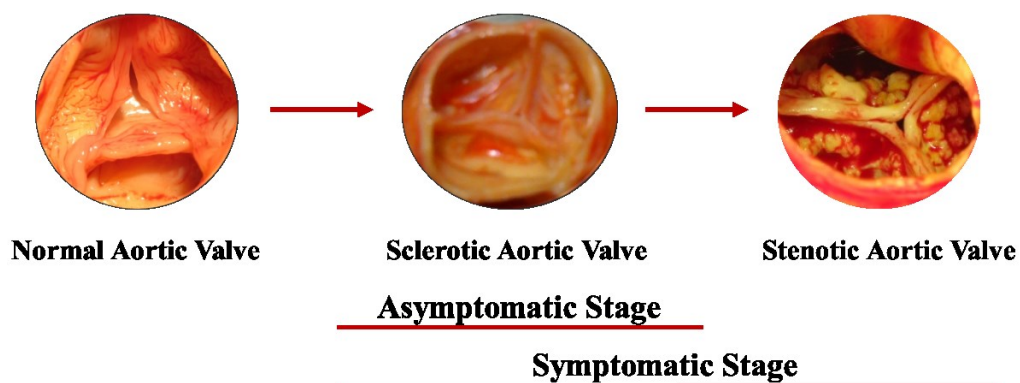


Figure 1.4. CAVS progression. CAVS begins with an asymptomatic phase known as AVSc, characterized by fibrocalcific thickening of the valve leaflets. AVSc may subsequently progress to aortic valve stenosis, the pathological and symptomatic phases, characterized by severe calcification.

1.3.1 CAVS's associated risk factors and Bicuspid Aortic Valve

As suggested by numerous evidences, CAVS shares many of the risk factors of atherosclerosis, including male gender, advanced age, smocking, hypertension³⁴, hypercholesterolemia, renal disease and metabolic syndrome^{35,36}.

However, in addition to the classical recognized risk factors, genetics abnormalities have also been identified that predispose patients to aortic valve calcification. A major genetic risk factors for development of CAVS is the presence of bicuspid aortic valve (BAV)³⁷. BAV disease is the most common congenital heart defect with a prevalence estimated between 0.5% and 2% in general population, and a male predominance of 3:1³⁸. Anatomically, the BAV has two functional commissures of normal height, thus making it a bicomissural valve. A third rudimentally commissure, also called *raphe*, is present in about 95% af BAV.

Patient with BAV, develop aortic valve calcification at an earlier age compared with degenerative tricuspid aortic valve (TAV). From a functional standpoint, significant aotic valve stenosis develops at age of approximately 50 to 60 years, wheareas regurgitation develops around the age of 30^{39,40}.

1.3.2 Clinical manifestation and Diagnosis

The main syntoms of aortic valve stenosis are exertion-related angina, dyspnea, congestive heart failure, presyncope, or syncope. Consequently, after left ventricular dysfunction and reduction in cardiac output, syntoms of congestive heart failure appear⁴¹.

In the clinical practice, echocardiography represents the key diagnostic tool in AS diagnosis. In particular, echocardiography is a non-invasive method classically performed *via* trantoracic; however, when the transthoracic examination is deemed insufficient or uninterpretable, the use of transesophageal echocardiography is necessary⁴².

This diagnostic method that provides some information regarding anatomy of valve, presence and extent of eventually calcium nodules and consequently severity of aortic valve stenosis. Standard measurements of aortic stenosis, including the mobility of the cusps, are calculated using Echo-Doppler. The calculated indicators are the maximum velocity (V_{\max}) across the stenotic valve, the mean transaortic pressure gradient (ΔP_{mean}) calculated with Bernulli equation and the effective aortic valve area (AVA) using the standard continuity equation (**Table 1.1**). Moreover, continuity equation

based AVA is considered a reliable parameter for prediction of the clinical outcome and for clinical decision making⁴³.

The early silent stage of CAVS, aortic valve sclerosis, is related to focal thickening and eventually micro-calcification of the aortic valve without obstruction of blood flow (**Figure 1.5**). Also for this stage of pathology, echocardiography can provide detail regarding tissue characterization; however, it cannot delineate histological properties and it is subject to instrumentation and artifact variables common to ultrasound imaging. Issues related to reporting of aortic valve sclerosis have been complicated by lack of a uniform definition for aortic valve sclerosis and differences within and between interpretations of valve sclerosis from published studies. Indeed, both subjective and qualitative evaluations of valve morphology are a primary limitation in defining aortic valve sclerosis^{44,45}.

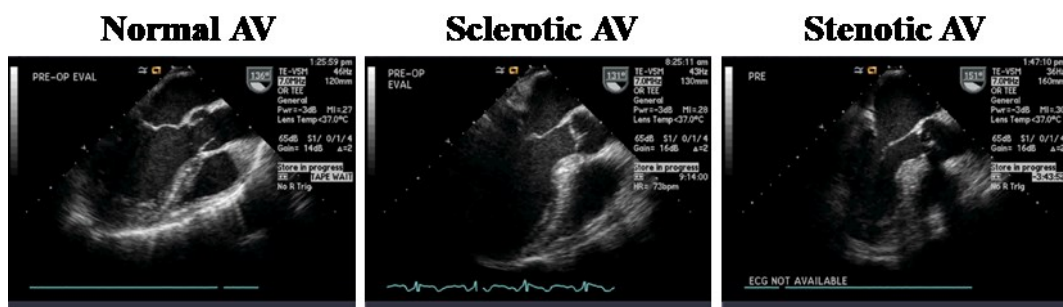


Figure 1.5. Echocardiographic calcific aortic valve degeneration phases.

Aortic valve sclerosis, is related to focal thickening and eventually micro-calcification of the aortic valve without obstruction of blood flow and finally aortic valve stenosis is characterized by massive calcification that causes impaired motion of leaflets.

Grading of severity	Echocardiographic indices		
	AV Vmax (m/s)	Mean gradient (mmHg)	AVA (cm ²)
Aortic sclerosis	<2.5	-	-
Mild	2.5-2.9	<20	>1.5
Moderate	3-3.9	20-39	1-1.5
Severe	4-4.9	40-59	<1
Very severe	≥5	≥60	≤0.6

Table 1.1 Echo-Dopler criteria for definition of aortic sclerosis and stenosis. Table from: *Ring et al., Echo Research Practice, 2021.*

1.3.3 Therapeutic options

To date, no tested drug therapy has proven effective for patient affected by CAVS.

For this reason, surgical treatment, performed with aortic valve replacement (AVR) or percutaneous treatment, achieved *via* transcatheter aortic valve implantation (TAVI) remain the only effective strategies.

1.3.3.1 AVR and TAVI

In the treatment of CAVS, medical therapy is only a temporary solution with aortic valve replacement (AVR) as the final outcome. Patients with severe AS have a life expectancy of less than 10 years and if there is a concomitant heart failure, 50% will die within a year^{46,47}.

An aortic valve replacement involves removing a faulty or damaged valve and replacing it with a new valve made of synthetic materials or animal tissue. AVR involves open-heart surgery under general anaesthesia *via* sternotomy and involved the use of extracorporeal circulation (<https://www.ahajournals.org/doi/full/10.1161/CIR.0000000000000503>).

Various alternatives are available for aortic valve replacement, and matching patients to the most-appropriate type of valve is not always straightforward. Matching the right valve for the right patient is a difficult but essential process to optimize the outcome for patients undergoing AVR⁴⁸. The ideal valve replacement should mimic the characteristics of a normal native valve. In particular, it should have excellent haemodynamics, long life, high thrombus resistance and excellent implantability. Unfortunately, the ideal prosthesis does not exist and all available prostheses present limitations⁴⁸. There are two main types of valve prosthesis: mechanical and biological.

(<https://www.escardio.org/Journals/E-Journal-of-Cardiology-Practice/Volume-9/How-a-prosthesis-in-aortic-valve-replacement-is-chosen>). As far as mechanical valves are concerned, there are mainly three types: *caged-ball*, *tilting disc valve* and *bileaflets heart valve*, which represent the majority of mechanical valves used today. All three types of mechanical valves are prone to thrombus formation due to high shear stress, stagnation and flow separation. For this reason, patient receiving this type of valve are forced to take oral anticoagulants (**Figure 1.6**) (<https://www.sciencedirect.com/topics/engineering/mechanical-valve>).

Mechanical valves are generally recommended for the treatment of young patients (younger than 65 years of age) thanks to their long service life.

Bioprosthetic heart valves are made with glutaraldehyde-fixed porcine aortic valves, or constructed with glutaraldehyde-fixed bovine pericardium and most of the times mounted on stent⁴⁹. Other types of bioprosthetic valves are pulmonary autograft and aortic valve homograft (**Figure 1.6**). The former, also known as Ross procedure⁵⁰, is used in young patients, particularly women in childbearing years, might not wish to take oral anticoagulation therapy⁴⁹. The latter is less in use because the realization that a homograft aortic valve has limited durability, is technically difficult to implant, is expensive to procure and cryopreserve, and might not be superior to other bioprosthetic valves.

Biological valves are generally used in those aged above 65 years although they are also increasingly being used in those aged 60-65 years (<https://www.escardio.org/Journals/E-Journal-of-Cardiology-Practice/Volume-9/How-a-prosthesis-in-aortic-valve-replacement-is-chosen>).

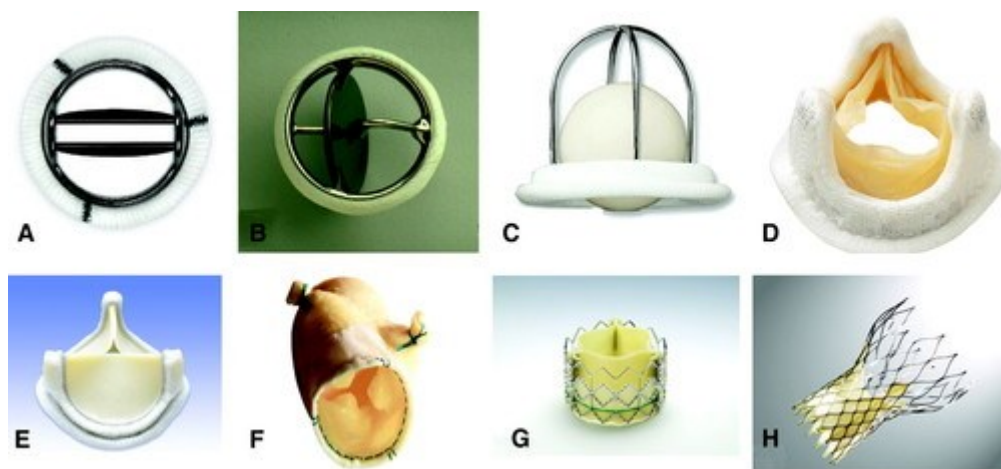


Figure 1.6. Different types of prosthetic valves. (A) Bileaflet mechanical valve (St Jude); (B) monoleaflet mechanical valve (Medtronic Hall); (C) caged ball valve (Starr-Edwards); (D) stented porcine bioprosthesis (Medtronic Mosaic); (E) stented pericardial bioprosthesis (Carpentier-Edwards Magna); (F) stentless porcine bioprosthesis (Medtronic Freestyle); (G) percutaneous bioprosthesis expanded over a balloon (Edwards Sapien); (H) self-expandable percutaneous bioprosthesis (CoreValve). Adapted from: *Pibarot et al., Circulation, 2009*.

Despite the disadvantages, AVR remains the gold standard of care for valve surgery. Indeed, thanks to improved in surgical and postoperative care driving perioperative mortality down to 1%-3%. The main perioperative complications include, conduction disease requiring permanent pacemaker insertion (1.5%–8.6%)⁵¹, cerebrovascular

accidents (2.4%– 8.1%)^{52,53}, cognitive decline (due to perioperative cerebral hypoperfusion microemboli or anaesthetic agent neurotoxicity)⁵⁴. An individual's risk of these complications can be estimated using surgical risk calculators such as EUROSCORE II and the Society of Thoracic Surgeons score⁵⁵.

However, the introduction of minimally invasive transcatheter aortic valve insertion (TAVI) over the last 10 years has completely changed the landscape for decision making regarding valve intervention in symptomatic patients (**Figure 1.7**).

Recent trials show non inferiority of this percutaneous technique compare with surgical intervention in both high-risk and intermediate risk patient^{53,54,56}. In addition, it should also be considered that the procedural risk could be further reduced with increasing in clinical expertise and advances in prosthesis design and engineering.

Several studies, have shown a significant decrease in major vascular complication (from > 10% to < 5%) (Ludman P. Transcatheter Aortic Valve Implantation: UK TAVI Audit 2016. [https://: www.bcis.org.uk/wp-content/uploads/TAVI-slide-deck-to-data-for-web-as-.pdf](https://www.bcis.org.uk/wp-content/uploads/TAVI-slide-deck-to-data-for-web-as-.pdf)). However, the long-term durability of these bioprostheses has not been demonstrated⁵⁵.

as a potential drug to slow down the progression of CAVS⁵⁷⁻⁵⁹. In order to observe the real effects of statins on CAVS progression, four clinical trials were carried out. However, the results showed no differences between patients taking statins and those taking placebo⁶⁰⁻⁶³. To better clarify, the effects of statin therapy on the incidence and onset of CAVS, Parolari et al.⁵⁷ performed a very complete meta-analysis. In particular, the authors showed that, in patients with non-rheumatic AS, statin treatment did not influence the occurrence of major events at 4 years of follow-up. However, the total ineffectiveness of statins in these clinical trials could have been explained by the fact that the patients enrolled were in advanced stages of diseases. Thus, it has been considered to start statin therapy at earlier stages of CAVS. Particularly, the SEAS trial showed that even in patients with mild-to-moderate AS, statin treatment did not able to reduce cardiovascular events CAVS associated⁶¹.

The use of this therapy could probably be tested in the AVSc phase, the earliest stage of CAVS. However, today AVSc is not recognized as a pathological condition and a reliable marker of stenosis. For this reason, the use of statins will not be sustainable in this particular context⁶⁴.

Since hypertension and CAVS often coexist, another class of drugs tested for CAVS patient's treatment is represented by anti-hypertensives⁶⁵ and in particular angiotensin-converting enzyme inhibitors (ACEi) or angiotensin II receptor blockers (ARBs). In particular, left ventricles pressure overload is associated with activation of the renin-angiotensin system (RAS), which plays a major role in the progression of myocardial hypertrophy and enhances the increase in collagen I and III mRNA expression leading to myocardial fibrosis. Systemic hypertension increases the diastolic transvalvular pressure gradient. This increased pressure gradient is sensed by the valve leaflets, which undergo remodeling with increased collagen deposition, inflammation, and endothelial dysfunction⁶⁶. Given the direct negative effects of RAS activation in AS patients, ACEi and ARBs may moderate myocardial hypertrophy and fibrosis and may have a beneficial effect on compromised left ventricles of AS patients⁶⁷. Anti-hypertensives have been tested on stenotic patient populations but also in these cases no significant difference was recovered between patients taking them and those given placebo^{68,69}.

Although these data are discouraging, there are few studies that demonstrate the potential of ACEi treatments in the early phase of CAVS⁷⁰. The American Heart Association/American College of Cardiology guidelines recommend treating

hypertension in patients with asymptomatic AS of any severity, with emphasis on careful titration and blood pressure monitoring^{71,72}. In addition, in patient undergoing TAVI, the use of ACEi may be considered to reduce the long-term risk of all-cause mortality⁷²⁻⁷⁴.

1.4 CAVS cellular and molecular mechanisms

CAVS is currently considered an actively regulated and progressive disease, characterized by a cascade of molecular signals able to generate cellular changes. These changes in the cells that comprise the valve leaflets are capable of causing fibrotic thickening first and massive calcification of the leaflets in the final stage of disease⁷⁵. Both endothelial and interstitial cells contribute to the pathological process leading to CAVS.

1.4.1 Endothelial dysfunction and oxidative stress

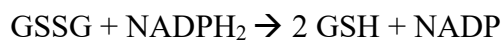
As in many vascular condition such as diabetes, hypertension and atherosclerosis, endothelial dysfunction is also strongly associated with the onset of CAVS⁷⁶. Indeed, VECs alteration leading to endothelial dysfunction represent an ineludible first step of CAVS development and progression.

In particular, is well known that histopatologically, AVSc is characterized by focal subendothelial lesion. These lesions are responsible for displacement of the *elastic lamina* and also extend to the adjacent *fibrosa* layer. At this level there are also extracellular accumulation of lipids, inflammation cells and eventually microscopic calcium accumulation, which together lead to tissue thickening, matrix remodeling and finally mineralization of leaflets^{33,77-79}. The main cause of these early lesion is probably related to endothelial damage. Oxidative stress is one of the factors chiefly accounting for this alteration⁸⁰. The term oxidative stress identifies a modification of the normal intracellular balance between reactive oxygen species (ROS) and the efficiency of antioxidant defence systems. In particular, ROS are all reactive oxygen-containing molecules including superoxide anion (O_2^-), hydrogen peroxide (H_2O_2), peroxynitrite ($ONOO^-$) and hydroxyl radical (HO^\cdot). These molecules, physiologically produced in cells as a result of metabolic reactions, may perform intracellular signaling function or be involved in pathogenetic mechanisms when their production is not adequately regulated⁸¹. In pathological situations, ROS are directly responsible for processes that cause cellular damage leading to apoptosis and necrosis⁸². It is now well

known that ROS when in excess, largely promote endothelial dysfunction which in turn is closely linked to the CAVS onset^{80,82}.

1.4.1.1 Dysregulation of glutathione system and protein Glutathionylation

Within the cells, there are several antioxidant mechanisms, involving a battery of enzymatic and non-enzymatic activities aiming to maintain tissue/cell redox homeostasis⁸³. Among them, soluble glutathione is the primary antioxidant system present in all cell's compartments⁸⁴. Glutathione is a low molecular weight tripeptide composed by a cysteine, a glycine and a glutamate. Within the cells it can exist in two different form: reduced (GSH) and oxidized (GSSG). Since the presence of GSH is essential for its anti-oxidant action, cells produce it in large quantities. In particular, cells produce GSH through the enzyme glutathione synthase or rather regenerate it from GSSG through the action of glutathione reductase (GR) which catalyses the following redox reaction:



The ratio GSH/GSSG typically serves to index tissue/cell oxidative stress and redox status. In particular, under physiological condition, the GSH/GSSG ratio is greater than or equal 100:1, while under oxidative stress condition approaches 1:1⁸⁵.

When dysregulated, however, the glutathione system can contribute to the pathogenesis of several cardiovascular diseases, including hypertension, atherosclerosis⁸⁶. In the presence of highly oxidizing conditions, redox sensitive proteins involved in many, if not all, cell function may undergo post-translational modification, including protein S-glutathionylation (P-SSG)⁸⁷.

This reversible modification consists of the interaction between molecules of GSH and/or GSSG with susceptible cysteine residues of protein⁸⁸. P-SSG has been found in various structural and functional proteins, including actin⁸⁷, modifying their characteristics and function⁸⁹. P-SSG can be part of many alteration affecting signaling mechanisms at the foundation of different cardiovascular disorders, serving as an early biomarker of pathological conditions⁹⁰. A progressive rise in the pro-oxidative milieu intervenes in the human valvular tissue during CAVS involution toward stenosis⁸⁰. However, direct specific quantification of ROS emission from human aortic valve leaflets is lacking, while previous relied on the evidence that both superoxide dismutase and catalase are down-regulated in CAVS^{91,92}. Regardless, no reports have

tested yet whether the ROS burden eventually varies with the disease stages, along with the possible role exerted by P-SSG post-translational modification in the CAVS disease progression.

1.4.1.2 *MicroRNA*

Non-coding RNAs (ncRNA), first described in 1993, are defined as transcripts that are not translated into functional protein⁹³. MicroRNA (miRNA) are a family of short (≈ 22 nucleotides) ncRNA, endogenously expressed, that regulate gene expression at post-translational levels^{94,95}. MiRNA are considered powerful post-transcriptional regulators, indeed each miRNA has more than 100 target genes⁹⁵. In recent decades, several studies showed that miRNA play a key role in regulation of protein-coding gene transcription⁹⁶, in chromatin remodeling⁹⁷ and in several diseases⁹⁸. In particular, they are able to induce gene silencing by pairing with a complementary sequence of target messenger RNA (mRNA) molecules. When a specific miRNA binds to the target mRNA, it either inhibits translational or induces degradation (Figure 1.8).

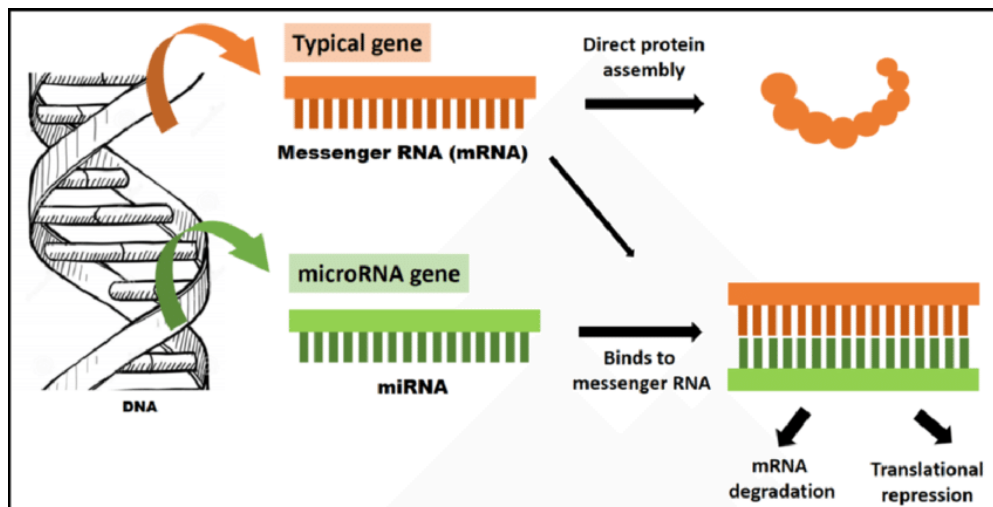


Figure 1.8. miRNAs molecular mechanism.

During the molecular mechanism involving miRNA they are able to bind target genes at mRNA level and inhibit protein production through mRNA degradation or translational repression.

Given their ability to regulate protein expression the inhibition or over expression of a single miRNA can lead to the activation of multifactorial physiological processes⁹⁵. Therefore, their regulation is crucial to tissue homeostasis. Altered expression of miRNA has been found in several pathological conditions including heart diseases⁹⁹. In particular, in cardiac tissue it has been observed that the loss of proper regulation of several miRNA is associated with arrhythmias, hypertrophy, vascular angiogenesis,

ischemia and infarction¹⁰⁰. However, in literature there are no evidence regarding differential expression of miRNA in endothelial cells isolated from stenotic BAV and TAV.

1.4.2 VICs phenotypic switching in osteoblastic-like cells

Several studies described the phenotypic differentiation of VICs during the early phase of disease. Indeed, during the progression of the pathology, this cell type becomes capable of differentiating into osteoblasts, cells able of depositing bone matrix in response to pro-osteogenic mediators released by infiltrating inflammatory cells during the early phase of disease.

During the onset of the pathology, the increase in mechanical and oxidative stress leads to endothelial damage followed by infiltration of inflammatory cells. This focal sub-endothelial lesions are characterized by the presence of inflammatory cells such as macrophages and T lymphocytes³³. Macrophages are capable of phagocytosing oxidized low-density lipoproteins (OxLDL), which have been observed in the sub-endothelial layer of subject with AVSc. Indeed, T lymphocytes release cytokines, including transforming growth factor beta (TGF β) and interleukin 1 β . These factors, activate VICs, stimulating their differentiation, proliferation and extracellular matrix synthesis¹⁰¹. Among the pro-osteogenic mediators, the most important seem to be none morphogenic protein (BMPs), belonging to the TGF β superfamily. These can be secreted by VECs following hemodynamic changes or by VICs themselves following activation mediated by other cytokines secreted by inflammatory cells. BMPs primarily induce the expression of the osteogenic transcription factor Runx2 through a signaling cascade mediated by protein complexes known as Smad. When activated, Runx2 increases the expression of calcification-related proteins such as osteopontin, bone sialoprotein II and osteocalcin¹⁰². BMPs, by Smad protein signaling, can also enhance the molecular pathway involving Wnt and β catenin, which was previously activated by the presence of subendothelial lipid deposits. Activation and enhancement of the Wnt/ β catenin pathway leads to increased expression of alkaline phosphatase (ALP) (**Figure 1.9**). ALPs are enzymes produced by osteoblasts, which play a key role in the process of bone mineralization. In particular, through their activity, they are able to convert pyrophosphatase into inorganic phosphate, promoting the deposition of mineral material on the organic matrix of the forming bone¹⁰¹.

In vitro studies on human VICs have shown the mechanism by which TNAP, a non-tissue-specific alkaline phosphatase highly expressed in VICs induces calcification. Specifically, when cells were stimulated with osteogenic medium (OM) composed by glycerophosphate and ascorbic acid require TNAP, to hydrolyse glycerophosphate into inorganic phosphate, which will then be incorporated into hydroxyapatite crystals to form the actual calcium nodules¹⁰³. In conclusion it can be said that the calcification process involves a dense and complex network of factors. Once started, this cycle of damage, inflammation and calcification is continually self-perpetuating, leading to the progression of the disease¹⁰⁴.

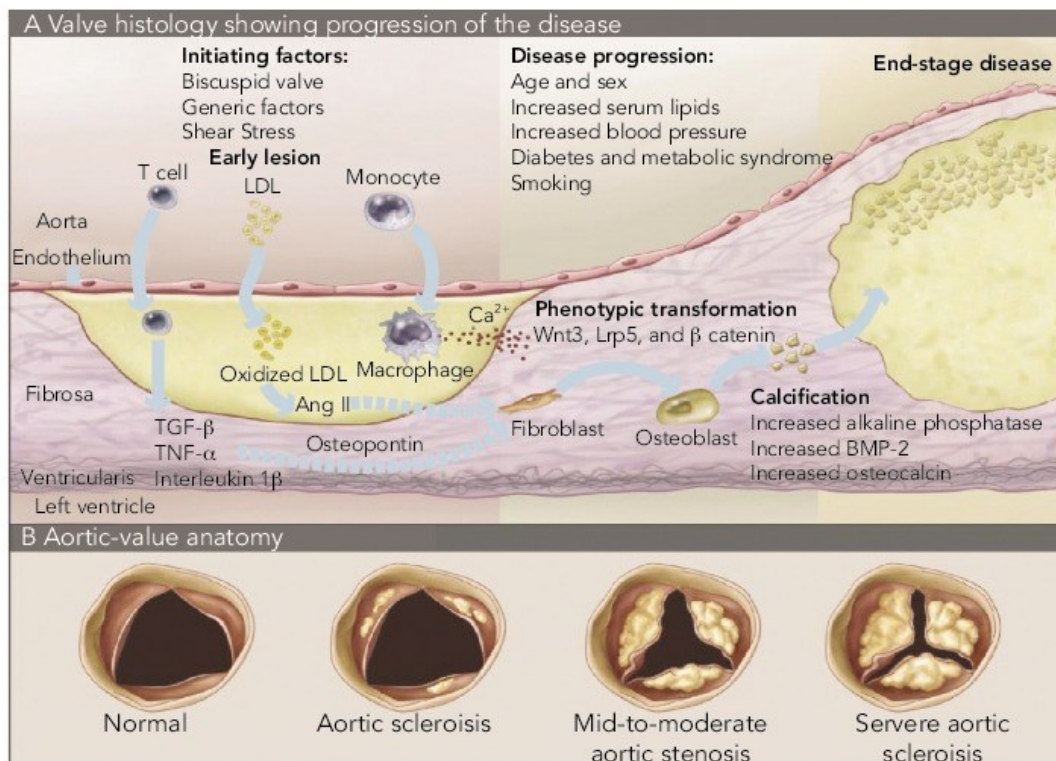


Figure 1.9. CAVS progression. The main players involved in AVSc are extracellular lipid stores (OxLDL), inflammatory cells (T lymphocytes and macrophages) and calcium nodules. In AS, the phenotypic transformation of VICs into osteoblasts takes place. Among the pro-ostrogenic mediators, the most important seem to be bone morphogenic protein (BMPs), belonging to the TGF β superfamily, which activate signaling pathways leading to increases in calcification-related proteins such as osteopontin, osteocalcin and alkaline phosphatase. Image from: *Lerman et al., European Cardiology, 2015.*

1.4.2.1 Potential players involved in VICs' calcification

Many factors are involved in the molecular mechanism that lead to VICs calcification. Among them, it is worth mentioning TGF- β signaling, Notch pathways, and Lp(a). With the aim of breaking new ground in the study of aortic valve calcification, we

decided to explore the role of two proteins whose role has never before been considered in this field: Cyclophilin A (CyPa) and Pro-protein convertase subtilisin/kexin tipe 9 (PCSK9).

As well as being interesting as known stimulators of pathological processes potentially involved in CAVS, have the distinction of having drugs for their inhibition already on the market. For this reason, in view of the absence of effective pharmacological treatments for CAVS, their study is particularly important for verifying and/or planning a possible pharmacological repositioning.

1.4.2.2 Cyclophilin A

CyPa is the largest member of cyclophilins family (CyPs). Human CyPs are composed of sixteen family members that are structurally distinct. This protein are peptidyl-propyl isomerases and catalyse the isomerization of prolines by interconverting this structurally important aminoacid between *cis* and *trans* isomers. In all cyclophilins there is a domain of approximately 109 aminoacid known as cyclophilin-like domain (CLD). For each family member, the CLD is surrounded by domain unique to each cyclophilin¹⁰⁵.

Initially purified from bovine thymocytes, CyPa has been identified as the primary cytosolic binding protein of the immunosuppressive drug cyclosporine A. CyPa is believed to be important player in many biological process including protein folding, tyraffiking, and T-cell activation^{106,107}.

Many evidences have shown the involvement of CyPa in many human pathologies end in particular in many cardiovascular diseases¹⁰⁶.

1.4.2.3 Structure and function

CyPa is a cytoplasmatic protein of 18 kDa. It is characterized by an eight-stranded antiparallel β -barrel structure, with two α -helices enclosing the barrel from either side¹⁰⁵ (**Figure 1.10**).

CyPa is believed to be important player in many biological process including protein folding, tyraffiking, and T-cell activation^{106,107}. Indeed, it is localized intracellularly but can nevertheless secreted by cells in response to inflammatory stimuli such as hypoxia, infection and oxidative stress. It is well known that secreted CyPa can act as an autocrine/paracrine factor, mediating intercellular communication. In fact, is involved in endothelial dysfunction, stimulating pro-inflammatory signal such as

NFKB and ERK in endothelial cells and smooth muscle cells (SMC)¹⁰⁸⁻¹¹⁰. It is also able to incentivate cell proliferation, senescence and apoptosis in several cell types. However, in addition to these well-known functions, it is also involved in osteoblastic differentiation process and bone metabolism^{111,112}. In particular, it has been demonstrated, *in vitro* that CyPa is able to enhance vascularSMC calcification stimulating ERK1/2 phosphorylation, runx2 expression and ALP activity. Moreover, CyPa inhibition, suppressed Pi-induced signaling and calcification¹¹³.

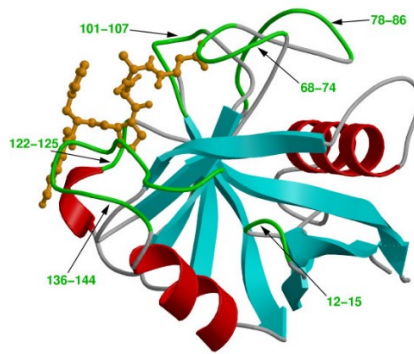


Figure 1.10. Tertiary structure of CyPa. Image from: Agarwal., *Microbial Cell Factories*, 2006.

1.4.2.2.2 CyPA in cardiovascular diseases

Several studies have highlighted the involvement of CyPa in the pathogenesis of many cardiovascular diseases.

Experiments in animal models have shown that this protein is involved in vascular remodeling. In particular, they demonstrate a significant link between CyPa expression and vascular SMC proliferation, suggesting the importance of CyPa in recruiting of inflammatory cells¹⁰⁹.

Moreover, it is also well known that CyPa contributes to the pathogenesis of abdominal aortic aneurism (AAA). In fact, it has been observed that its deletion in mice prevent the formation of AAA after angiotensin II infusion due to the reduction of inflammation, oxidative stress and matrix degradation^{114,115}.

Another disease in which chronic inflammation play a pivotal role is atherosclerosis, one of the leading causes of AAA and a condition with many points in common with aortic valve stenosis. In this regard, several pathological mechanisms by which CyPa contributes to atherosclerosis' development have been identified. In particular, CyPa is involved in: stimulation of low-density lipoprotein (LDL) uptake in the vessel, increment of endothelial dysfunction through enlargement in vascular cell adhesion

molecule 1 (VCAM-1) expression, decrease in endothelial nitric oxide synthase (eNOS) expression *via* kruppel-like factor 2 (KLF2) repression, promotion of apoptosis by the expression of tumor necrosis factor alpha (TNF- α) and in recruiting of inflammatory cells¹¹⁶.

In literature, it has been also showed that CyPa is a determinant factor in those cardiac pathologies characterized by oxidative stress, inflammation and calcification such as cardiac hypertrophy, myocardial ischemia, reperfusion injury and coronary artery disease¹¹⁷⁻¹¹⁹.

Nothing is known about CyPa's possible involvement in CAVS, a disease characterized by oxidative stress, inflammation and calcification, pathological processes in which CyPa is typically involve.

1.4.2.3 Pro-protein convertase subtilisin/kexin tipe 9

The PCSK9 is one of nine members of the pro-protein convertase (PCs) family (**Figure 1.11**). The PCs family is a group of seine proteases responsible for the proteolytic maturation of secreted proteins such as hormones, cytokines, grow factors, as well as membrane proteins such as receptors and integrines. Convertase are characterized by the presence of an active site able to catalyze the enzymatic hydrolysis of peptides. The first seven (PC1, PC2, furin, PC4, PC5, PACE 4 and PC7) activate protein precursor by cutting at basic residues while the isozyme subtilisin kexin 1 (SKI-1) and the proprotein convertase subtilisin/kexin type 9 (PCSK9) regulate lipid homeostasis by cutting at non-basic residues or inducing receptor degradation. PCs are now considered attractive targets for the development of new therapies¹²⁰.

PCSK9 is produced and secreted mainly by the liver, to a lesser extent by the kidney and intestine, and is transiently expressed in the central nervous system durin embryogenesis¹²¹.

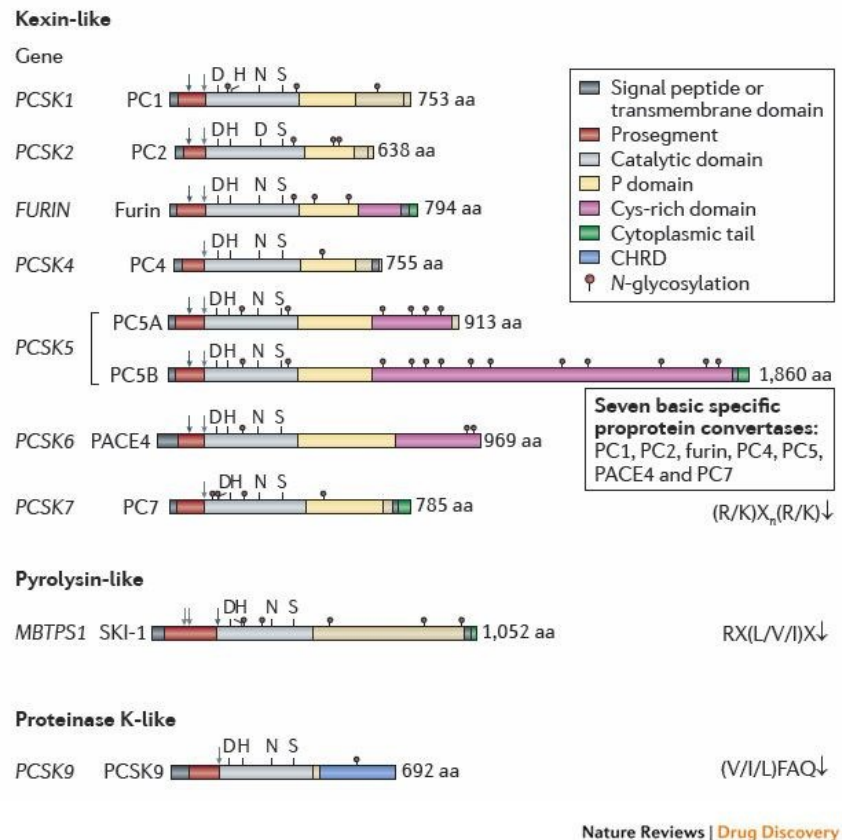


Figure 1.11. Primary structure of human pro-protein convertases. Image from: *Seidah et al., Nature Reviews. Drug discovery, 2012.*

1.4.2.3.1 Structure and processing

PCSK9 is a 692 aminoacid glycoprotein synthesised in an immature form, prepro-PCSK9, from its gene located in the short arm of chromosome 1 (1p32.3). Starting from the N-terminal end, preproPCSK9 is composed of a signal peptide (aa 1-30), a prodomain with autocatalytic activity (aa 31-152) a catalytic domain (aa 153-404) containing the proteolytic active site (catalytic triad amino acids 186,226,386), a hinge region (aa 405-454) and the C-terminal cysteine- and histidine-rich domain (CHRD) (aa 452-692)^{122,123}. The signal peptide guides the synthesised protein to the endoplasmic reticulum (ER). Upon reaching the ER, the signal peptide is cut and proPCSK9 undergoes an autocatalytic cut at position 152 (Asp151↓Gln152). This cut is necessary to generate the active structure of the protein, which can then be secreted. Unlike other PCs, the pro-domain remains associated with the catalytic site of the protein through hydrogen bonds, leading to the formation of the PCSK9/pro-domain complex. This complex prevents protein substrates from entering the catalytic site,

thereby inhibiting protease activity. This step is necessary for the exit of the mature protein from the ER (**Figure 1.12**). It then leave the ER, and it is transported to the Golgi apparatus *via* vesicles coated with COP-II cargo proteins¹²⁴.

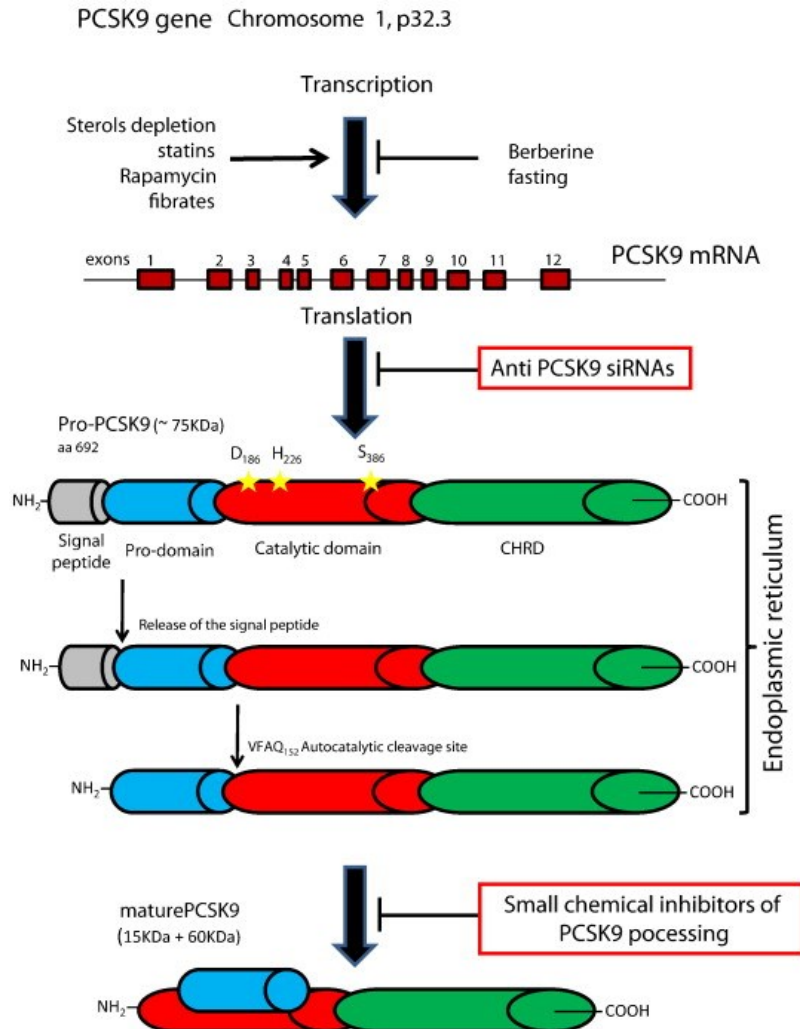


Figure 1.12. PCSKO syntesys and maturation. Starting from the top of the picture, the genetic locus, the transcribed mRNA and its translation into the preproPCSK9 protein are schematically represented. The signal peptide allows the protein to be transported to the endoplasmic reticulum. Here, the signal peptide is cut, and proPCSK9 undergoes an autocatalytic process at aa 152 (Asp151↓Gln152), creating the mature form of the protein consisting of the catalytic domain and the C-terminal domain rich in cysteines and histidines (60kDa); and a pro-domain (15 kDa) that remains covalently attached to the mature protein, covering access to the catalytic site. Image from: *Norata et al., Vascular pharmacology, 2014.*

The mature secreted protein also undergoes post-translational modifications, such as phosphorylation or glycosylation, which give it its final tertiary structure (**Figure 1.13**).

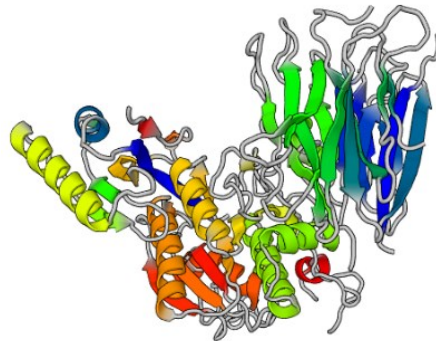


Figure 1.13. Tertiary structure of PCSK9. Image downloaded from: <https://www.nextprot.org/entry/Q8NBP7/gh/Alain-Gateau/Protein-3D-structure>

In circulation, PCSK9 may also be proteolytically cut at position 218 of the catalytic domain by furin. This cut produces a less active cut form of the protein, which in humans has been shown to account for approximately 15-40% of total circulating PCSK9¹²³.

1.4.2.3.2 PCSK9 function: role in low-density lipoprotein receptor

The discovery of PCSK9 in the liver has made it possible to identify an important new modulator of cholesterol homeostasis through its action in the binding and degradation of the LDL receptor (LDLR). Physiologically, circulating LDL binds to LDLR present on hepatocytes; this binding leads to endocytosis of the complex. Within the endosome, the acidic pH causes a rearrangement of the extracellular domain of LDLR, which reduces the binding affinity between it and LDL, and consequently leads to recycling of the receptor in the membrane and release of LDL into the cell^{122,123,125}. However, in the systemic circulation, the mature form of PCSK9 interacts with “A” domain of LDLR, on the hepatocytes’ cell surface. The formed PCSK9-LDLR complex is internalized in the cell by clatrin mediated endocytosis¹²³. Within endosomes, the acidic pH promotes the formation of a more stable bond between the C-terminal domain of PCSK9 and the ligand binding domain (LBD) of LDLR. This binding allows the receptor to be directed to the lysosome for degradation¹²⁵.

In addition to this extracellular degradation pathway, a minor degradation pathway has also been demonstrated at the intracellular level. In this case, the binding of PCSK9 to the LDLR receptor occurs directly at the Golgi, and transport to the lysosome occurs via a trans-Golgi network (TGN), mediated by clathrin light chains. Through these two different degradation pathways, the presence of LDLR in the membrane decreases, thus increasing the presence of LDL in the circulation¹²⁶ (**Figure 1.14**).

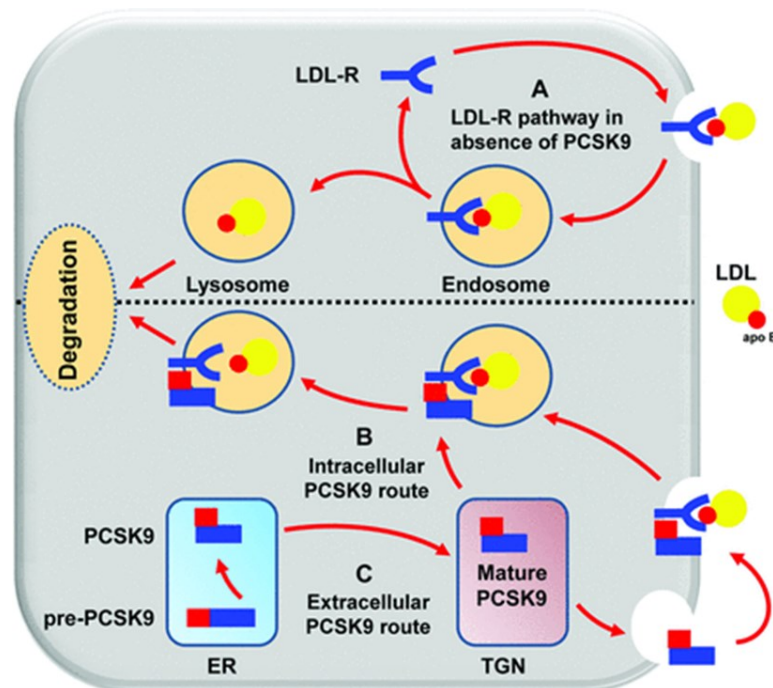


Figure 1.14. PCSK9-mediated intracellular and extracellular LDL degradation. A) The LDLR receptor binds LDLc, the complex is incorporated by endocytosis. The LDLR receptor is recycled in the membrane, while the LDLc particle is degraded within the lysosome. (B) PCSK9 after autocatalytic cleavage in the ER degrades LDLR via the intracellular, TGN-mediated pathway. (C) PCSK9 is secreted into plasma, where it binds the EGF-A domain on LDLR. The LDLR-PCSK9 complex is internalized through endocytosis and directed to lysosomal degradation. Image from: *Awan et al. Clinical Chemistry, 2014.*

PCSK9 is therefore a crucial regulator of cholesterol metabolism. In humans, PCSK9 has been shown to be one of three genes causing autosomal dominant hypercholesterolaemia, along with the LDLR and APOB genes.

Mutations leading to a gain-of-function (GOF) of PCSK9 have been associated with high levels of circulating LDL and premature atherosclerosis (*e.g.* S127R); while

mutations leading to loss-of-function (LOF) of the gene are associated with low levels of circulating LDL and protection against coronary heart disease (*e.g.* R46L)¹²⁷.

Based on this evidence, PCSK9 inhibitors have been developed to reduce cardiovascular events, particularly in subjects affected by familial hypercholesterolaemia.

Evolocumab and Alirocumab are two monoclonal antibodies that inhibit PCSK9 binding to LDLRs, thereby increasing LDL uptake and reducing LDL in circulation currently used for the treatment of adults patients with primary hypercholesterolaemia or mix dyslipidemia. Furthermore, it has been shown that adding a PCSK9 inhibitor to statin therapy can lead to a reduction of up to 60% in plasma LDL levels and a reduction in cardiovascular events¹²⁸. A promising drug currently in clinical phase III (ORION-1 study) is Inclisiran, a synthetic double-stranded oligonucleotide (siRNA) that is selectively absorbed in the liver and activates a silencing complex that degrades the mRNA responsible for PCSK9 synthesis¹²⁹. Another approach currently in Phase I is a possible vaccine, AT04A, an agent that induces an antibody response against PCSK9¹³⁰.

1.4.2.3.3 PCSK9 in aortic valve calcification

As mentioned above, PCSK9 plays a crucial role as a regulator of cholesterol metabolism and CAVS is strongly associated with high levels of plasma lipids. Therefore, various studies have been developed to assess the possibility of a correlation between PCSK9 and this disease.

In particular, two population studies demonstrated a possible association between PCSK9 and aortic valve calcification. The first was a cross-sectional population study involving patients with and without aortic valve calcification who were measured for plasma PCSK9 levels. This study found that subjects with high levels of circulating PCSK9 correlated with the presence of CAVD¹³¹.

The second population-based study showed that the loss-of-function R46L mutation of PCSK9 is not only associated with low LDL and Lp(a) levels, but also with a reduced risk of aortic valve calcification¹³².

Finally, other studies have recently been performed in animal models of wild type (WT) and PCSK9 knockout (KO) mice. Colorimetric assays for calcium identification performed on aortic valve tissues extracted from 12-month-old WT and KO mice fed a standard diet showed that calcification developed was 5-fold lower in KO mice than

in WT mice. In addition, VICs isolated from both groups of mice were used to assess calcification *in vitro* under basal conditions and with pro-osteogenic growth medium: under both conditions VICs isolated from KO mice showed lower levels of calcium than WT cells¹³³.

2. Material and Methods

2.1 Blood and Aortic Valve Collection

We prospectively obtained human aortic valve leaflets from patients who were to undergo aortic valve replacement (AVR) at Centro Cardiologico Monzino IRCCS (CCM). All performed studies was approved by the Institutional Review Board and by the Ethical Committee of CCM according to the principles outlined in the Declaration of Helsinki (1964). We ask each enlisted patient to sign informed consent to use the removed aortic valve leaflets. In particular, we enrolled patients with tricuspid aortic valve (TAV) intended for surgery because they suffer from aortic valve insufficiency without (control) or with sclerosis (AVSc), and severe stenosis (AS) and patients with bicuspid aortic valve (BAV) candidate to surgery due to severe stenosis. We evaluated the morphology and functionality of the aortic valve pre-operatively by echocardiography.

We used the following inclusion criteria: 1) elective and isolated surgical procedure; 2) over 18 years of age; 3) ejection fraction >30%; and 4) normal sinus rhythm. The following exclusion criteria were adopted: previous cardiac surgery, rheumatic heart disease, endocarditis, active malignancy, chronic liver or kidney diseases, calcium regulation disorders (hyperparathyroidism, hyperthyroidism, and hypothyroidism), and chronic or acute inflammatory states (sepsis, autoimmune disease, and inflammatory bowel disease) were considered exclusion criteria.

C-reactive protein levels were collected from the clinical routine evaluation: pre-operatively, at 3rd day, at 5th day and at discharge (postoperative day 6th-7th). Blood samples for research purposes were obtained the day before surgery.

After the surgical procedure, the aortic valve leaflets removed were collected and processed within 30 minutes.

2.2 Echocardiographic Evaluation

Pre-operative echocardiographic evaluation with M-mode, two-dimensional and pulsed, continuous and colour-flow Doppler capabilities were performed for all patients. Morphology and function of the aortic valve were assessed. Specifically, the presence of AVSc was recognized as non-uniform thickening with or without spotty calcified areas of the aortic valve leaflets without a significant transvalvular gradient (maximum aortic velocity < 2.5 m/s) as described by Otto et al.¹³⁴

2.3 Blood Sampling and Biochemical Measurement

Whole blood: 6 mL of peripheral blood sample was drawn from patients and controls while fasting, into tubes containing EDTA (9.3 mM; Vacutainer Systems, Becton Dickinson, Franklin Lakes NJ, USA) kept on ice. 250 μ L of whole blood was immediately precipitated with 250 μ L of 10% trichloroacetic acid (Sigma-Aldrich, St Louis, MO, USA) plus 1 mM EDTA solution. Samples were stored at -80 °C until analysis.

Plasma EDTA: anti-coagulated blood was centrifuged at 1700 g for 10 min at 4 °C within 30 min after being drawn. Plasma was separated and aliquots were stored at -80 °C until analysis.

2.3.1 *Glutathione Measurement*

Reduced (GSH) and oxidized glutathione (GSSG) forms were determined in whole blood by liquid chromatography-tandem mass spectrometry (LC-MS/MS) method. The separation of analytes was conducted on a Luna PFP analytical column (100 x 2.0 mm, 3 μ m, Phenomenex) eluted at 35 °C under isocratic conditions at 250 μ L/min by 1% methanol in 0.75 mM ammonium formate adjusted to pH 3.5 with formic acid. LC-MS/MS analysis was performed using an Accela HPLC (high performance liquid chromatography) system coupled with a triple quadrupole mass spectrometer TSQ Quantum Access (Thermo Fisher Scientific, Waltham, MA, USA) using electrospray ionization source and multiple reaction monitoring (MRM) in positive mode. Data were obtained after comparison with calibration curves using GSH and GSSG pure standard solutions (Sigma-Aldrich, St Louis, MO, USA). The intra- and inter-CVs (%) obtained with standard samples were <5% for both the analytes. The limits of detection were 0.031 μ mol/L for GSH and 0.008 μ mol/L for GSSG. Levels of GSH and GSSG were corrected for haemoglobin (Hb) and expressed as μ mol/g Hb.

2.3.2 *Asymmetric Dimethylarginine Measurement*

The assessment of asymmetric dimethylarginines (ADMA) was performed by LC-MS/MS using a target metabolomic approach. Briefly, the chromatographic analysis was conducted on a Luna HILIC (hydrophilic interaction liquid chromatography) analytical column (50 x 2.0 mm, 3 μ m, Phenomenex, Torrance, CA, USA). The mobile phases consisted of aqueous 1.5 mM ammonium formate (pH 3.2)

(A) and 1.5 mM ammonium formate in acetonitrile/methanol (95.5:0.5, v/v) (pH 3.2) (B) at flow rate of 250 μ L/min. The mobile phase gradient ran from 10% A to 70% A over 7 min, ran from 70% A to 94.5% A over 2 min and was held at 94.5% A for 5 min, returning to 10% A over 2 min and held at 10% A for re-equilibration. The sample injection volume was 10 μ L, the column temperature was set at 30 $^{\circ}$ C and the sample injector was maintained at 10 $^{\circ}$ C. Total run time per sample, including column cleaning and re-equilibration, was 25 min. The mass spectrometric analysis was performed using a TSQ Quantum Access (Thermo Fisher Scientific, Waltham, MA, USA) triple quadrupole mass spectrometer equipped with an electrospray ionization (ESI) interface operated in positive mode. The analytes were detected by tandem mass spectrometry (MS/MS) using multiple reaction monitoring (MRM). The LOQ value is \leq 0.25 μ M for all compounds, making this method suitable for the analysis of samples containing relatively low concentrations of the analytes, with a satisfactory precision as documented by the intra- and inter-day CVs of less than 10%. The method is linear in a wide range of concentrations (between 0 and 20 μ M), with correlation coefficients greater than 0.99 and limit of detection (LOD) around 3–10 nm for all compounds.

2.4 Electron Paramagnetic Resonance (EPR)

ROS measurements were conducted using electron paramagnetic resonance (EPR) spectroscopy, as previously described¹³⁵. Flash-frozen human aortic valve tissue (~20 mg) was homogenized using a hand-held homogenizer in phosphate-buffered saline (PBS) containing protease inhibitor cocktail (Roche Applied Science) and 0.1 mM of the metal chelator, diethylenetriaminepentaacetic acid (DTPA), at pH 7.4. Non-soluble fractions were removed by centrifugation at 15,000 g for 10 min (4 $^{\circ}$ C). The homogenates were kept on ice and analyzed immediately. Stock solutions of the spin probe 1-hydroxy-3-methoxycarbonyl-2,2,5,5-tetramethyl-pyrrolidine hydrochloride (CMH; Enzo Life Sciences) were prepared daily in nitrogen-purged 0.9% (w/v) NaCl, 25 g/L Chelex 100 (Bio-Rad) and 0.1 mM DTPA, and kept on ice. The samples were treated with 1 mM CMH at 37 $^{\circ}$ C for 2 min, transferred to 50- μ L glass capillary tubes, and analyzed immediately on a Bruker E-Scan (Billerica, MA) EPR spectrometer at room temperature. Spectrometer settings were as follows: sweep width, 100 G; microwave frequency, 9.75 GHz; modulation amplitude, 1 G; conversion time, 5.12 ms; receiver gain, 2×10^3 ; number of scans, 16. In all cases, the

samples were in the linear response region. EPR signal intensities were assessed by measuring EPR signal peak-to-peak amplitude. The reported ROS levels represent EPR signal intensities normalized to the tissue homogenates' protein concentrations as determined by Pierce BCA protein assay kit (Life Technologies).

2.5 Histological Evaluation

Aortic valve leaflets assigned to histological studies were washed 3 times in phosphate-buffered saline (PBS) 1× and were fixed in 4% formalin, dehydrated, included in paraffin, and cut into 5- to 7- μ m slides. Before staining, slides were rehydrated.

2.5.1 Immunohistochemistry

For immunohistological staining, slides were incubated in antigen retrieval solution (Target Retrieval Solution Citrate [pH 6], Dako Cytomation, Glostrup, DK) at 98°C for 20 min and then cooled at room temperature for 20 min. Slides were treated with 3% H₂O₂ to block endogenous peroxidases and then washed 3 times with 1× PBS with 0.1% Triton (PBST). Blocking solution (PBST and 5% bovine serum albumin) was added and kept for 45 min at room temperature. Slides were incubated with primary mouse monoclonal anti-PCSK9 (Abcam, Cambridge, UK) or mouse monoclonal anti-GSH (Santa Cruz, Dallas, Tx, USA) at 4°C overnight. Slides were washed 3 times with PBST and incubated with biotinylated anti-mouse secondary antibody (Vector Laboratories, Burlingame, CA, USA) for 60 min at room temperature. Slides were washed 3 times and ABC complex (ABC kit, Vector Laboratories, Laboratories, Burlingame, CA, USA) was added and incubated for 30 min at room temperature. Slides were washed 3 times, and ImmPACT DAB Peroxidase (HRP) Substrate (Vector Laboratories, Laboratories, Burlingame, CA, USA) was added and let react for 25 s. Slides were immediately rinsed in distilled H₂O and then incubated for 10 s with hematoxylin. Slides were dehydrated, mounted with EUKITT (O. Kindler/Orsatec), and images were taken with AxioScope (Carl Zeiss, Oberkochen, DE). The quantification of PCSK9 immunohistochemistry has been performed implementing the ImageJ v1.50i software (NIH, Bethesda, MD, USA) with the plugin IHC Tool box. The automated color detection, which allows the generation of deconvoluted images, has been performed with the default model H-DAB for brown color detection. The integrate pixel density has been calculated on binary panoramic images and normalized with the total area of the section (pixel²).

2.5.2 *Von Kossa Staining*

Von Kossa staining was carried out with silver nitrate added on top of each section and exposed to ultraviolet illumination at room temperature for 20 min. Slides were washed in deionized H₂O and then incubated in sodium thiosulfate solution 2 g/dl (Sigma-Aldrich, St Louis, MO, USA) at room temperature for 5 min. Slides were washed 3 times in deionized H₂O and then incubated for 10 s with hematoxylin. Slides were dehydrated, mounted with EUKITT (O. Kindler/Orsatec, Bobingen, DE), and images were taken with AxioScope (Carl Zeiss, Oberkochen, DE).

2.6 **Isolation of aortic valve endothelial and interstitial cell**

Aortic valve endothelial and interstitial cells isolation was performed using mechanical disruption and enzymatic digestion. Particularly, aortic valve leaflets were placed in 2 mg/mL type II collagenase (Worthington Biochemical Corp., Lakewood, NJ, USA) in Advanced Dulbecco's modified Eagle's medium (Ad DMEM – Life Technologies, Carlsbad, CA, USA) containing 10% fetal bovine serum (FBS), 1% Penicillin, 1% Streptomycin solution and incubated for 20 min at 37 °C. Loosened endothelial layer was removed by wiping the leaflet surfaces with sterile cotton swabs. The resulting cells were washed and isolated using Dynabeads® conjugated with an endothelial marker, platelet endothelial cell adhesion molecule (CD31 – Life Technologies, Carlsbad, CA, USA), and cultured in supplemented Medium 200 (Life Technologies, Carlsbad, CA, USA) on 0.1% gelatine (Sigma-Aldrich, St Louis, MO, USA) coated tissue culture plate. After removal of the endothelial cell layer, the specimens were finely shredded with bisturi and then incubated over night at 37°C in a tube containing complete Ad DMEM with 1 mg/ml type II collagenase, to process the extracellular matrix protein. At the end of incubation, the resulting valve interstitial cells (VIC) were plated in tissue culture plates in complete Ad DMEM and maintained at 37°C and 5% CO₂. All the experiments were performed on cultured cells between the second and sixth passage.

2.7 **Gene expression**

2.7.1 *RNA Isolation from tissues and cells*

After collection, aortic valve samples were stored at –80 °C in an appropriate amount of RNA Later solution (Sigma-Aldrich, St Louis, MO, USA). Then, dried tissues were crushed by the Bessman Tissue Pulverizer (Spectrum Europe, Lake

Forest, CA, USA) and RNA was isolated with the TRIzol® solution (Thermo Fisher Scientific, Waltham, MA, USA). RNA extraction was performed from valve VECs using Total RNA Purification Plus Kit (Norgen Biotek Corp., Thorold, ON, CA) according to the manufacturer's instructions. RNA quantification was determined with a spectrophotometer (ND-1000, NanoDrop®, EuroClone®).

2.7.2 Reverse Transcription and Real Time PCR

Reverse transcription was performed following the manufacturer's instructions with the SuperScript III (Invitrogen™, Carlsbad, CA, USA) or with TaqMan Reverse transcription Reagent (Applied Biosystems, Foster City, CA, USA). Quantitative real-time polymerase chain reaction was executed by the use of the iQTM SYBR Green SuperMix (Bio-Rad, Hercules, CA, USA) or the SYBR Green PCR MasterMix (Applied Biosystems, Foster City, CA, USA). All reactions were performed in a 96-well format with the iQ5TM (Bio-Rad, Hercules, CA, USA) or with AB7900 (Applied Biosystems, Foster City, CA, USA). The relative quantities of specific mRNA were obtained with the use of the comparative Ct method and were normalized to glyceraldehyde 3-phosphate dehydrogenase gene (GAPDH). The primer sequences used to gene amplification were: PPIA_Foward: 5'-CCACCGTGGTCTTCGACATT-3'; PPIA_Reverse: 5'- CCTTGCTGCAAACAGCTCA-3'; PCSK9_Foward: 5'-TGTCTTTGCCCAGAGCATC-3'; PCSK9_Reverse: 5'-GTCACTCTGTAGCTGGTGTC-3'; GAPDH_Foward: 5'-ATGTTTCGTCATGGGTGTGAA-3'; GAPDH_Reverse: 5'-GTCTTCTGGGTGGCAGTGAT-3'; PECAM1_Foward: 5'- CAG GCC CCA TTG TTC CC -3'; PECAM1_Reverse: 5'- ATT GCT CTG GTC ACT TCT CC -3'; CDH5_Foward: 5'- GAT CAA GTC AAG CGT GAG TCG -3'; CDH5_Reverse: 5'- AGCCTCTCAATGGCGAACAC -3'; ACTA2 Fw 5'- AGA GTTACGAGTTGCCTGATG -3'; ACTA2 Rv 5'- CTG TTG TAG GTG GTT TCA TGG A -3'.

2.7.3 TaqMan human miRNA card A and B arrays

The TaqMan Human microRNA Card A and B Arrays version 3.0 (Thermo Fisher Scientific, Waltham, MA, USA) were used for evaluating the expression a total of 754 miRNAs. The megaplex pool primers were used for reverse transcription (RT), pre-, and amplification steps and performed according to the manufacturer's protocol

on 7900HT Real-Time PCR System (Thermo Fisher Scientific, Waltham, MA, USA). In particular, 350 ng of RNA were retrotranscribed with 40 cycles at 16 °C for 2 min, 42 °C for 1 min, and 50 °C for 1 s, followed by an incubation at 85 °C for 5 min. The pre-amplification was performed by a serial incubation at 95 °C for 10 min, 55 °C for 2 min, 72 °C for 2 min, 12 cycles at 95 °C for 15 s and 60 °C for 4 min, followed by an incubation at 99.9 °C for 10 min. Finally, the samples were loaded into the run plate and incubated at 50 °C for 2 min, 94.5 °C for 10 min, 40 cycles at 97 °C for 30 s and 59.7 °C for 1 min. Analyses were performed using the Expression Suite software v1.0.3 (Thermo Fisher Scientific, Waltham, MA, USA) as previously described⁹⁴. We filtered out miRNA that did not pass the quality controls. The excluded miRNAs had one or more of the following: low signal in linear phase; bad passive reference signal (ROX); low Cq confidence; cT algorithm failed; exponential algorithm failed; and thresholding algorithm failed. In addition, we considered only miRNAs that were expressed and passed the quality tests in all the samples. The expression value of each miRNA is expressed as log₂ fold change (log₂FC).

2.7.4 Functional analysis

To evaluate miRNA-mRNA interactions, we used Cytoscape (v3.7.1), a web-bioinformatics tool (<http://www.microrna.org>), and ClueGO (v2.5.3). Cytoscape is an open source software platform for visualizing complex networks (<https://cytoscape.org>)¹³⁶. MiRNA target prediction was carried out with miRanda¹³⁷ and mirSVR¹³⁸ algorithms. ClueGO application was used to calculate enrichment (Fisher's exact test) p-values for the gene ontology (GO) pathway performed with iScript™ Advanced cDNA Synthesis Kit (Bio-Rad, Hercules, CA, USA) and total RNA (3 µg) was converted into cDNA. Real Time PCR (qPCR) was carried out on ABI Prism 7900 HT (Applied Biosystems, Foster City, CA, USA), according to the manufacturer's instructions and analysis were performed using software SDS2.4 (Life Technologies, Carlsbad, CA, USA).

2.8 Protein expression

2.8.1 Western and Dot Blot

Tissue whole-protein extracts were obtained by pulverizing frozen aortic valve leaflets. The powder was suspended in 1x RIPA buffer with the addition of protease

inhibitors (Sigma-Aldrich, St Louis, MO, USA) as well as VECs and VICs to obtain cell lysates.

Total protein concentration was quantified with BCA kit (Thermo Fisher Scientific, Waltham, MA, USA). Protein extracts were subjected to Dot blot and Western Blot. After procedures were transferred onto a nitrocellulose membrane. The membranes were blocked for 30 min at room temperature in 5% nonfat dry milk (Sigma-Aldrich, St Louis, MO, USA) in Wash Buffer (Tris Buffer Sulfate 1×, 0.1% Tween 20) and then incubated overnight (O/N) at 4 °C with the appropriate primary antibody. The primary antibodies used were specific for CyPA (R&D system Inc., Minneapolis, MN, USA), GSH (Santa Cruz Biotechnology, Dallas, Tx, USA), γ H2AX (Cell Signaling) GAPDH (Santa Cruz Biotechnology, Dallas, Tx, USA) and bActin (Cell Signaling Technology, Danvers, MA, USA). Then, the membranes were washed and incubated with peroxidase-conjugated secondary antibodies (GEHealthcare) or IRDye conjugated secondary antibody (LI-COR Bioscience) respectively for 1 h and 20 min. Finally, the membrane were washed to remove any excess of secondary antibody and acquired using Alliance Mini 2M (UVITec Cambridge) or Odyssey Infrared conjugated Imaging System (LI-COR Bioscience, Lincoln NE, USA). Densitometric analysis of membranes was performed using the Alliance Mini 4 16.07 software (UVITec Cambridge) or the software ImageJ (Version 1.48v -National Institute of Health). In order to normalize, GAPDH or β -Actin were used as a total protein loading control.

2.8.2 Immunoprecipitation

Five hundred micrograms of VECs protein extract were pre-cleaned at 4 °C for 30 min with 0.5 μ g of non-immune IgG coupled to 10 μ L of protein G agarose beads (Bio-Rad, Hercules, CA, USA). Pre-cleaned extracts were centrifuged for 60 seconds at 300 x g and the supernatant was immunoprecipitated overnight at 4 °C with 10 μ L of protein G agarose beads and 3 μ g of GSH antibody (Santa Cruz Biotechnology, Dallas, Tx, USA) *per* 100 μ g of protein. After washing three times with lysis buffer, the beads were boiled in reducing Laemmli buffer for 5 min and subjected to a Western Blot.

2.8.3 ELISA assay

The supernatant culture media of VICs cultured in normal and osteogenic medium were collected. The PCSK9 quantification was carried out with an enzyme-linked immunosorbent assay (ELISA - R&D system Inc., Minneapolis, MN, USA) following

the manufacturer's instructions. The secreted CyPA levels detection was performed by an other ELISA kit (BioVendor, Brno, CZ) following the manufacturer's instructions.

2.9 In vitro model of Protein S-Glutathionylation and Oxidative Stress

An in vitro model using human umbilical vein endothelial cells (HUVEC) was performed. The block glutathione reductase was achieved with a specific compound known as 2-acetylamino-3-[4-(2-acetylamino-2-carboxyethylsulfanylthiocarbonylamino)phenylthiocarbamoylsulfanyl]propionic acid (2-AAPA Sigma-Aldrich, St Louis, MO, USA) at two different concentration, 50 and 100 μM .

Then, this model was implemented in porcine VEC (pVEC) titrating the dose of 2-AAPA as follow: 12.5, 25, 50, 75, and 100 μM . Briefly, HUVEC and pVECs were treated with 2-AAPA for 4 h in full M200 media (Thermo Fisher Scientific, Waltham, MA, USA). Then, cells were let recover for 24 h in fresh full media. At the end of the recovery time, GSH/GSSG levels, MTT, proteins and mRNA transcripts were evaluated. We found that minimum effective dose of 2-AAPA in pVECs was 50 μM ; therefore, we treated human VECs (hVEC) with this drug concentration and performed assays such as protein level, GSH/GSSG, MTT, and apoptosis assessment using this 2-AAPA dosage.

2.10 MTT assay

hVECs and pVECs were seeded in 96 well plates coated with 0.1% gelatin (Sigma-Aldrich, St Louis, MO, USA) in a complete M200 growing medium (Life Technologies, Carlsbad, CA, USA). After cell adhesion, a starvation protocol was carried out overnight in M200 without FBS. After one day, starvation was terminated, and the cells treated with 2-AAPA or H_2O_2 in M200 with 0.5% FBS. After the 4 hours treatment and 24 hours of recovery, the medium was removed, and the 3-(4, 5-dimethyl thiazolyl-2)-2,5-diphenyltetrazolium bromide (MTT - Sigma-Aldrich, St Louis, MO, USA) solution (0.5 mg/ml) was added into each well and incubated at 37°C, 5% CO_2 for 4 hours. After incubation, the MTT solution was discarded, and dimethylsulfoxide (DMSO - Sigma-Aldrich, St Louis, MO, USA) was added into each well and was incubated for 10 minutes. Finally, the corresponding absorbance was measured using

the microplate reader (TECAN pro infinite M200) at a dual-wavelength of 590 nm and 620 nm (reference).

2.11 Apoptosis detection

The Annexin V, a standard marker of apoptotic cells, was used to measure apoptosis levels after 2-AAPA treatments. Annexin V assay was performed on hVECs using Gallios (Beckman Coulter, Brea, CA, USA) flow cytometer. hVECs were treated for 4 hours with 2-AAPA 50 μ M and after they were subjected to 24h of recovery in Medium 200 or for 72h with two different concentration of H₂O₂ (100 and 200 μ M). Subsequently, cells were detached by a non-enzymatic method (TripLE Select – Gibco – Thermo Fisher Scientific, Waltham, MA, USA), re-suspended in 100 μ L of FACS buffer (PBS supplemented with 0.1% BSA (Gibco – Thermo Fisher Scientific, Waltham, MA, USA) and 5 mM EDTA (Gibco – Thermo Fisher Scientific, Waltham, MA, USA)) and incubated in the dark for 15 min with the antibody Annexin V conjugated with Alexa Fluor488 (Thermo Fisher Scientific, Waltham, MA, USA). After incubation and wash with the FACS buffer, the cells were centrifuged for 10 min at 400 x g to remove eventually unbound antibody. Finally, cells were re-suspended in 500 μ L of FACS buffer and analysed at cytofluorimeter. hVECs were gated on a side scatter-forward scatter dot plot to eliminate cell debris, and a total of 20000 events in the hVECs gated area were acquired. Acquisition analysis were performed thanks to the Kaluza software (Beckman Coulter, Brea, CA, USA).

2.12 Intracellular ROS detection

pVECs were grown to sub-confluency in 60 mm plates (Corning® Costar®, New York NY, USA) coated with 0,1% of gelatin (Sigma-Aldrich, St Louis, MO, USA) in a complete M200 medium (Life Technologies, Carlsbad, CA, USA). After 4 hours of 2-AAPA 50 μ M treatment (Sigma-Aldrich, St Louis, MO, USA) and 24 hours of recovery, ROS detection was performed by CellROX® green Assay Kit (Thermo Fisher Scientific, Waltham, MA, USA), executed following the manufacturer's instruction. The staining was analyzed by ImageStream X imaging flow cytometer (ImageStream X Mark II, Amnis). The analysis was performed using the IDEAS 6.2 software.

2.13 In vitro osteogenic stimuli on VECs and VICs

During the calcification assays, we seeded VECs in 24 well plate and treated them with different stimuli: a) a pro-calcifying one, consisting of a standard medium supplemented with 2 mM inorganic phosphate (Pi) administered every two days while changing the medium every time; b) a pro-oxidative challenge by providing 2-AAPA (50 μ M for 4 hours) and changing the media every two days; and c) an antioxidant treatment encompassing 1 hour of pretreatment with 2 mM N-acetyl-L-cysteine (NAC), followed by for 4 hours with 2-AAPA (50 μ M) + NAC (2 mM) and NAC (2 mM) was administered every two days while changing the medium.

Similarly, VICs were seeded in 24 well plate and than they were subjected to different treatment: osteogenic medium (10 mmol/l b-glycerophosphate and 50 μ g/ml ascorbic acid) with or without a neutralizing antibody anti-PCSK9 (NAb anti-PCSK9, 0.8 ng/ml, BPS Bioscience, San Diego, California) or immunoglobulin G1 as control (IgG1, 0.8 ng/ml, Novus Biologicals, Centennial, Colorado); medium with different concentration of human recombinant CyPa (10,100 and 100 ng/mL) or MM284 (250 ng/mL). Each assay lasted 1 week.

2.14 Calcium assay

After removing the culture media, extracellular calcium crystals were dissolved with 0.6 M hydrochloric acid (HCl) for 5 h in gentle agitation. Subsequently, HCL samples were recovered and stored +4°C; meanwhile, the layer of cells present in each well was treated with 0.1 M sodium hydroxide (NaOH) and 0.1% sodium dodecyl sulfate (SDS) to ensure cellular lysis necessary for total protein quantification. Extracellular calcium quantification was performed using a colorimetric assay kit (BioVision Inc., Milpitas, CA, USA) following the manufacturing company's protocol. The absorbance was read off at the Infinite® 200pro (TECAN) spectrophotometer.

2.15 Human aortic valve cell transfection

Transfection was performed seeding 2×10^5 endothelial cells and treated with 50 nM of a miR mimic, a miR inhibitor, or negative control (Ambion, Thermo Fisher Scientific, Waltham, MA, USA). In particular, 5 μ L of Lipofectamin RNAiMAX Transfection Reagent (Invitrogen, Thermo Fisher Scientific, Waltham, MA, USA) were used following manufacturer's protocol. RNA evaluation was performed after 48

h following transfection, while apoptosis evaluation was carried out treating ECs with 200 μ M H₂O₂ for 72 h.

2.16 Genetic association study of PCSK9 R46L variant and CAVS

We investigated the association between the R46L PCSK9 variant and CAVS in a meta-analysis of 1 published (Copenhagen General Population Study, Copenhagen City Heart Study, and Copenhagen Ischemic Heart Disease Study, totaling 1,437 cases and 99,040 control patients¹³²) and 9 unpublished studies (UK Biobank 1,350 cases and 349,043 control patients; EPIC-Norfolk [European Prospective Investigation into Cancer and Nutrition– Norfolk] 508 cases and 20,421 control patients; MDCS [Malmo Diet and Cancer Study] 682 cases and 5,963 control patients; GERA [Genetic Epidemiology Research on Aging], 3,469 cases and 41,234 control patients, the Estonian Biobank 481 cases and 7,223 control patients, the QUEBEC-CAVS study 1,009 cases and 11,625 control patients, and 3 French cohorts 3,123 cases and 6,532 control patients). This meta-analysis was performed after each study had tested the impact of this variant on CAVS using logistic regression adjusted for age and sex, and the first 10 ancestry-based principal components when available. We performed a fixed-effect meta-analysis using the inverse-variance weighted method as implemented in the *rmeta* package (version 3.0) in R version 3.5.1 software (R Foundation for Statistical Computing, Vienna, Austria). The design of each study and the definition of CAVS is presented in the Appendix. All study protocols were approved by local ethics committees, and all patients provided informed consent. A summary of the definition of CAVS in each cohort is described in **Supplemental Table 1** showed in **Supplemental Appendix**.

2.17 Statistical Analysis

The data were analyzed using IBM SPSS statistic 26 software and Graph Pad Prism software (version 7). Quantitative variables with normal or skewed distribution were reported as mean \pm SD or median and interquartile range, respectively. Categorical variables were reported as frequency and percentage. Group comparisons for normal, skewed, and categorical variables were performed by Student t-test for independent samples, by Wilcoxon rank-sum test, and χ^2 test, respectively. Between-group differences were evaluated by one-way ANOVA with Bonferroni or Tukey correction, as appropriate. The association between AVSc and mortality was assessed by Kaplan-Meier survival curves with log-rank test and by multivariable Cox regression analysis.

The sensitivity analysis was carried out implementing a Cox model adjusted for all the variables significantly associated with AVSc. To assess whether AVSc adds to prediction of short-term mortality on top of EuroScore II (ESII) the integrated discriminating improvement (IDI) index was employed. A value of $p < 0.05$ was considered statistically significant.

3. Results

3.1 Aortic valve sclerosis add to prediction of short-term mortality in patients with documented coronary atherosclerosis

3.1.1 Study design

All patients who underwent isolated CABG from 2004 to 2015, at Centro Cardiologico Monzino, were included into this study. Demographic information, preoperative, intraoperative, and postoperative data were retrieved from the institutional database. The number of anastomosis, the on- or off-pump technique, as well as the graft used (e.g., saphenous vein, radial artery, and/or internal thoracic artery) were chosen by staff surgeons according to European guidelines¹³⁹. A total of 2246 patients were identified. At the 90th day post-surgery, 2215 patients were still alive, whereas 31 were deceased (all-cause mortality: 1.5%). Deceased patients were eligible for the study only if the cause of death was cardiac (n = 29), their echocardiographic images were of good quality and they have no sign of significant valve pathologies (e.g., aortic valve stenosis, mitral regurgitation, or rheumatic heart disease). Therefore, the final analysis included 2244 patients. The flow chart with patient's selection is shown in **Figure 3.1**.

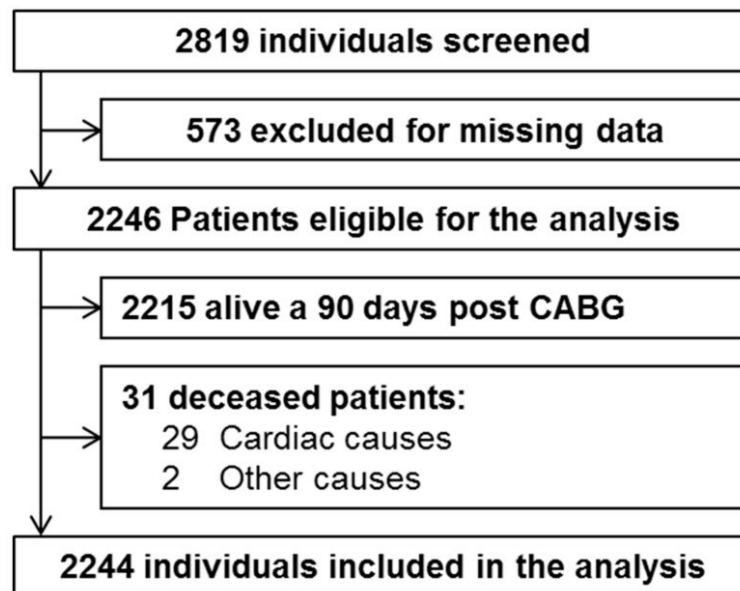
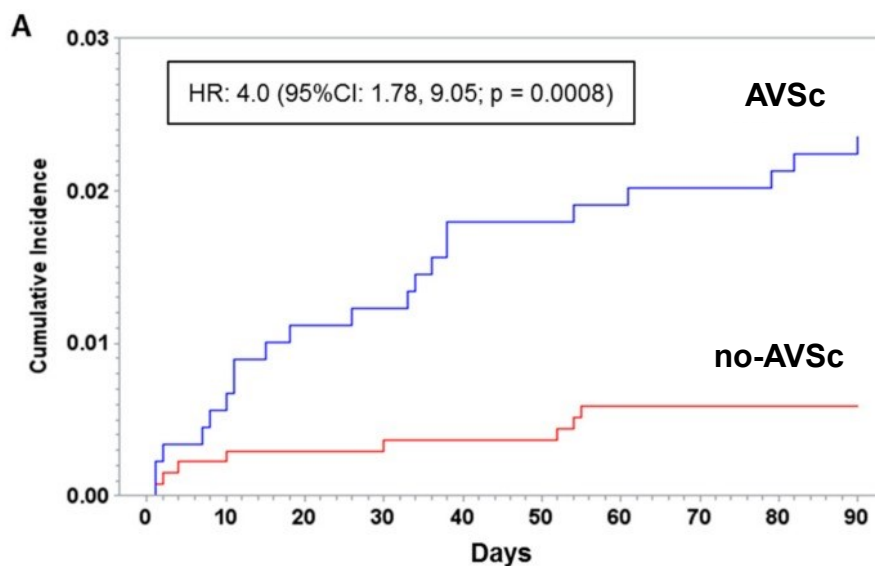


Figure 3.1. Case study selection.

3.1.2 Presence of AVSc: independent predictor of short-term mortality

The examined population was predominantly of male sex (84%) with an average age of 67 years and medium-low risk (ESII: 1.8 [95%CI: 1.1; 3.6]). Most patients (77%) had a three-vessel coronary disease with a mean left ventricular EF of 57%. Among patients enrolled in the study who met the inclusion criteria (n = 2244), 1352 had normal aortic valve leaflets and were classified as no-AVSc and the remaining 892 (39.8%) had non-uniform thickening of the aortic leaflets and were classified as AVSc. **Supplemental Table 2** in **Supplemental Appendix**, shows the characteristics of patients with and without AVSc. The groups significantly differed for age, sex, prevalence of diabetes, New York Heart Association (NYHA) class, EF, CBP and clamping time, and number of transfused units per patient. No differences were observed in terms of CAD severity, with the exception of the circumflex artery, which shows an increased number of patients with a stenosis >50% in the AVSc group. Kaplan-Meier cumulative incidence curves, stratified by presence/absence of AVSc, showed a significant increase in short-term mortality in AVSc patients (**Figure 3.2**). After 90 days from CABG, the mortality rate in AVSc patients was 2.6% compared to 0.6% in no-AVSc patients. The unadjusted hazard ratio (HR) was 4.0 (95%CI: 1.78, 9.05; p = 0.0008), the ESII adjusted HR was 2.9 (95%CI: 1.26, 6.56; p = 0.01), while the propensity score adjusted HR was 2.7 (95%CI: 1.17, 6.23; p = 0.02). In the sensitivity analysis, the adjusted HR was minimally changed (HR: 2.44, 95%CI: 1.03, 5.77; p = 0.04). In the IDI analysis, the model including AVSc and ESII performed better than the model including only ESII (IDI = 0.009, 95%CI: 0.004, 0.013; p < 0.001).



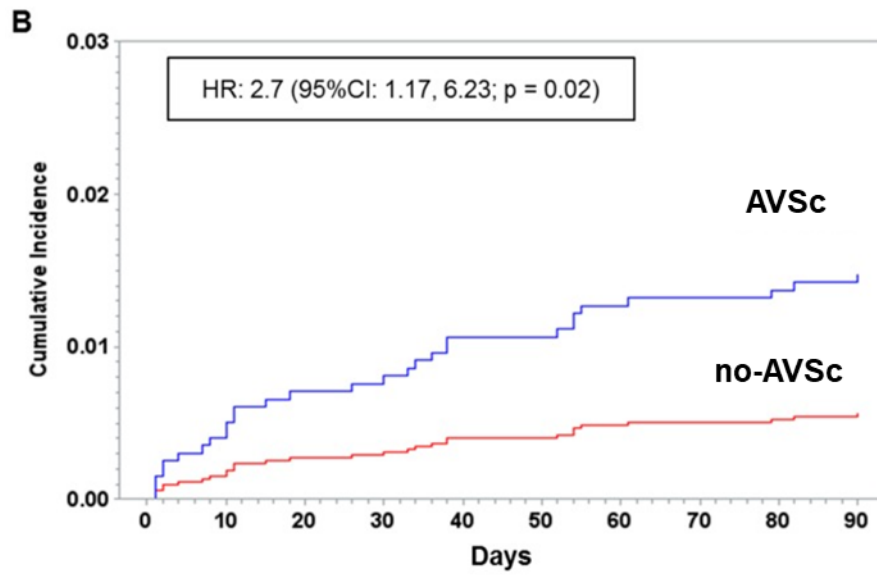


Figure 3.2. Kaplan-Meier cumulative incidence of patients that underwent surgical myocardial revascularization. (A) unadjusted and (B) adjusted for propensity score survival curves. Patients are stratified accordingly to normal aortic valve morphology (no-AVSc) or to aortic valve sclerosis (AVSc).

3.2 Aortic valve sclerosis as an important predictor of long-term mortality in patients with 2 carotid atheromatous plaque requiring carotid endarterectomy (CEA)

3.2.1 Study design

In total, 806 adult patients with the severe atherosclerotic disease who underwent isolated CEA 4 from 2006 to 2018, in the vascular surgery department at Centro Cardiologico Monzino (University 5 Hospital), were identified and included in this retrospective observational study. Indications for 6 CEA intervention were the presence of carotid artery stenosis $\geq 50\%$ in symptomatic and $\geq 70\%$ in 7 asymptomatic patients¹⁴⁰. Twenty-seven patients (5%) were considered symptomatic due to 8 transient ischemic attack, amaurosis fugax, or stroke within 6 months before surgery. Patients with 9 concomitant open-heart surgery and CEA were excluded. Patients with significant valve pathologies 10 such as aortic valve stenosis, mitral valve regurgitation, rheumatic valve disease, and with 11 insufficient quality of echocardiographic images were also excluded from the study. Demographic 12 characteristics, preoperative, intraoperative, and postoperative data were retrieved from the 13 institutional database. The follow-up was carried out through a regional registry. This study was 14 approved by the Institutional Review Board of Centro Cardiologico Monzino IRCCS (CCM 591- 15 RE2674). The study protocol conforms to the ethical guidelines of the 1975 Declaration of Helsinki.

For all CEA patients, in addition to a comprehensive echocardiographic evaluation, previously described in **Material and Methods** section, preoperative MDCT angiography was performed. Plaque type was classified according to density measurements based on previously reported criteria¹⁴¹. In detail, soft plaques, associated with lipid-rich cores, were defined as those with a median density of less 2 than or equal to 60 Hounsfield units (HU); mixed/fibrotic plaques, associated with large amounts of 3 fibrous tissue, were categorized as those with a median density of between 61 and 130 HU; 4 calcified plaques consisted of lesions having a median density of greater than 130 HU.

3.2.2 High AVSc prevalence in CEA patients

Of the 806 patients initially screened, 541 (mean age 70.8 ± 7.6 years, 333 men) were enrolled in the study (**Figure 3.3**). In our cohort, 423 (78%) patients had hypertension, 405 (75%) had dyslipidemia, and 147 (27%) were diabetic, while 89 (16%) and 189 (35%) were current and ex-smokers, respectively. The prevalence of previous cerebrovascular events and myocardial infarction were 23 and 12%, respectively. The presence of non-uniform thickening of one or more aortic valve leaflets, classified as AVSc, was found in 348 patients (64%). Patient baseline characteristics, stratified by the presence of AVSc, are shown in **Supplemental Table 3** showed in **Supplemental Appendix**. In the univariate analysis, the patients with AVSc were significantly older (72.4 ± 6.6 vs 67.8 ± 8.2 , $p < 0.001$), and presented lower eGFR levels (67.7 ± 17.4 vs 72.1 ± 18.8 , $p = 0.006$), while patients without AVSc had a higher prevalence of diabetes (33% vs 24%, $p = 0.033$). We did not find any difference regarding sex, hypertension, dyslipidemia, smoking, BMI, previous myocardial infarction (MI) and cerebrovascular events (CVE), left ventricular ejection fraction (LVEF), NYHA class, and severity of carotid artery stenosis between the two groups. The multivariate analysis including age, diabetes and Egfr revealed that only age ($p < 0.001$) was independently associated with AVSc presence.

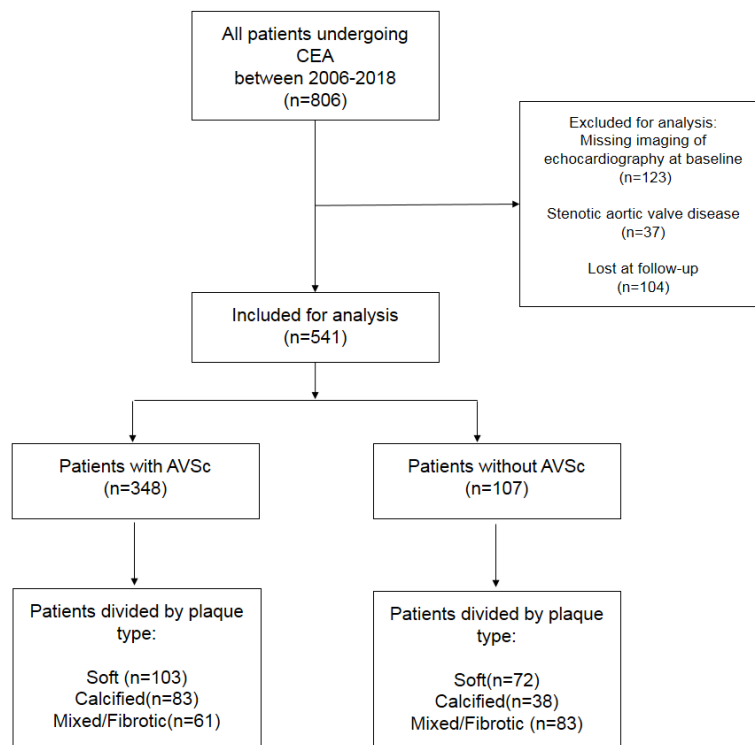


Figure 3.3. Patient flow chart. The number in the brackets indicates the number of patients. AVSc: 3 aortic valve sclerosis; CEA: carotid endarterectomy.

3.2.3 AVSc predicts long-term all-cause mortality

During the 5-year follow-up, we registered 73 deaths (13.5%) for any cause. In **Supplemental Table 4** showed in **Supplemental Appendix**, we presented the baseline characteristics of these patients compared to the 17 survived ones. The groups significantly differed in age, sex, eGFR, LVEF, NYHA class, and AVSc. No difference was observed in terms of diabetes, hypertension, dyslipidemia, smoking, BMI, previous MI and CVE, and the severity of carotid stenosis. In addition, the multivariate analysis revealed that old age, low eGFR, reduced – but within normal levels – LVEF and AVSc presence were independent predictors of all-cause mortality. The five-year all-cause mortality rate in patients with AVSc was 16.7%, while in patients without AVSc was 7.8% ($p = 0.004$). The survival analysis showed a strong association between AVSc and mortality at five years (log-rank $p = 0.005$; **Figure 3.4A**) better evidenced by the inset depicted in **Figure 3.4B**, while **Figure 3.4C** shows the breakdown of the patients at risk per year in two groups. **Figure 3.4D** shows the

unadjusted hazard ratio (HR) for all-cause mortality of patients with AVSc and the HR adjusted for baseline demographic and clinical characteristics identified by the multivariate analysis. In particular, after adjustment for age as well as cardiac and renal function, AVSc was still an independent predictor of 2 long-term mortality (HR: 1.92, 95% CI: 1.04-3.54; $p = 0.038$).

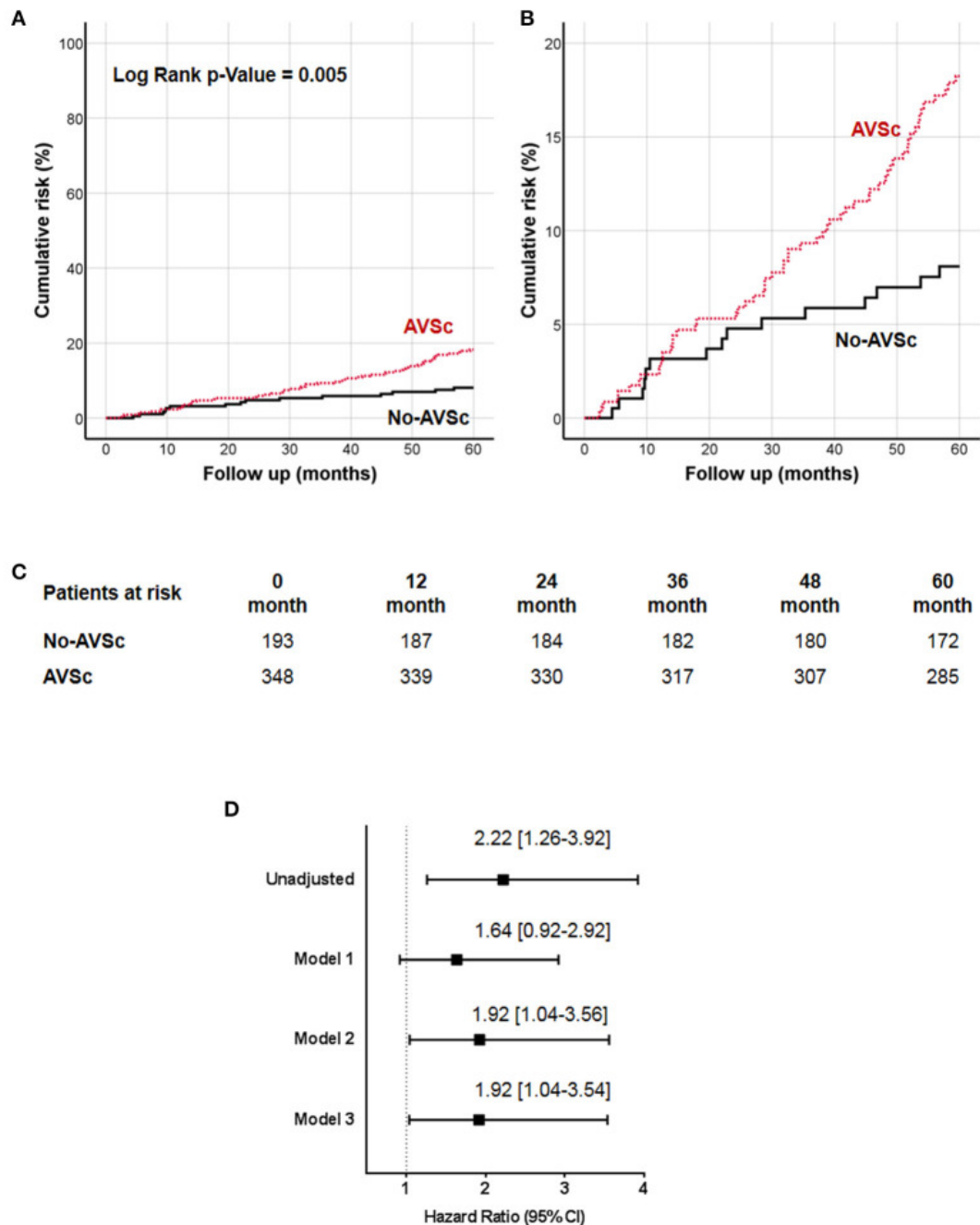


Figure 3.4. Cumulative incidence curves for 5-year all-cause mortality. (A) All-cause mortality was compared between CEA patients with (red dash line) and without (black solid line) aortic valve sclerosis (AVSc). (B) Inset of (A) to better evidence the differences between the two groups. (C) Breakdown of

the patients at risk per year in the two groups. **(D)** Cox regression analysis showing the hazard ratio (HR) unadjusted and adjusted for age (Model 1), for age and estimated glomerular filtration rate (eGFR; Model 2), and for age, eGFR, and left ventricular ejection fraction (LVEF; Model 3).

3.2.4 All carotid plaque types are associated with AVSc

To better understand the prediction capabilities of AVSc presence, we stratified our patients based on plaque-type: soft, calcified, and mixed/fibrotic. We did not find any difference in AVSc prevalence between soft (59.1%), calcified (69.2%), and mixed/fibrotic (65.7%) plaque. **Supplemental Table 5** in **Supplemental Appendix** shows patient baseline characteristics with different plaque types. In all the three groups, patients with AVSc were significantly older than patients without AVSc (all $p < 0.01$). The presence of diabetes was significantly higher in patients with calcified and mixed/fibrotic carotid plaque in patients without AVSc compared to patients with AVSc (all $p < 0.05$). In patients with mixed/fibrotic plaque, patients with AVSc presented lower eGFR levels compared to patients without AVSc (66 ± 17 vs 73 ± 20 , respectively; $p = 0.008$). However, multivariate analysis revealed that only old age was independently associated with AVSc in all examined groups (**Supplemental Table 6** in **Supplemental Appendix**).

3.2.4 AVSc is associated with all-cause mortality in CEA patients with mixed/fibrotic plaques

We examined the impact of different plaque types on all-cause mortality (**Supplemental Table 7**), and we found that low eGFR was associated with higher all-cause mortality in all three groups, while AVSc was correlated with higher mortality only in the mixed/fibrotic plaque group. Since our work was focused on AVSc, multivariate analysis was performed only for a mixed/fibrotic plaque group. The analysis highlighted that low eGFR ($p = 0.02$) and AVSc ($p = 0.01$) were independent predictor of all-cause mortality in patients with mixed/fibrotic plaque. The five-year all-cause mortality rate in patients with AVSc and mixed/fibrotic plaque was 15.5% compared to 2.4% in patients without AVSc ($p < 0.001$). The survival analysis showed a strong association between the presence of mixed/fibrotic plaque and AVSc in CEA patients and mortality at five years (log-rank $p = 0.005$; **Figure 3.5A**) better evidenced by the inset depicted in **Figure 3.5B**, while **Figure 3.5C** shows the breakdown of the patients at risk per year in the two groups. **Figure 3.5B** shows the unadjusted hazard ratio (HR) for all-cause mortality of patients with AVSc and the HR adjusted for

baseline demographic and clinical characteristics. In particular, after adjustment for age as well as cardiac and renal function, AVSc was still an independent predictor of long-term mortality (HR: 12.83, 95% CI: 1.71-96.35; $p = 0.013$). Finally, we assess the predictive ability of eGFR and AVSc, separately and in their combination. ROC curve analyses are reported in **Figure 3.6**. In particular, the combination of eGFR and AVSc showed a good predictive ability for 5-year all-cause mortality in patients with mixed/fibrotic plaque with an AUC of 0.77 (95% CI: 0.76-0.79), a sensitivity of 0.88 (95% CI: 0.86-0.90), and a negative predictive value of 0.84 (95% CI: 0.82-0.86).

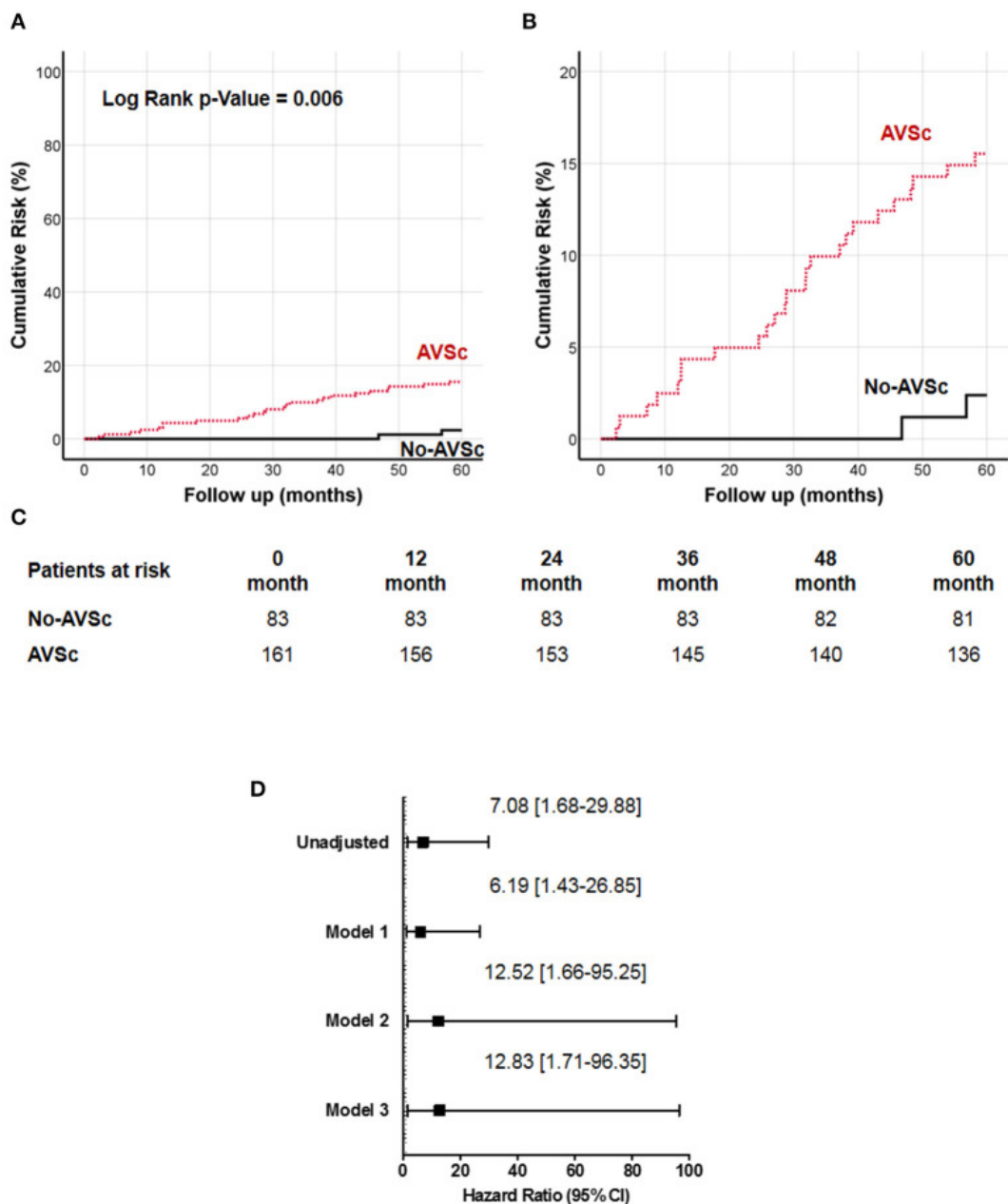


Figure 3.5. Cumulative incidence curves for 5-year all-cause mortality in patients with 12 mixed/fibrotic carotid plaque. (A) All-cause mortality was compared between CEA patients with (red

dash line) and without (black solid line) aortic valve sclerosis (AVSc). **(B)** Inset of **(A)** to better evidence the differences between the two groups. **(C)** Breakdown of the patients at risk per year in the two groups. **(D)** Cox regression analysis showing the hazard ratio (HR) unadjusted and adjusted for age (Model 1), for age and estimated glomerular filtration rate (eGFR; Model 2), and for age, eGFR, and left ventricular ejection fraction (LVEF; Model 3).

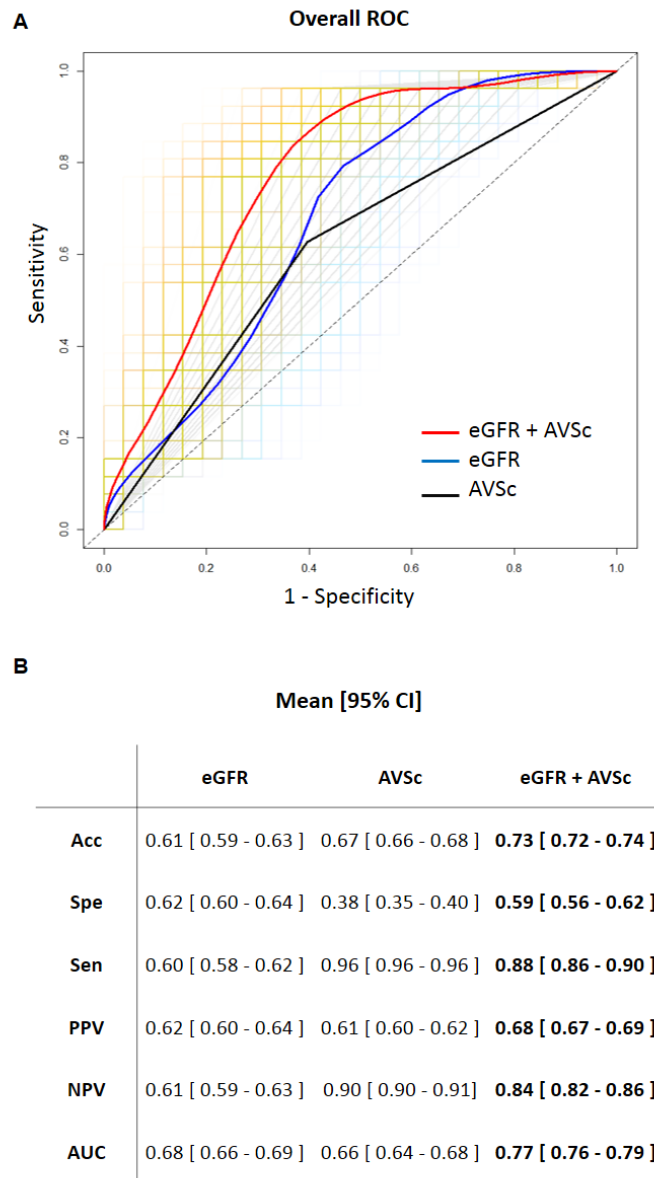


Figure 3.6. Predictive ability of eGFR and AVSc for the 5-year all-cause mortality in patients 18 with mixed/fibrotic plaque. **(A)** The average performance of the three logistic models are shown 19 as ROC curves, where the predictors are aortic valve sclerosis (AVSc; black line), estimated 20 glomerular filtration rate (eGFR; blue line), and the combination of AVSc and eGFR (red line). The 21 grids represent the 1000 bootstrap iterations (ROC curves) plotted for AVSc (gray), eGFR (light 22 blue), and the combination of AVSc and eGFR (red). **(B)** Classification accuracy (Acc), specificity 23 (Spe), sensitivity (Sen), positive predicted value (PPV), negative predicted value (NPV), and area 24 under the ROC curve (AUC) are summarized as mean and 95% CI for each model took into account.

3.3 Systemic and valvular oxidative stress in calcific aortic valve disease

3.3.1 Patient population and characteristics

Fifty-eight patients that underwent coronary artery bypass grafting (CABG) were enrolled in the study between January and June 2011. Inclusion and exclusion criteria were previously described in **Material and Methods** section, with the addition of the presence of bicuspid aortic valve morphology in the inclusion criteria for this study. The isolated CABG population included 58 patients. Their demographic, laboratory and clinical features are listed in **Supplemented Table 8**. Fifty percent of patients (n = 29) had normal aortic valve morphology (No-AVSc group), while the remaining 50% (n = 29) was classified as aortic valve sclerosis morphology (AVSc group). The two groups were comparable for all studied variables, including age, hypertension, dyslipidaemia, diabetes mellitus, smoking habits, body mass index, NYHA class, the severity of coronary artery disease, echocardiographic parameters and pharmacological treatments. In addition, the two groups also had comparable pre-operative C-reactive protein (CRP) levels.

3.3.2 Systemic oxidative stress and endothelial dysfunction

To evaluate systemic glutathione homeostasis, we measured the circulating levels of GSH and GSSG. Pre-operatively, GSSG/GSH ratio was significantly higher in AVSc patient's group (0.070 ± 0.007) than No-AVSc patients (0.047 ± 0.004 ; $p = 0.006$, **Figure 3.7A**). To assess endothelial dysfunction, we measured ADMA levels. Pre-operatively, ADMA concentration was significantly higher in AVSc patients ($0.47 \pm 0.009 \mu\text{M}$) compared to No-AVSc patients ($0.39 \pm 0.007 \mu\text{M}$; $p < 0.0001$, **Figure 3.7B**).

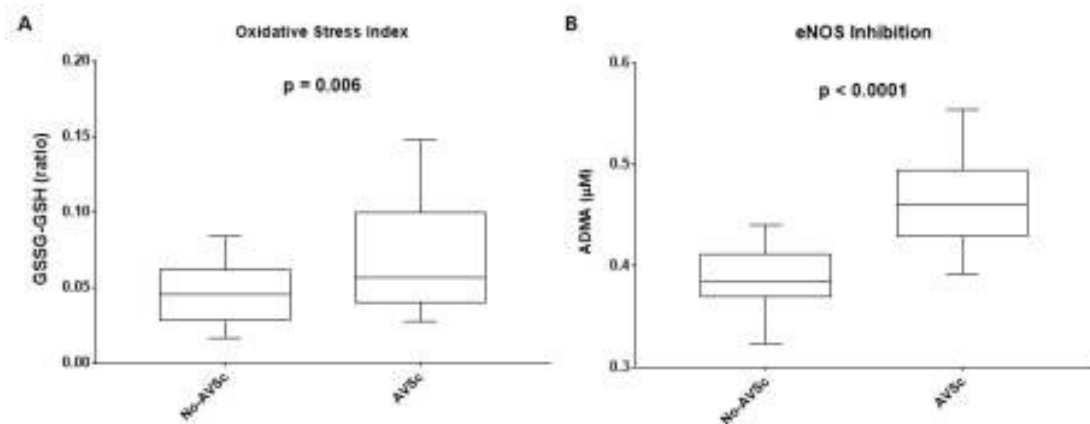


Figure 3.7. Imbalance of systemic glutathione homeostasis and endothelial dysfunction. (A) Box plot representing the ratio between the reduced (GSH) and the oxidized (GSSG) forms of glutathione in patients with normal aortic valve leaflet (No-AVSc; n = 29) and aortic valve sclerosis (AVSc; n = 29). (B) Box plot representing ADMA levels in patients with No-AVSc (n = 29) and AVSc (n = 29).

3.3.3 Systemic inflammation status

Since CRP pre-operative levels were similar between the two groups (No-AVSc = 2.01 ± 0.25 and AVSc = 2.31 ± 0.33), we considered CRP levels at other subsequent time points (at 3rd-day post-intervention, at 5th-day post-intervention and at discharge). We found that at 3rd-day after the intervention, CRP levels were significantly higher (+30.7, 95%CI: +3.9, +57.5; $p = 0.02$) in AVSc patients compared to No-AVSc ones (**Figure 3.8**), indicating a possible different burst of inflammation caused by the intervention in these two groups. However, at 5th-day after the intervention and at discharge the levels between the two groups were comparable (**Figure 3.8**).

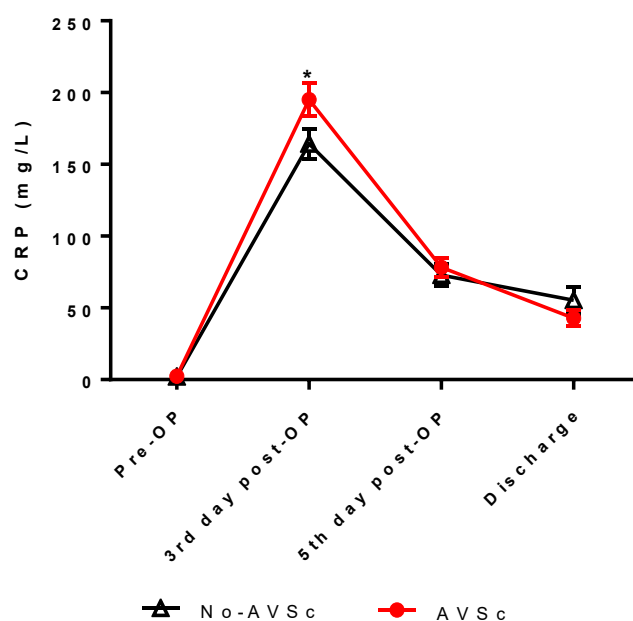


Figure 3.8. Systemic inflammation status. Graph representing C-reactive protein (CRP) levels measured in clinical routine preoperatively, at 3rd-day post-surgery, at 5th-day post-surgery, and at discharge. Black line denotes patients with normal aortic valve leaflets (No-AVSc; n = 29), while red line denotes patients with increase aortic valve leaflet thickness (AVSc; n = 29). * p < 0.05. No-AVSc: patients with a normal aortic valve leaflets. AVSc: patient with aortic valve sclerosis.

3.3.4 Aortic valve protein S-glutathionylation in AVSc patients

The systemic imbalance of glutathione homeostasis could also reflect a confined alteration leading to aberrant protein glutathionylation (Pr-SSG) in loco (i.e., in aortic valve leaflets). We evaluated this reversible post-translational modification in aortic valve whole protein extracts from patients that underwent concomitant CABG and aortic valve replacement (AVR) due to aortic valve insufficiency. Three specimens had normal morphology (No-AVSc), while six had AVSc. Dot-blot analysis revealed that AVSc specimens had significantly increased Pr-SSG levels ($+6.5 \pm 1.5$) than No-AVSc (p = 0.01, **Figure 3.9A, B**). In addition, immunohistochemistry revealed that protein glutathionylation occurred in valve endothelial cells of both groups (No-AVSc and AVSc), while in valve interstitial cells Pr-SSG was present only in AVSc group was present only in AVSc group (**Figure 3.9C** and **Figure 3.10**).

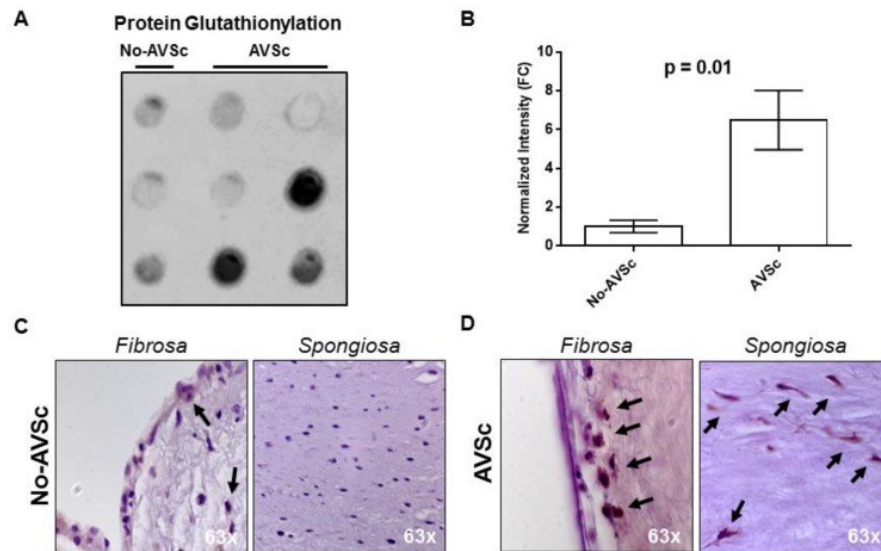


Figure 3.9. Aortic valve protein S-glutathionylation. (A) Dot-blot evaluation of total glutathione (GSH) expression in aortic valve leaflets (No-AVSc $n = 3$; AVSc $n = 6$) and relative quantification showed in the bar graph (graph (dot-blot analyses using ImageJ; plugin: Dot-blot Analyzer v1.0). (C-D) Representative images showing histological analysis of human aortic valve in *Fibrosa* and *Spongiosa* layers. No-AVSc: patients with a normal aortic valve leaflets. AVSc: patient with aortic valve sclerosis. Black arrows indicate positive cells for GSH staining.

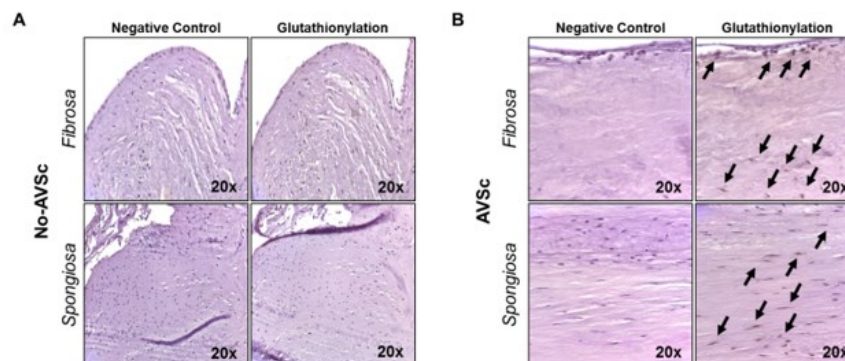


Figure 3.10. Protein S-glutathionylation in aortic valve leaflets. (A-B) Immunohistochemistry showing glutathione (GSH) expression in *Fibrosa* and *Spongiosa* layers of the aortic valve (A) in patients with normal aortic valve leaflets (No-AVSc) and (B) in patients with increased aortic valve leaflets thickness (AVSc). Black arrows indicate positive cells for GSH staining.

3.3.5 Increased ROS emission and protein S-glutathionylation mark the transition from sclerosis to stenosis in human aortic valves.

Oxidative stress may herald CAVS onset and progression⁸⁰. However, no data are available regarding specific quantification of ROS emission from human aortic valve leaflets at different disease stages. To fill this gap in our knowledge, we tackled these questions using an electron paramagnetic resonance (EPR) approach that is the only

method for the direct detection of paramagnetic species, such as ROS. We employed this approach in aortic valve specimens obtained from three different patients' populations, *i.e.*, control subjects and patients with aortic sclerosis or aortic stenosis (see patients' enrollment description). A one-way ANOVA analysis revealed significant differences between the three groups (ANOVA $p = 0.01$; p -trend = 0.003). In detail, ROS levels in specimens from aortic sclerosis patients (72.0 ± 18.7 AU) were not statistically significant either from those observed in control or aortic stenosis specimens. However, aortic stenosis samples displayed a striking rise in ROS levels over controls (147.1 ± 41.3 AU vs. 21.0 ± 4.3 AU, respectively; $p = 0.007$; **Figure 3.11A, B, C**), thus attesting that an increment in valve ROS emission accompanies human CAVS disease progression.

Next, we tested whether protein S-glutathionylation (P-SSG) parallels this escalation in valve ROS emission, likely affecting aortic valve tissue biology and function. To this end, we measured P-SSG levels in whole tissue extracts that include proteins from both interstitial and endothelial valve cell types (*i.e.*, VICs and VECs). Using a Western blot analysis, we found significant differences between the three groups (ANOVA $p < 0.05$). More specifically, specimens from patients with aortic sclerosis harbored slightly but not significantly higher P-SSG levels as compared to controls ($\log_2FC = +1.1 \pm 0.3$; $p = 0.11$). Conversely, aortic samples from patients suffering from aortic stenosis had significantly more elevated P-SSG levels than control subjects ($\log_2FC = +1.5 \pm 0.4$; $p = 0.04$; **Figure 3.11D, E**). Of note, sclerotic samples did not differ from stenotic ones. This set of data suggests P-SSG as a new possible signature of aortic valve disease progression towards stenosis.

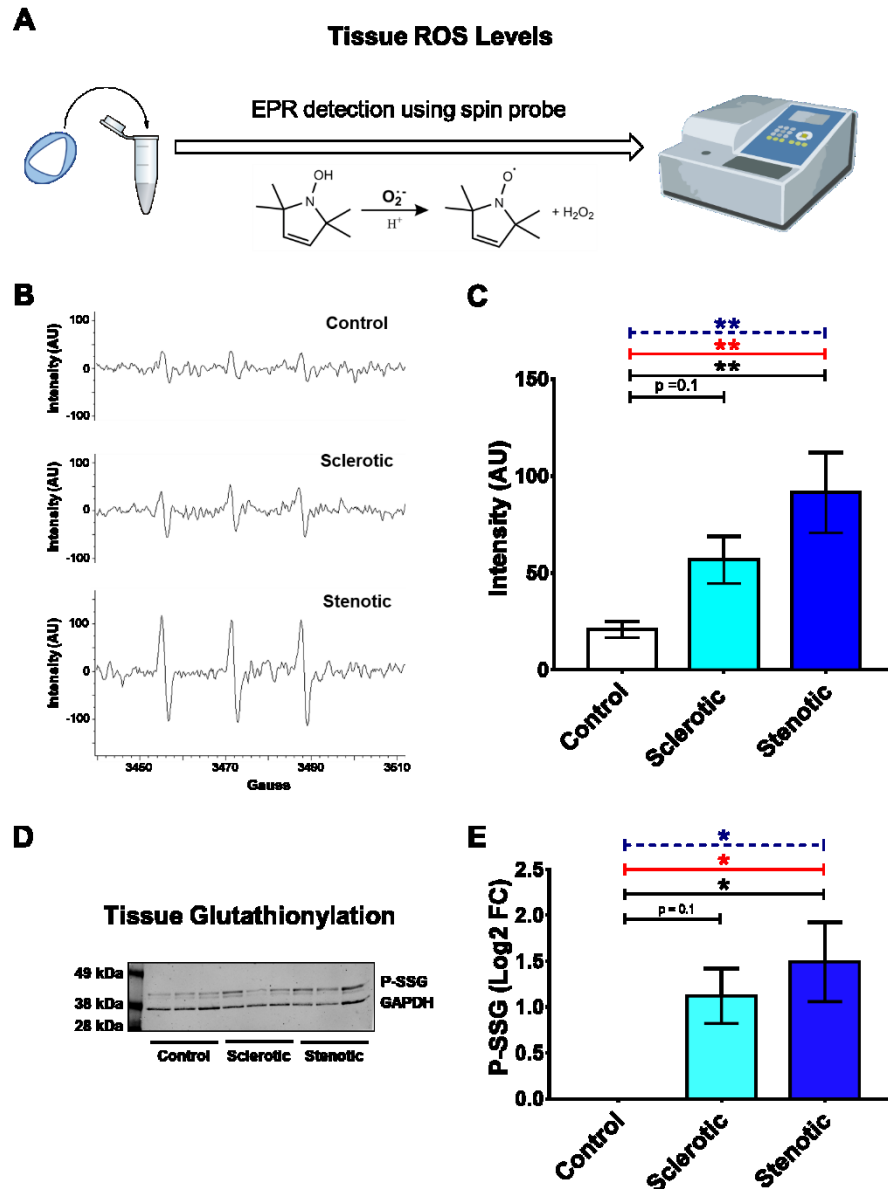


Figure 3.11. ROS levels and protein S-glutathionylation during calcific aortic valve stenosis progression. (A) Scheme showing Electron Paramagnetic Resonance (EPR) performed using a spin probe that reacts with extra- and intracellular oxygen free radicals to generate the detectable EPR. (B) EPR representative spectra for Control, Sclerotic, and Stenotic tissue samples. (C) Bar graph representing EPR quantification. (Control = 11; Sclerotic = 11; Stenotic = 12) (D) Western blot representative images of protein S-glutathionylation (P-SSG) in whole extracts of aortic valve leaflets at different stages of the pathology. (E) Bar graph representing Western blot relative quantification by ImageJ. (Control = 3; Sclerotic = 5; Stenotic = 4) ** $p \leq 0.01$; * $p < 0.05$; blue dashed line: Test for trend; red line: ANOVA; black line: Tukey post-test.

3.4 Protein S-glutathionylation and valve endothelial cells

3.4.1 *In vitro* model of oxidative stress and protein S-glutathionylation in HUVEC

To study the effects of aberrant Pr-SSG as a trigger of endothelial damage, we implemented an *in vitro* model using HUVEC. As shown in **Figure 3.12A**, both 2-AAPA concentrations were able to drastically reduce the GSH/GSSG ratio ($p < 0.05$). As expected, the drop in GSH/GSSG ratio led to a significant increment of Pr-SSG. In particular, we noticed an increment of Pr-SSG by $+2.3 \pm 0.6$ fold change (2-AAPA 50 μM) and by $+2.1 \pm 0.5$ fold change (2-AAPA 100 μM) when compared to untreated cells or DMSO controls ($p < 0.001$, **Figure 3.12B**). Interestingly, the glutathionylated bands were at the same molecular weight of β -actin. Indeed, immunoprecipitation confirmed that β -actin was actually the protein that underwent glutathionylation (Supplemental Figure S3). In addition, we noticed that 2-AAPA, at both concentrations, induced the phosphorylation of histone 2AX (γH2AX), indicating DNA double-strand breaks (**Figure 3.12C**).

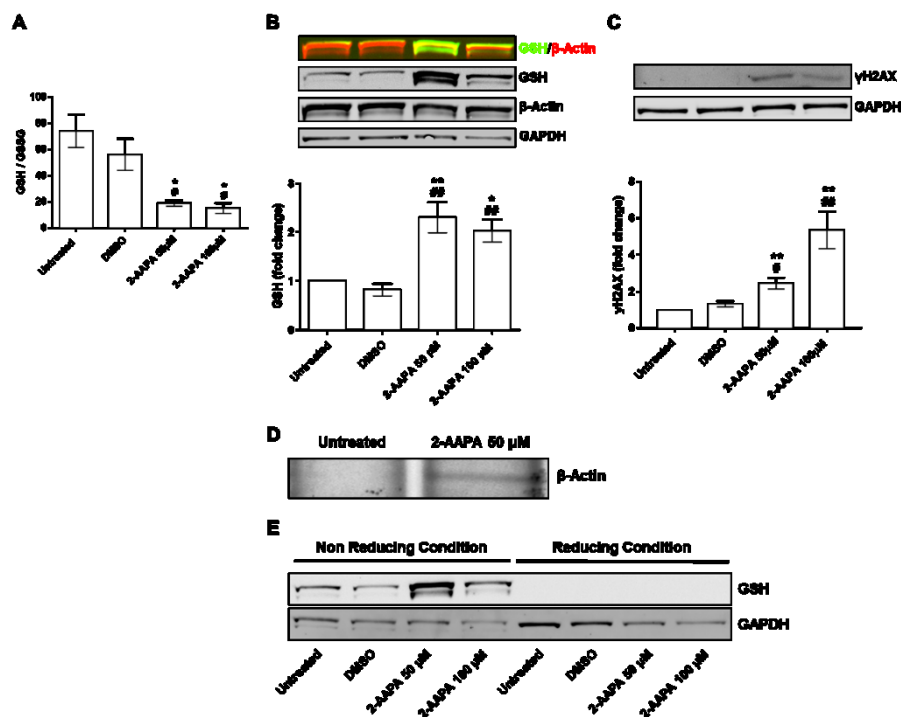


Figure 3.12. *In vitro* model of protein S-glutathionylation. (A) Bar graph representing the ratio between the reduced (GSH) and the oxidized (GSSG) form of glutathione (GSH/GSSG ratio) in human umbilical vein endothelial cells (HUVEC) after 4 h of treatment (2-AAPA 50 and 100 μM) and 24 h of recovery ($n = 3$). (B) Western blot representative images of HUVEC treated with 2-AAPA (50 and 100 μM) for 4 h and 24 h of recovery ($n = 4$); GSH is shown in green and β -actin is shown in red; Bar graph

representing Western blot quantification by ImageJ. (* $p < 0.05$ vs. Untreated; ** $p < 0.001$ vs. Untreated; ## $p < 0.001$ vs. Dimethyl Sulfoxide (DMSO)). (C) Western blot evaluation of histone 2AX phosphorylation (γ H2AX) in HUVEC after 2-AAPA (50 and 100 μ M) treatment for 4 h and 24 h of recovery ($n = 4$); Bar graph representing Western blot quantification by ImageJ. (** $p < 0.001$ vs. Untreated; # $p < 0.05$ vs. DMSO; ## $p < 0.01$ vs. DMSO). Glyceraldehyde-3-Phosphate Dehydrogenase (GAPDH) has been used for normalization. (D) Immunoprecipitation of glutathione (GSH) and Western blot for β -actin in HUVEC treated with 2-AAPA 50 μ M for 4 hours and 24 hours of recovery. (E) Western blot showing GSH in non-reducing and in reducing conditions in HUVEC untreated, treated with DMSO, 2-AAPA 50 μ M, and 2-AAPA 100 μ M.

3.4.2 Protein S-glutathionylation and endothelial-to-mesenchymal transition in HUVEC

To evaluate the involvement of Pr-SSG in endothelial-to mesenchymal transition (EndMT) we treated the HUVECs with the minimum dose of 2-AAPA that caused Pr-SSG and DNA damage (50 μ M). We, therefore, assessed endothelial specific genes, such as platelet and endothelial cell adhesion molecule 1 (PECAM1) and cadherin 5 (CDH5) and activated fibroblast specific gene, such as alpha-smooth muscle actin 2 (ACTA2). First, we checked for the best housekeeping gene in our experimental conditions with the implementation of four different algorithms. The comprehensive gene stability analysis allowed us to recognize glyceraldehyde-3-phosphate dehydrogenase (GAPDH) as the most stable gene (**Figure 3.13**). Finally, as shown in **Figure 3.14**, we found significant downregulation of both PECAM1 and CDH5 and a significant upregulation of ACTA2 in HUVEC treated with 2-AAPA in comparison to untreated and DMSO treated cells (all $p < 0.001$).

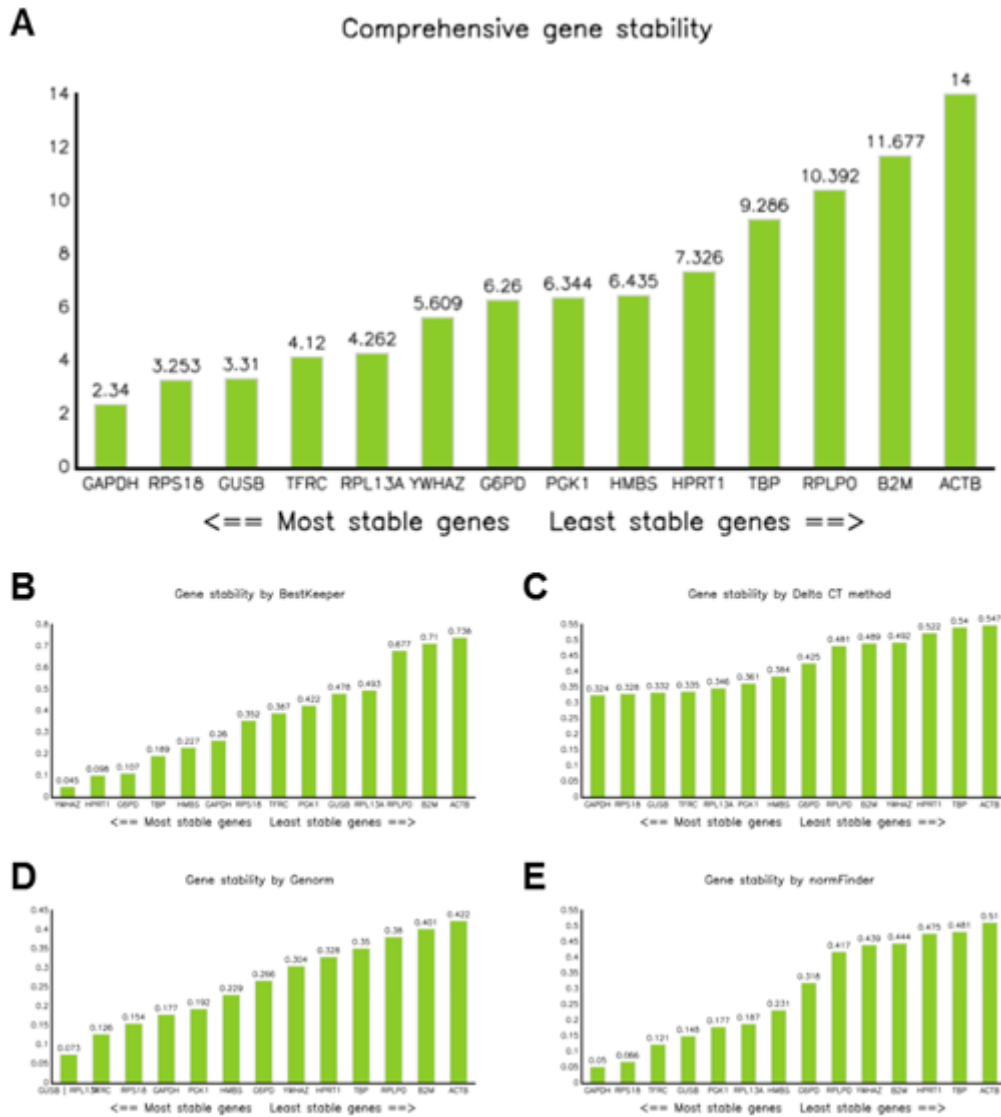


Figure 3.13. Comprehensive gene stability. (A) Histograms showing the evaluation of comprehensive gene stability comparing untreated vs. 2-AAPA 50 μ M cells (n = 3) assessed by following different algorithm: (B) Bestkeeper; (C) Delta CT method; (D) Genorm; and (E) Normfinder.

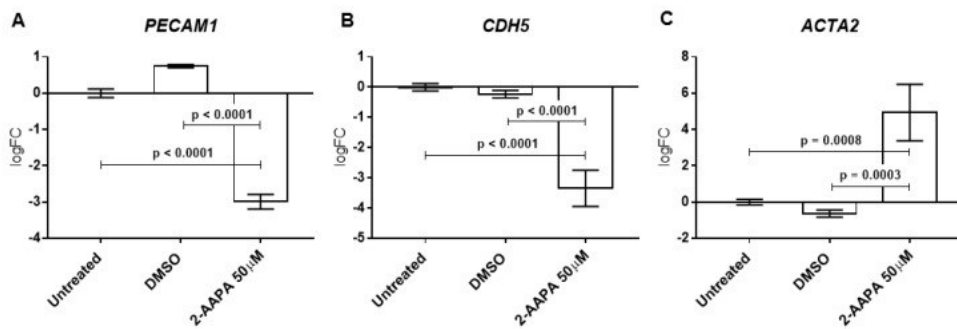


Figure 3.14. Protein S-glutathionylation and endothelial-to-mesenchymal transition. Quantitative Polymerase Chain Reaction (qPCR) of the gene encoding endothelial markers (A) CD31, (B) VE-

cadherin and mesenchymal marker (C) ACTA2 after 4h of 2-AAPA (50 μ M) treatment and 48h of recovery (n = 3). (n = 3). qPCR data are expressed as log₂ fold change (log₂FC) in comparison to untreated cells.

3.4.3 *Blocking glutathione reductase builds-up ROS emission and Protein S-glutathionylation in porcine valve endothelial cells*

To get mechanistic insights into P-SSG-induced changes in endothelial cells, we employed an *in vitro* model of aberrant aortic valve P-SSG using pVECs. To this end, we used 2-AAPA to disrupt cells' ability to detoxify ROS, leading to increased intracellular oxidative stress, thus enhancing the chance of P-SSG formation. **Figure 3.15** reveals that 2-AAPA treatment significantly augmented P-SSG levels (ANOVA p = 0.0005). More in detail, we observed that, compared to untreated and DMSO control conditions, 2-AAPA at 50 μ M led to a sizable increment in P-SSG (log₂FC = +4.8 \pm 1.5; p = 0.01). Moreover, consistent with previous studies³, the P-SSG positive bands had the same molecular weight as β -actin, which could result in an altered ratio between soluble and polymerized protein, leading to significant cell architecture perturbations⁴. We also noticed a marked rise in the phosphorylated form of the histone H2AX (γ H2AX; ANOVA p = 0.001; **Figure 3.16**), thus denoting the presence of foci of DNA repair due to double-strand breaks. This effect was dose-dependent (p-trend < 0.0001). Indeed, pVECs treated with different concentrations of 2-AAPA (50, 75, and 100 μ M) led to significant escalating γ H2AX levels when compared to untreated cells (log₂FC = +2.6 \pm 0.8; log₂FC = +2.6 \pm 0.7; log₂FC = +3.0 \pm 0.4, respectively; all p < 0.05). Since 50 μ M 2-AAPA was the minimum effective dose able to induce P-SSG and DNA damage, we next interrogated whether or not this concentration imbalanced VECs' redox status. To this end, we measured ROS production. As shown in **Figure 3.15C, D, e**, the cytofluorimetric analysis showed that 2-AAPA 50 μ M triggered a sizable ROS production compared to cells treated with DMSO (26.2 \pm 4.8 vs. 13.9 \pm 4.4 %, respectively; p = 0.04). Hand-in-hand with this finding, the MTT assay revealed that treating VECs with 50 μ M 2-AAPA abated cell viability drastically (ANOVA p < 0.001; **Figure 3.17**). Finally, we sought to determine whether adding N-acetyl-L-cysteine (NAC) would reduce/prevent the extent of this post-translational modification in pVECs. We found that NAC (2mM) supplementation, before and during 2-AAPA administration, substantially attenuated P-SSG deposition compared to 2-AAPA treatment alone (log₂FC = +1.97 \pm 1.0 vs.

+5.9±0.8, respectively; $p = 0.006$; **Figure 3.15 F, G**). We interpreted these findings to indicate that blocking glutathione reductase and thioredoxin activity, in VECs *via* 2-AAPA, is sufficient to build up P-SSG in a sizable and likely functionally relevant manner, as suggested by the above-reported decrement in VECs viability and mounting oxidative stress.

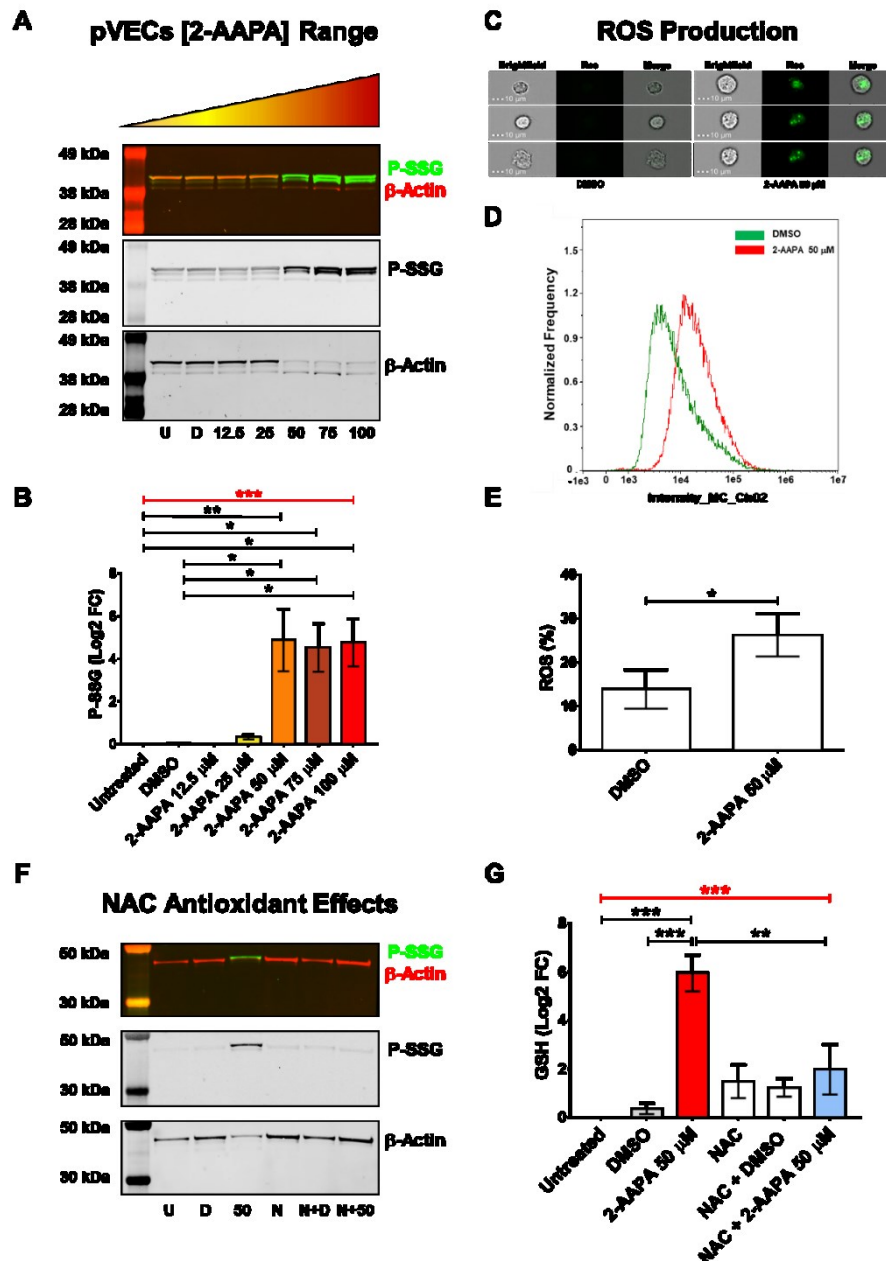


Figure 3.15. *In vitro* model of protein S-glutathionylation in porcine valve endothelial cells. (A) GSH and β-actin Western blot representative images of porcine aortic valve endothelial cells (pVEC) after 4 hours of treatment with DMSO and increasing concentrations of 2-AAPA and 24 hours of recovery. GSH is shown in green and β-actin is shown in red. (B) Bar graph of Western blot relative quantification performed with ImageJ (U = Untreated, n = 4; D = DMSO, n = 3; 12.5 = 2-AAPA 12.5 μM, n = 3; 25 = 2-AAPA 25 μM, n = 3; 50 = 2-AAPA 50 μM, n = 4; 75 = 2-AAPA 75 μM, n = 4; 100 = 2-AAPA 100 μM n = 4). (C-D) Image flow cytometry analysis of ROS levels in pVECs treated with DMSO and 2-AAPA 50 μM (40X). (E) Bar graph showing the percentage of pVECs positive cells after 2-AAPA 50 μM treatment and 24 hours of recovery (n = 3). (F) Western blot representative images of μ-actin S-glutathionylation when pVECs are treated with N-acetyl-L-cysteine (NAC) before and during 2-AAPA 50 μM treatment. GSH is shown in green and β-actin in red. (U = Untreated; D = DMSO; 50 = 2-AAPA 50 μM; N = NAC 2mM; N+D = NAC 2 mM + DMSO; N + 50 = NAC 2 mM + 2-AAPA

50 μM). (G) Bar graph representing Western blot relative quantification performed with ImageJ. *** $p \leq 0.001$; ** $p \leq 0.01$; * $p \leq 0.05$; dotted line: ANOVA; solid line: Tukey post-test ($n = 3$).

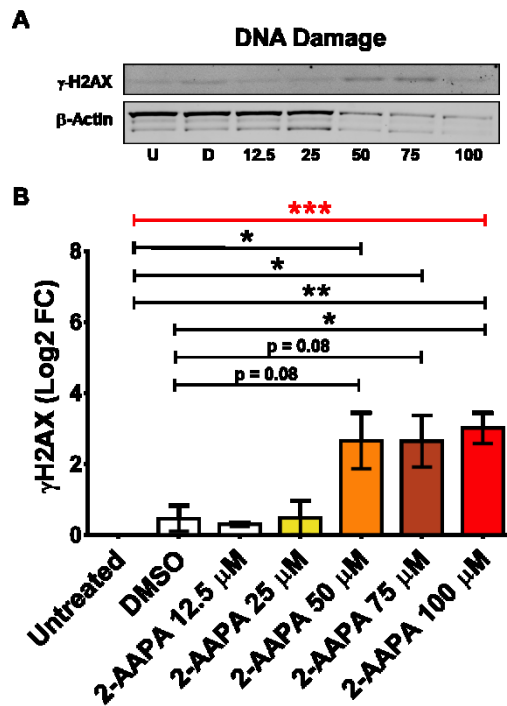


Figure 3.16. Effect of 2-AAPA on DNA damage in porcine valve endothelial cells.

(A) $\gamma\text{-H2AX}$ and $\beta\text{-actin}$ Western blot representative images of porcine aortic valve endothelial cells (pVEC) after 4 hours of treatment with increasing concentrations of 2-AAPA and 24 hours of recovery. (U = Untreated; D = DMSO; 12.5 = 2-AAPA 12.5 μM ; 25 = 2-AAPA 25 μM ; 50 = 2-AAPA 50 μM ; 75 = 2-AAPA 75 μM ; 100 = 2-AAPA 100 μM). (B) Bar graph of Western blot quantification performed with ImageJ ($n = 3$). *** $p \leq 0.001$; ** $p \leq 0.01$; * $p \leq 0.05$; blue dashed line: Test for trend; red line: ANOVA; black line: Tukey post-test.

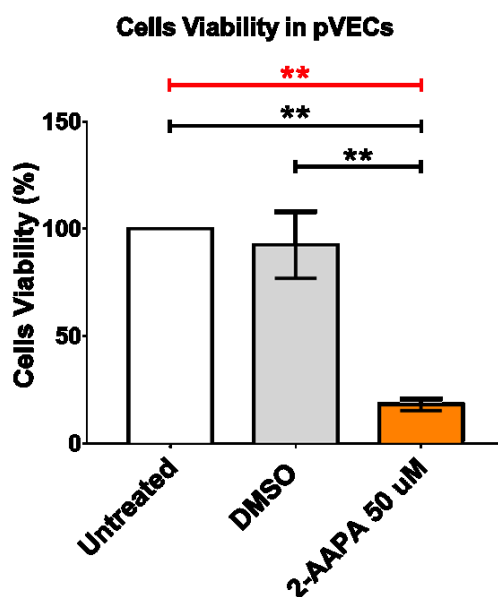


Figure 3.17. Effect of 2-AAPA treatment on porcine valve endothelial cells viability.

Bar graph showing percentage of porcine aortic valve endothelial cells (pVEC) viability after 4 hours of 2-AAPA 50 μ M treatment and 24 hours of recovery (n = 3). ** p \leq 0.01; red line: ANOVA; black line: Tukey post-test .

3.4.4 Human valve endothelial cells' resilience against oxidative stress during CAVS progression

Next, we interrogated whether changes in the GSH/GSSG ratio, a metric of oxidative stress in cells, occur in CAVS patients and if these alterations are stage-dependent in human CAVS due to progressive increments in P-SSG, as described above. We used a state-of-art methodology to monitor the GSH/GSSG ratio, such as liquid chromatography-tandem mass spectrometry (LC-MS/MS) ³. In control, healthy endothelial cells, this ratio typically ranges around 100^{5,6}. Intriguingly, we noticed a progressive rise in the GSH/GSSG ratio, escalating with the CAVS disease's worsening. First, group analysis revealed significant differences between the three groups (ANOVA p = 0.0003; **Figure 3.18A**) with an increment during CAVS progression (p-trend < 0.0001). Then, we found that sclerotic hVECs had a significantly higher GSH/GSSG ratio than control cells (211.3 \pm 16.8 vs. 65.3 \pm 17.2, respectively; p = 0.01). However, stenotic hVECs displayed the highest P-SSG content (306.4 \pm 50.0; p = 0.0002 vs. the control group). This evidence suggests that stenotic hVECs have higher GSH (*i.e.*, reduced glutathione) bioavailability compared to the sclerotic and control groups, hinting at the intriguing possibility that these stenotic hVECs are more protected against oxidative stress, thus less prone to P-SSG induction.

To test this hypothesis directly, we induced oxidative stress using 2-AAPA (50 μ M) treatment. In control hVECs, this oxidative challenge led to a drastic (85%) decrease in the GSH/GSSG ratio compared to untreated and DMSO conditions (ANOVA $p < 0.01$; **Figure 3.18B**). The same drastic drop was evident in sclerotic hVECs (ANOVA $p < 0.0001$) in which the ratio declined by 82% and 59% compared to untreated ($p < 0.0001$) and DMSO ($p = 0.0008$), respectively (**Figure 3.18C**). Conversely, in stenotic hVECs, we captured a less pronounced decline in the GSH/GSSG ratio after 2-AAPA treatment than in untreated stenotic ones (**Figure 3.18D**). We interpret these findings to indicate that, owing to a higher basal GSH/GSSG ratio (**Figure 3.18A**), the stenotic hVECs are more protected against further oxidative insults (**Figure 3.18E**).

Concerning P-SSG, we did not find any basal difference among hVECs at the three pathological stages considered ($p = 0.505$), but we noticed an increment in the induction of this post-translational modification after 2-AAPA treatment in all three hVECs groups (**Figure 3.19**). In particular, in control hVECs, P-SSG drastically increased after 2-AAPA treatment ($\log_2FC = +2.0 \pm 0.5$; $p < 0.01$) compared to untreated and DMSO-treated ones (**Figure 3.19A, B**). In sclerotic hVECs we noticed a similar P-SSG rise ($\log_2FC = +2.0 \pm 0.9$; $p < 0.01$; **Figure 3.19C, D**). Conversely, in stenotic hVECs, the P-SSG increment was less evident ($\log_2FC = 0.7 \pm 0.2$; $p < 0.05$; **Figure 3.19E, F**). To validate that stenotic hVECs are more resilient to oxidative stress than control and sclerotic cells, we tested the extent of 2-AAPA-induced cell apoptosis and viability. As shown in **Figure 3.20**, the 2-AAPA treatment induced apoptosis and decreased the survival rate in all three groups. However, this regimen increased Annexin V-detected apoptotic marker in control and sclerotic hVECs (**Figure 3.20B, C**) compared to DMSO (control hVECs = $+33.8 \pm 0.8$ % and sclerotic hVECs = $+38.9 \pm 0.9$ %, both $p < 0.0001$ vs DMSO treatment). Conversely, after 2-AAPA treatment, stenotic hVECs showed a lower percentage of annexin V positive cells compared to DMSO-treated ones ($+11.3 \pm 0.3$ %; $p < 0.0001$; **Figure 3.20D**) as well as vs. controls and sclerotic treated cells (**Figure 3.21A**). At the same time, control and sclerotic hVECs exhibited a drastic drop in viability rate vs. DMSO treated ones (control hVECs = -60.1 ± 14.4 % and sclerotic hVECs = -66.2 ± 1.3 %, $p < 0.05$ vs. DMSO and $p < 0.0001$ vs. DMSO respectively). While stenotic hVECs displayed a moderate viability reduction compared to DMSO (-44.0 ± 8.5 %, $p < 0.05$; **Figure 3.20G**) as well as vs. controls and sclerotic treated cells (**Figure 3.21B**). These data collectively suggest that those endothelial cells that survived during CAVS

progression over the years harnessed adaptive/compensatory mechanisms, such as boosted antioxidant systems, including the glutathione one.

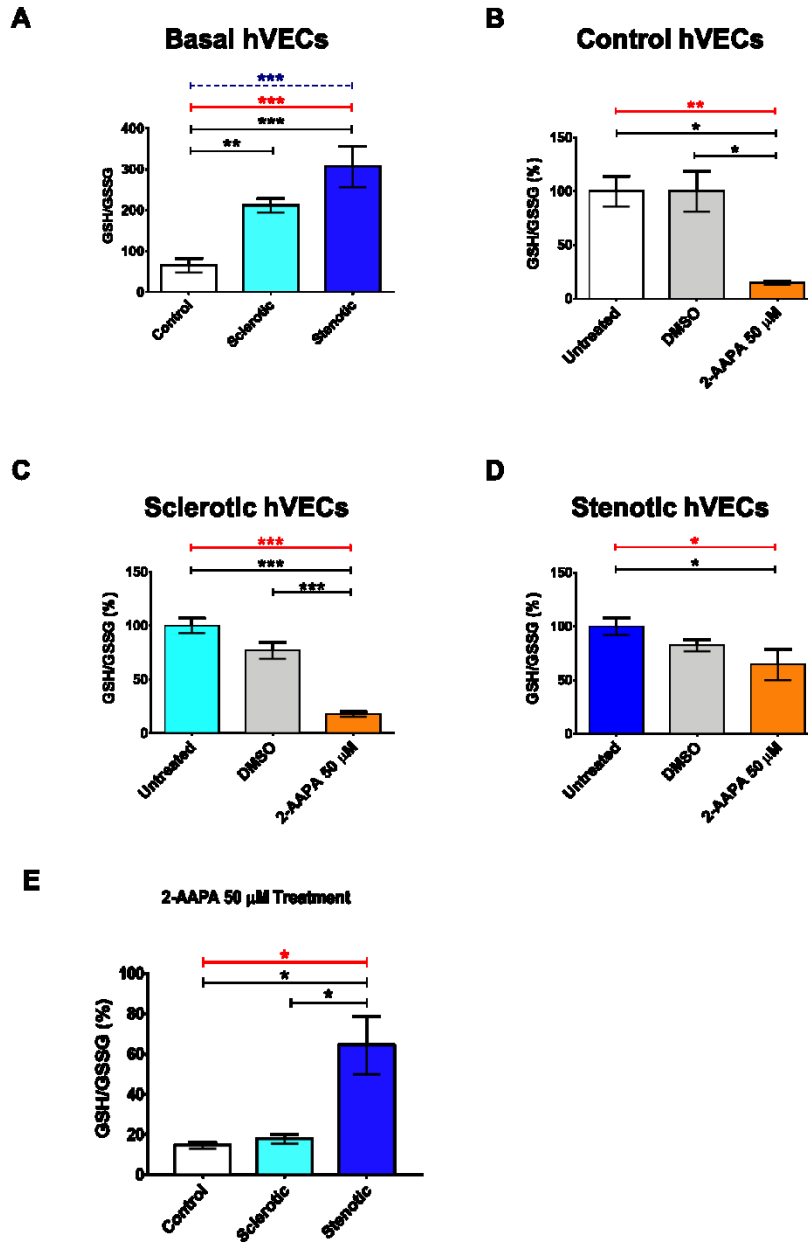


Figure 3.18. Imbalance of glutathione system during calcific aortic valve stenosis progression in human valve endothelial cells. (A) Bar graphs representing the ratio between reduced (GSH) and oxidized (GSSG) form of glutathione in human aortic valve endothelial cells (hVEC) at steady-state. (Control n = 6; Sclerotic n = 6; Stenotic n = 6) (B-C-D) Bar graph showing the percentage of GSH/GSSG ratio after 4 hours of DMSO or 2-AAPA 50 μ M and 24 hours of recovery in control, sclerotic, and stenotic hVECs (Untreated n = 6; DMSO n = 6; 2-AAPA 50 μ M n = 3). *** p \leq 0.001; ** p \leq 0.01; * p \leq 0.05; dashed line = Test for trend; dotted line: ANOVA; solid line: Tukey post-test. (E) Bar graph representing the comparison of the reduced (GSH) and oxidized (GSSG) form of glutathione, expressed as percentage GSH/GSSG ratio, in control, sclerotic, and stenotic human valve

endothelial cells after 4 hours of 2-AAPA 50 μM treatment and 24 hours of recovery. The untreated samples were used to calculate the ratio percentages. (n = 3). * $p \leq 0.05$; red line: ANOVA; black line: Tukey post-test.

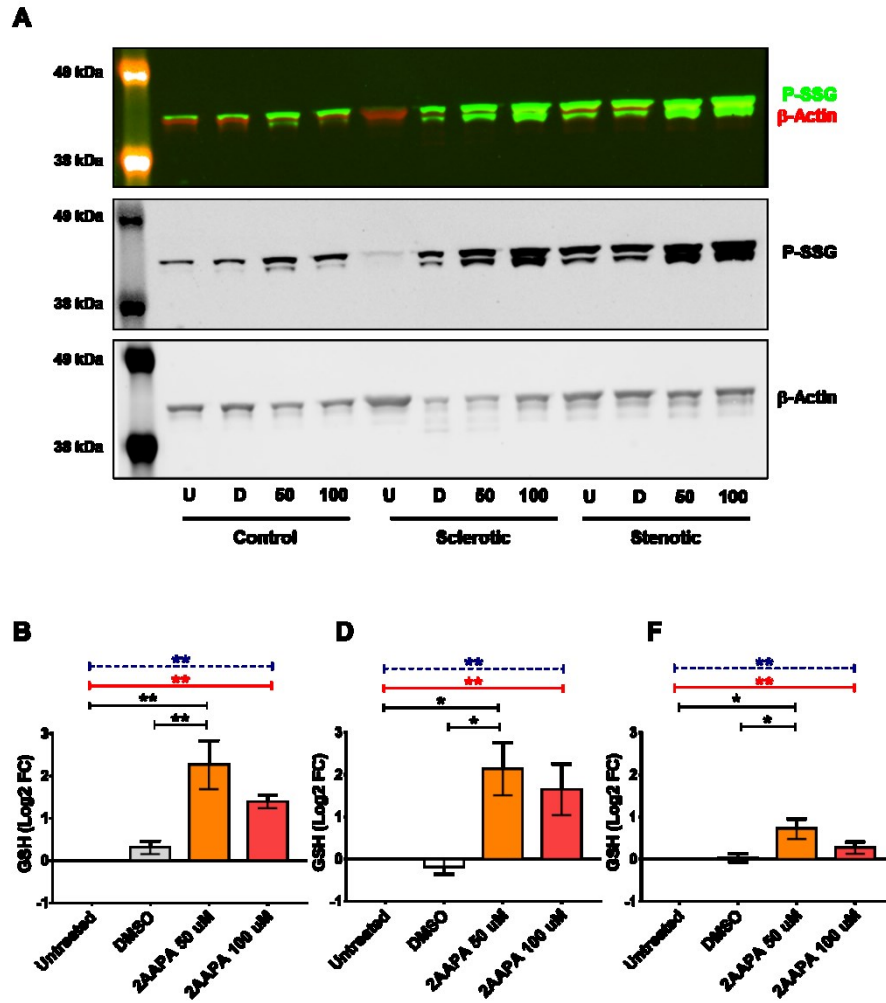


Figure 3.19. Human valve endothelial cells *in vitro* protein S-glutathionylation. (A-C-E) Western blot representative images of control, sclerotic, and stenotic human aortic valve endothelial cells (hVEC) after 4 hours of DMSO and 2-AAPA 50 μM treatment and 24 hours of recovery. (B-D-F) Bar graphs of Western blot relative quantification performed by ImageJ. (Control: Untreated n = 4; DMSO n = 4; 2-AAPA 50 μM n = 4; 2-AAPA 100 μM n = 3; Sclerotic: Untreated n = 5; DMSO n = 4; 2-AAPA 50 μM n = 5; 2-AAPA 100 μM n = 5; Stenotic: Untreated n = 5; DMSO n = 5; 2-AAPA 50 μM n = 5; 2-AAPA 100 μM n = 4). ** $p \leq 0.01$; * $p \leq 0.05$; dashed line = Test for trend; dotted line: ANOVA; solid line: Tukey post-test.

Apoptosis In hVECs

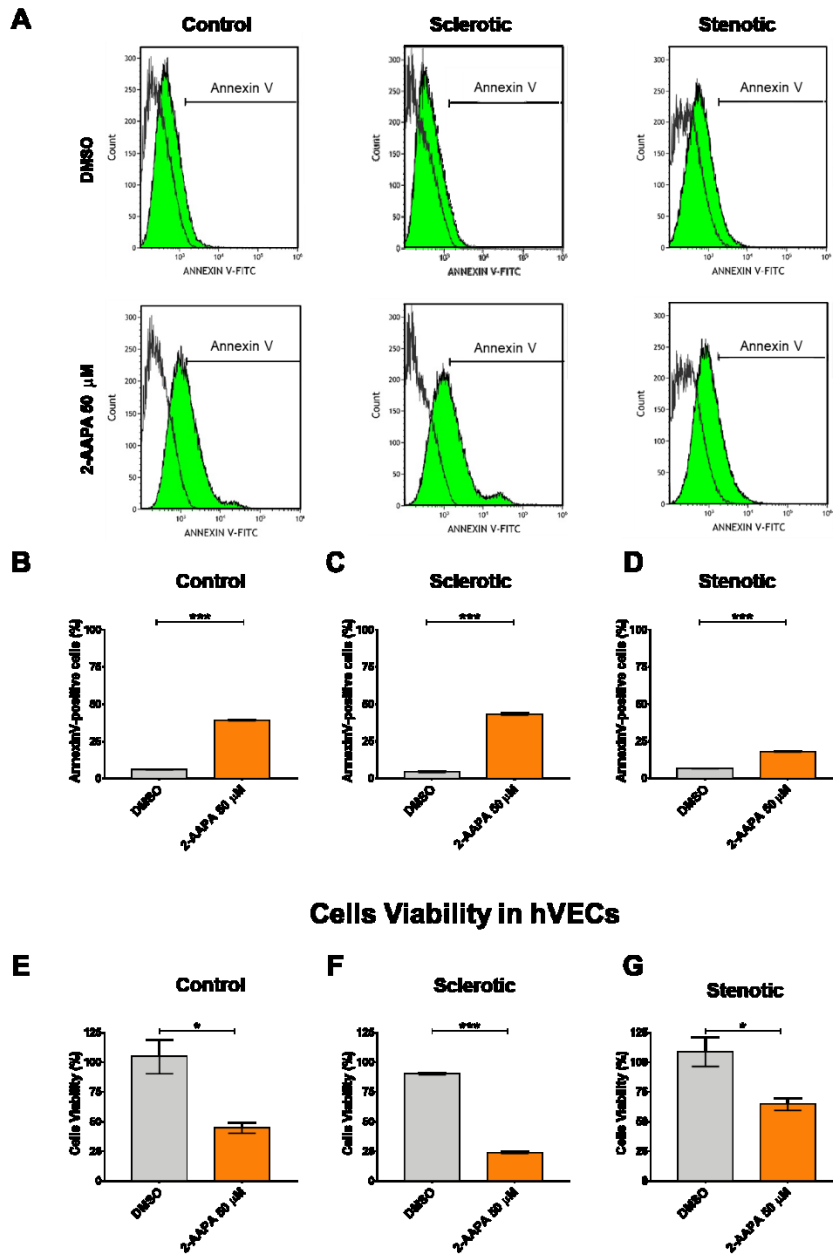


Figure 3.20. Glutathione imbalance effects on apoptosis and survival rate in human valve endothelial cells. (A) Flow cytometry representative analysis of Annexin V in control, sclerotic, and stenotic human valve endothelial cells (hVEC) after DMSO or 2-AAPA 50 μ M treatments and 24 hours of recovery. (Grey area: Annexin V positive cells). **(B-C-D)** Bar graphs showing Annexin V positive cells percentages after 4 hours of DMSO or 2-AAPA 50 μ M and 24 hours of recovery in control (DMSO n = 6; 2-AAPA 50 μ M n = 5), sclerotic (DMSO n = 6; 2-AAPA 50 μ M n = 6), and stenotic (DMSO n = 6; 2-AAPA 50 μ M n = 6) hVECs. **(E-F-G)** Bar graphs representing the percentage of cell viability after 4 hours of 2-AAPA 50 μ M and 24 hours of recovery in control (n = 3), sclerotic (n = 3) and **(G)** stenotic (n = 3) hVECs. * ≤ 0.05 ; *** $p \leq 0.001$.

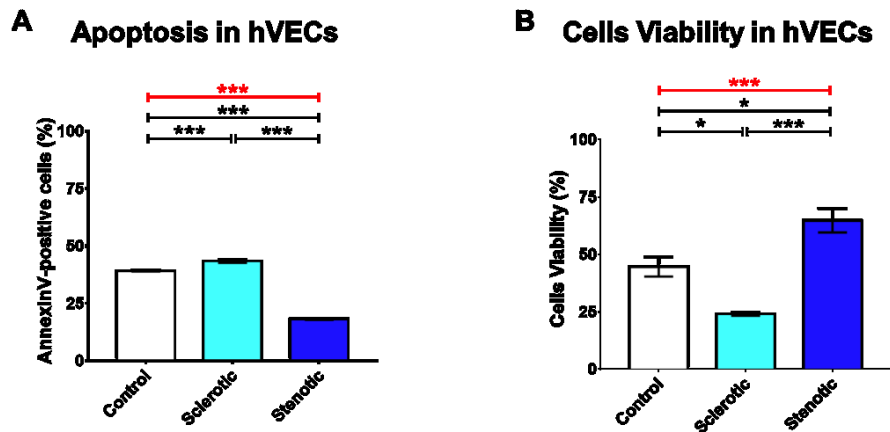


Figure 19. Apoptosis and survival rate after 2-AAPA treatment at different stages of CAVS. (A) Bar graph showing percentage of Annexin V positive cells in control (n = 6), sclerotic (n = 6), and stenotic (n = 6) human valve endothelial cells (hVEC) after 4 hours of 2-AAPA 50 μ M and 24 hours of recovery. The untreated samples were used as reference (100%) to calculate the ratio percentages. (B) Bar graph showing percentage of cells viability in control (n = 3), sclerotic (n = 3), and stenotic (n = 3) hVECs after 4 hours of 2-AAPA 50 μ M and 24 hours of recovery. *** p \leq 0.001; * p \leq 0.05; red line: ANOVA; black line: Tukey post-test.

3.4.5 Protein S-glutathionylation favors endothelial morphological/functional changes in hVECs

The above-reported findings suggest that, despite an acquired resistance against oxidative stress, hVECs undergo a profound structural (and likely functional) remodeling during CAVS progression. Therefore, using an immunofluorescent staining approach, we started dissecting possible mechanisms underlying these alterations. First, we observed that hVECs had the classical actin filament configuration under basal conditions (**Figure 3.22** top and middle panels). In particular, in the 2D monolayer configuration, actin filaments were arranged below the plasma membrane thus identifying the cortical actin and in the cytoplasm¹⁴². However, after 2-AAPA treatments, besides a P-SSG deposition rise, we noticed salient morphological changes (**Figure 3.22** lower panels). Namely, the cytoskeleton was de-structured with a predominant colocalization between glutathione and β -actin filaments, suggesting β -actin S-glutathionylation (negative staining control are in **Figure 3.23**). Correspondingly, we found a significant fall in a specific endothelial marker, CD31 (log2FC = -1.6 \pm 0.3; ANOVA p < 0.0001; **Figure 3.22B, C**). This fact suggests the loss of cell-cell junction and adhesion. Concomitantly, we found a significant increment in metalloproteinase type 2 (MMP2) active form (C-MMP2

$\log_2FC = +0.53 \pm 0.2$; ANOVA $p = 0.02$; **Figure 3.22B, E**). Since MMPs could directly influence cell surface proteins' expression¹⁴³, the latter finding may help explain the loss of CD31. In aggregate, these data indicate that the P-SSG induction is conducive to morphological and functional changes.

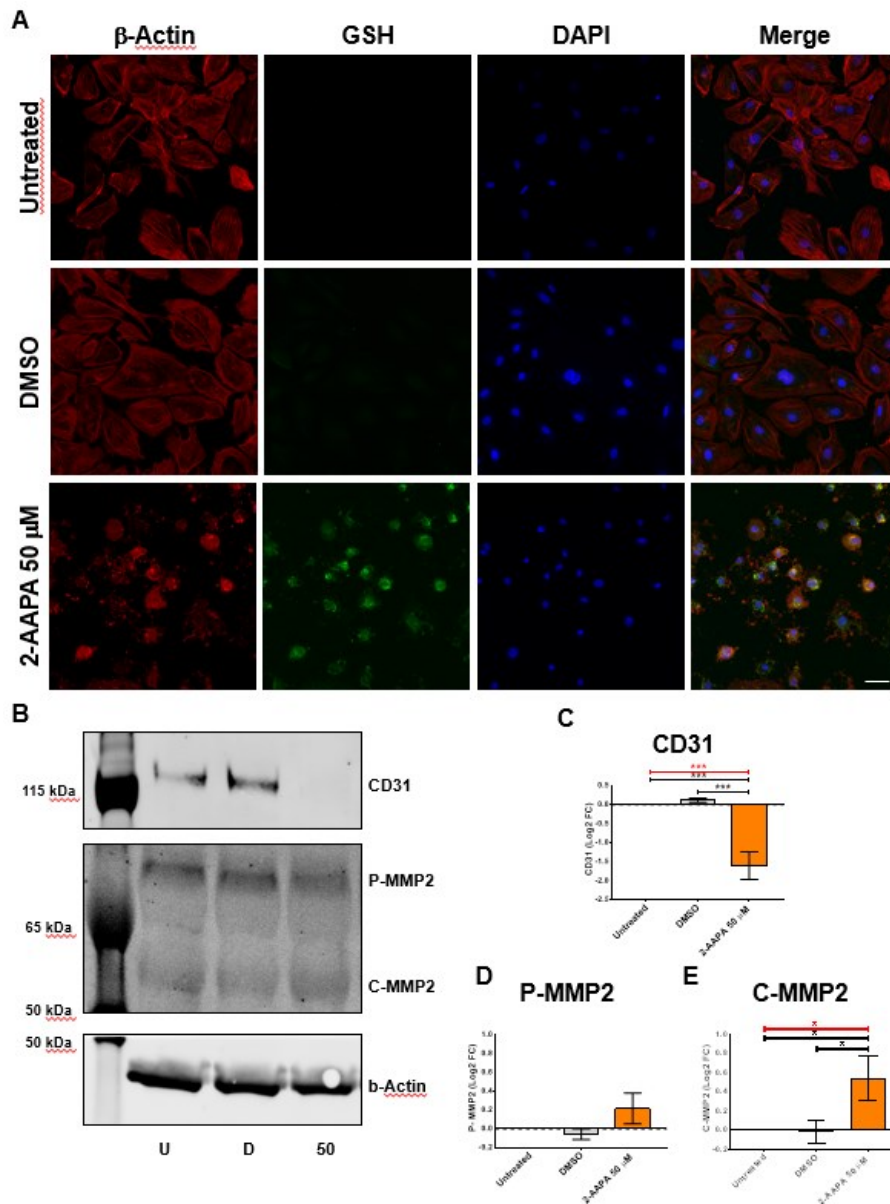


Figure 3.22. Morphological and protein expression changes in stenotic human valve endothelial cells under oxidative stress conditions. (A) Immunofluorescent staining representing GSH (green) and β -actin filaments (red) arrangement in stenotic human aortic valve endothelial cells (hVEC) at steady-state and after 4 hours of treatment with DMSO or 2-AAPA 50 μ M and 24 hours of recovery. Cell nuclei were visualized with DAPI (blue). Scale bar: 50 μ M. (B) Western blot representative images of stenotic hVECs after 4 hours of 2-AAPA 50 μ M treatment and 24 hours of recovery. Antibodies against CD31, MMP2, α SMA, and β -Actin were used. P-MMP2: pro-MMP2; C-MMP2: cleaved-MMP2. (C) Bar graphs of Western blot relative quantification performed by ImageJ (CD31: Untreated n = 11; DMSO n = 9; 2-AAPA 50 μ M n = 11; P-MMP2 Untreated n = 8; DMSO n = 7; 2-AAPA 50 μ M n = 8; C-MMP2 Untreated n = 8; DMSO n = 8; 2-AAPA 50 μ M n = 8). *** $p \leq 0.001$ * $p \leq 0.05$; dotted line: ANOVA; solid line: Tukey post-test.

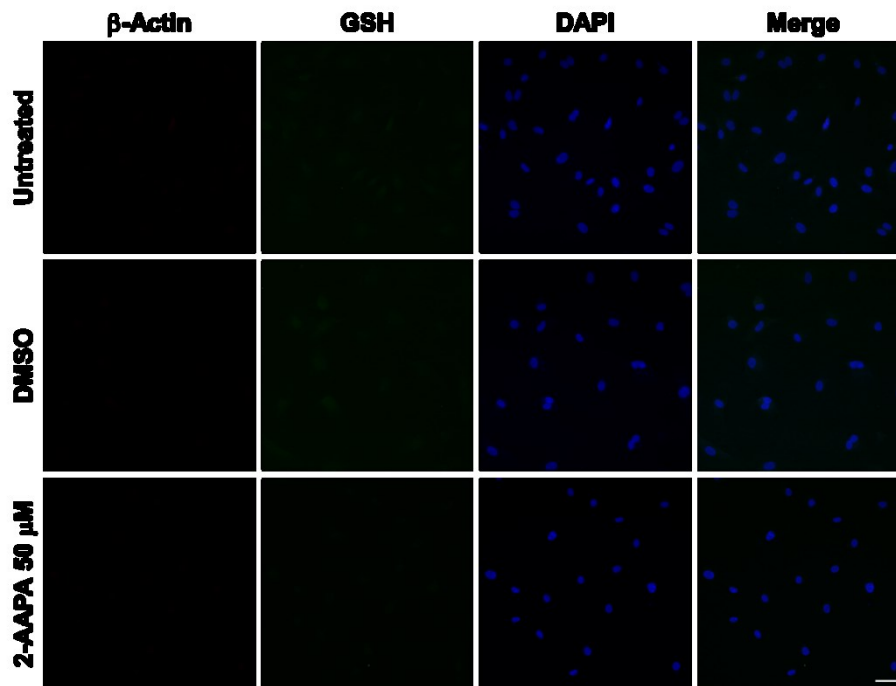


Figure 3.23. Negative control for GSH and β -actin immunostaining. Immunofluorescent staining performed under the same conditions as in Figure 6 but using secondary antibody without primary antibody anti-GSH and anti- β -actin. Scale bar: 50 μ M.

3.4.6 NAC fend off P-SSG and consequent calcium deposition in hVECs

Aortic valve calcification is a stenotic CAVS signature, contributing to narrowing the aortic valve¹⁴⁴. Thus, we felt it necessary to determine whether excessive P-SSG deposition predisposes hVECs to calcification. To this purpose, we first evaluated the calcium deposition susceptibility of these cells after a challenge with a well-known calcification inducer¹⁴⁵. A treatment with inorganic phosphate (Pi) caused hVECs calcification compared to untreated cells (53.0 ± 6.4 vs. 8.3 ± 1.1 ng of calcium/ μ g protein, respectively; $p < 0.0001$; **Figure 3.24A**). Then, we observed that the oxidative stress generated by 2-AAPA (50 μ M) prompted hVECs calcification, differently from what occurred with DMSO alone (97.7 ± 14.3 vs. 7.9 ± 0.6 ng of calcium/ μ g protein, respectively; $p < 0.0001$; **Figure 3.24B**). Finally, we proved that the addition of 2 mM NAC, 1 hour before and during the 2-AAPA treatment, drastically lowered the calcium deposition (-78.4 ± 5.6 %; $p < 0.0001$) when compared to hVECs treated with 2-AAPA alone (**Figure 3.24C**). This data set corroborate that oxidative stress via P-SSG plays a pivotal role in CAVS progression, inducing maladaptive mechanisms in hVECs, eventually leading to calcium deposition.

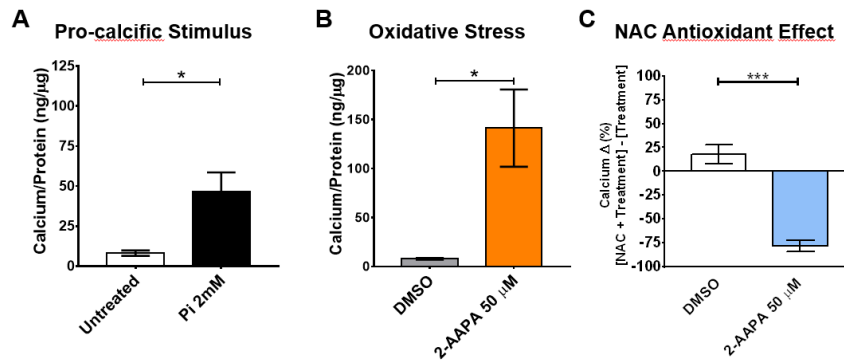


Figure 3.24. Calcium deposition potential of human stenotic valve endothelial cells. (A) Bar graph representing extracellular calcium quantification on human aortic valve endothelial cells (hVEC) treated with normal medium or 2 mM inorganic phosphate (Pi) for 7 days (n = 4). (B) Bar graph showing calcium quantification on hVECs after 4 hours of DMSO or 2-AAPA 50 μM and 7 days of recovery (n = 4). (C) Bar graph showing the calcification delta between treatment and treatment with N-acetylcysteine (NAC). Treatment: 4 hours of DMSO or 2-AAPA 50 μM and 7 days of recovery (n = 3). * p ≤ 0.05; *** p ≤ 0.01.

3.5 Different susceptibility to oxidative stress of endothelium in aortic valve with different morphology

3.5.1 BAV and TAV human valve endothelial cells characterization

Endothelial cells were isolated using a classical procedure with collagenase digestion (as described in **Material & Method** section) from aortic valve leaflets of 17 patients affected by CAVS and undergoing surgical repair. hVECs from both type of valve morphology (BAV and TAV) showed a cobblestone shape at contrast microscopy (**Figure 3.25A**). In addition, imaging flow cytometry confirmed that all isolated cells expressed at membrane level platelet endothelial cell adhesion molecule (CD31) while, at intracellular level, endothelial nitric oxide synthase (eNOS) and vimentin (**Figure 3.25C**). Of notice, ECs doubling time differed significantly between the two types (p = 0.04). BAV ECs had a doubling time of 28.4 ± 1.6 h whereas TAV ECs of 24.2 ± 1.8 (**Figure 3.25B**).

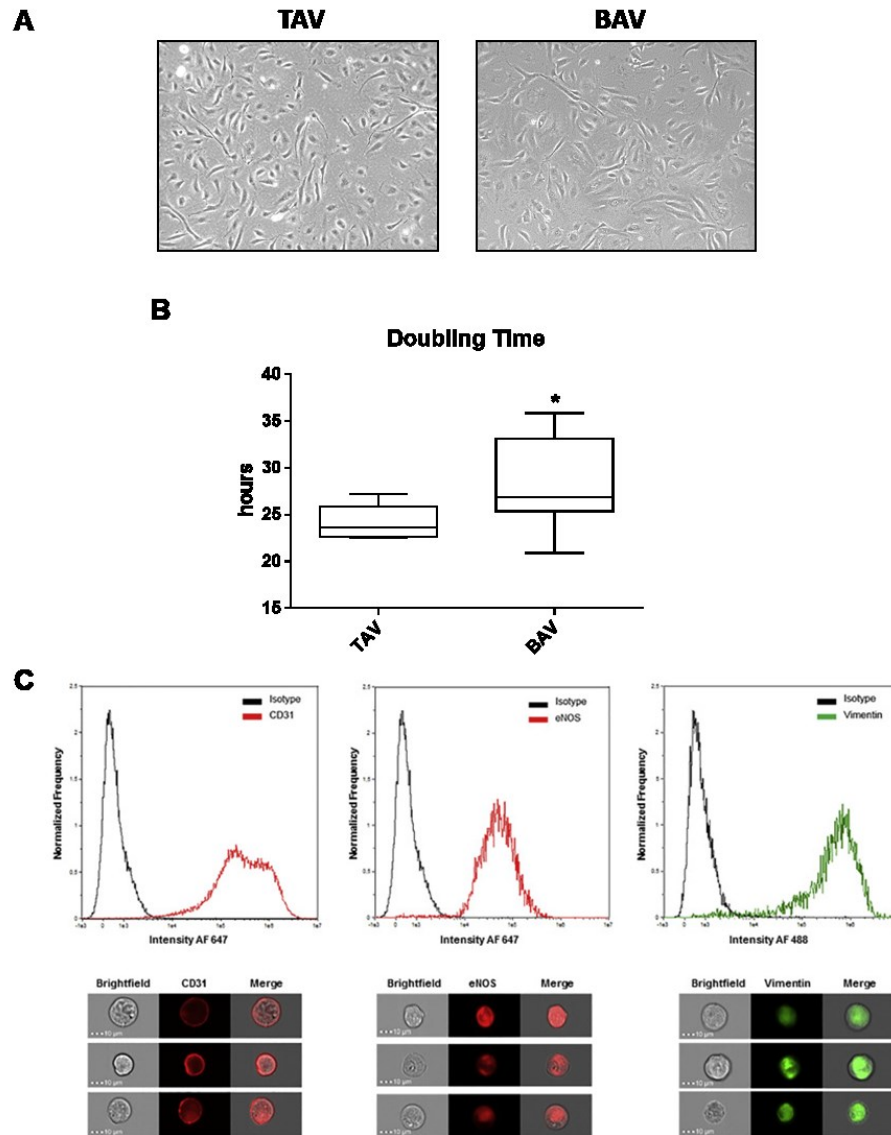


Figure 3.25. Human valve endothelial cells characterization. (A) Representative phase contrast images on BAV and TAV hVECs. (B) Whisker box plot representing the average doubling time of ECs derived from BAV and TAV patients. * $p < 0.05$. (C) Representative imaging flow cytometry analysis. Graph and fluorescent images showing the expression of platelet endothelial cell adhesion molecule (CD31), endothelial nitric oxide synthase (eNOS), and vimentin.

3.5.2 *MiRNA profile of BAV and TAV hVECs*

To investigate possible differences between the two groups of hVECs, we evaluated basal levels of 754 miRNAs. We identified eight miRNAs significantly up regulated in BAV hVECs compared to TAV hVECs (all $p < 0.05$; **Figure 3.26**). In particular, miR-26b-3p log₂ fold change (log₂FC) was +5.6 (95%CI: 5.0; 6.2), miR-139-3p log₂FC was +10.1 (95%CI: 9.4; 10.8), miR-197-3p log₂FC was +1.4 (95%CI: 0.4; 2.3), miR-328-3p log₂FC was +2.5 (95%CI: 1.5; 3.5), miR-520 g-3p log₂FC was +8.3 (95%CI: 8.0; 8.5), miR-561-3p log₂FC was +2.1 (95%CI: 1.4; 2.8), miR-573 log₂FC

was +12.7 (95%CI: 11.1; 14.2), and miR-1180-3p log₂FC was +11.8 (95%CI: 10.0; 13.6).

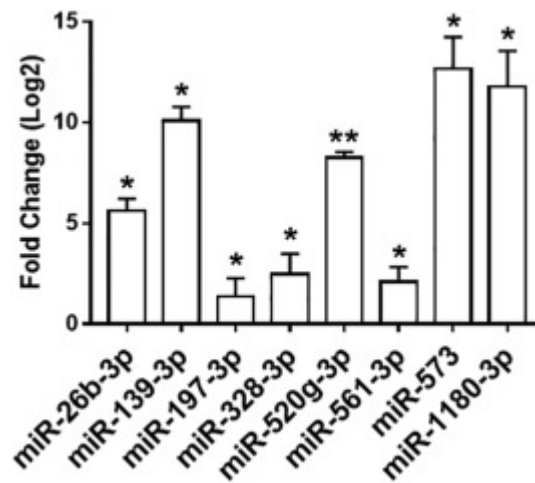


Figure 3.26. MiRNA expression profile. Significant miRNAs differentially expressed in BAV ECs (n = 4) compared to TAV hVECs (n = 3). Graph represent the log₂ fold change of miRNA in BAV hECs compared to TAV ECs. * p < .05; ** p < 0 .01.

3.5.3 Differentially activated signaling pathways in BAV and TAV hVECs

Functional analysis revealed that the identified miRNAs could regulate > 2'000 mRNA transcripts that are implicated in several pathways. Specifically, the significantly modulated pathways in BAV ECs compared to TAV ECs were the cellular response to DNA damage stimulus (i.e. hydrogen peroxide – H₂O₂) with direct consequences on the activation of the intrinsic apoptotic signaling pathway via p53 (**Figure 3.27**).

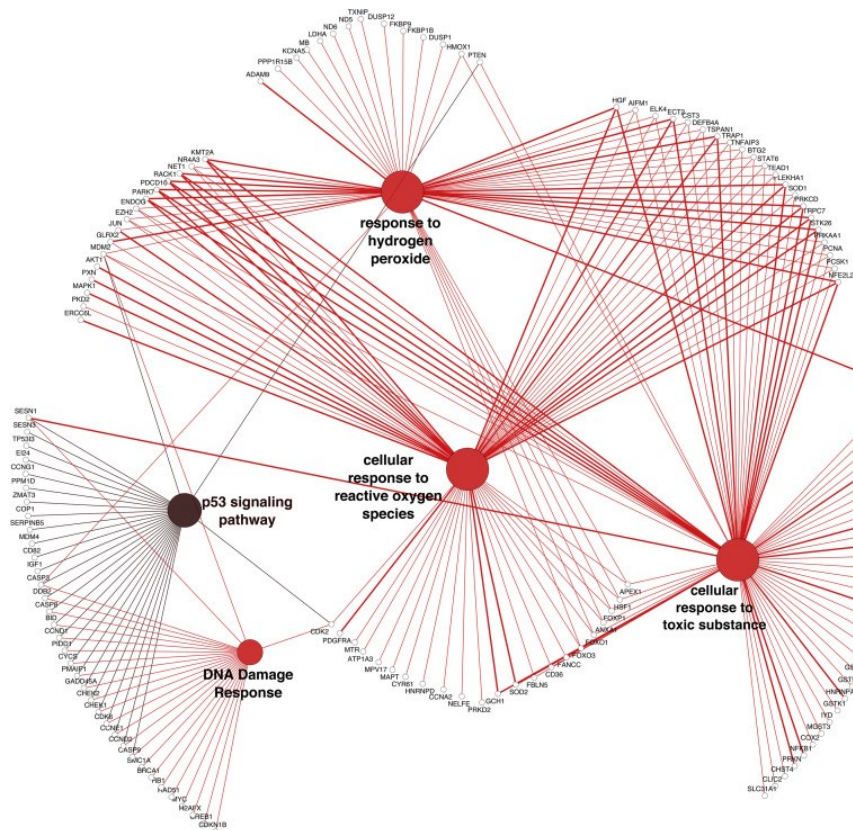


Figure 3.27. Functional pathway analysis. Signaling pathways directly modulated by upregulated miRNAs in BAV hVECs compared to TAV hVECs. The colour of the nodes represents the p value; red ($p < 0.01$) and brown ($p < 0.05$).

3.5.3 BAV ECs have an enhanced susceptibility to hydrogen peroxides

Since the functional analysis uncovered a possible difference in the H_2O_2 metabolism in the two hVEC groups, we evaluated the mRNA expression levels of 20 enzymes that are involved in the H_2O_2 homeostasis. We found that the glutathione peroxidase 3 (GPX3) was down regulated in BAV ECs ($FC = 0.48 \pm 0.16$; $p = 0.05$) than TAV hVECs and the sulfiredoxin 1 (SRXN1) was also down regulated in BAV hVECs ($FC = 0.72 \pm 0.07$; $p = 0.01$) compared to TAV hVECs (**Figure 3.28A, B, C, and Supplemental Table 9 in Supplemental appendix**). The GPX3 is directly implicated in the reduction of H_2O_2 by glutathione and thereby it protects cells against oxidative damage, while SRXN1 binds to peroxiredoxins (Prxs) and contributes to oxidative stress resistance by reducing Prxs cysteine-sulfinic acid formed under the exposure to oxidants.

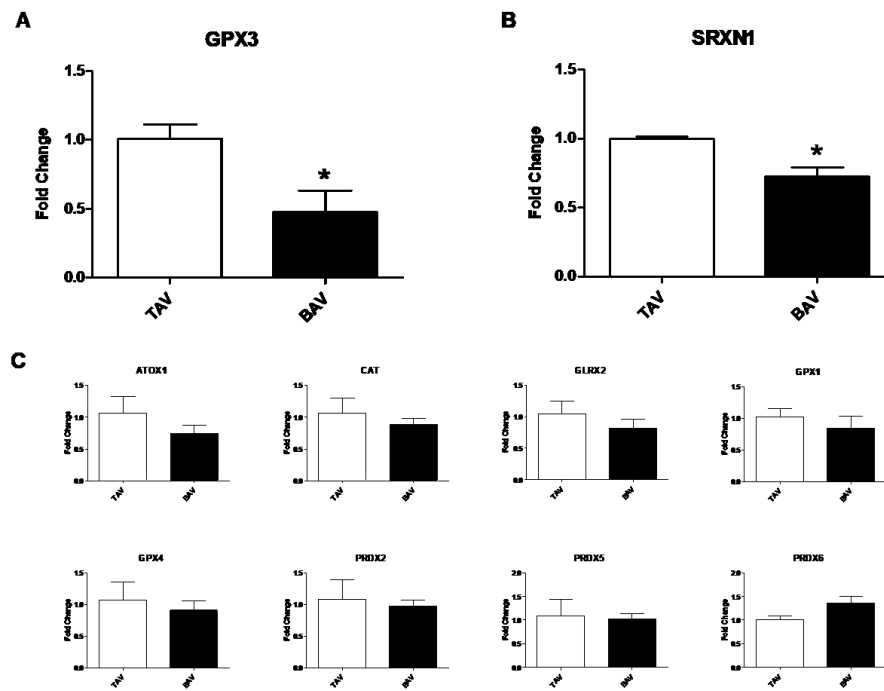


Figure 3.28. Differential expression of transcripts involved in hydrogen peroxide metabolism.

(A) Quantitative PCR (qPCR) of glutathione peroxidase 3 (GPX3) and (B) sulfiredoxin 1 (SRXN1) in valve ECs derived from TAV (n = 3) and BAV (n = 3). * p < 0.05. (C) Quantitative PCR (qPCR) of non-modulated transcripts in TAV (n = 3) and BAV (n = 3) ECs.

ATOX1: Antioxidant 1 Copper Chaperone; CAT: Catalase; GLRX2: Glutaredoxin 2; GPX1: Glutathione Peroxidase 1; GPX4: Glutathione Peroxidase 4; PRDX2: Peroxiredoxin 2; PRDX5: Peroxiredoxin 5; PRDX6: Peroxiredoxin

To prove that BAV hVECs have an impairment in the reduction of H₂O₂, we treated hVECs from both groups with 100 μM H₂O₂ for one hour in phosphate buffered saline. During the recovery, we evaluated the phosphorylation of the histone 2AX (γH2AX) as a direct indicator of the number of DNA double-strand breaks (DSB)¹⁴⁶. As shown in **Figure 3.29A** and **B**, both BAV and TAV hVECs presented an activation of γH2AX after 15 min of recovery (p < 0.001) and γH2AX activation remained up to 48 h of recovery (p < 0.05). Of notice, the γH2AX activation was significantly higher in BAV ECs than TAV hVECs at 15 min (p < 0.01), 30 min (p < 0.01), 2 h (p < 0.01), 4 h (p < 0.05), and 24 h (p < 0.05), while it was comparable at 48 h (**Figure 3.29C**), indicating that H₂O₂ treatment induced more DSB in BAV hVECs compared to TAV ECs. However, the hVECs survival rate at 48 h was comparable between the two groups (BAV hVECs = 61.2 ± 2.9; TAV hVECs = 53.7 ± 1.3; **Figure 3.29D**), suggesting that BAV ECs were able to repair efficiently most of the DSB.

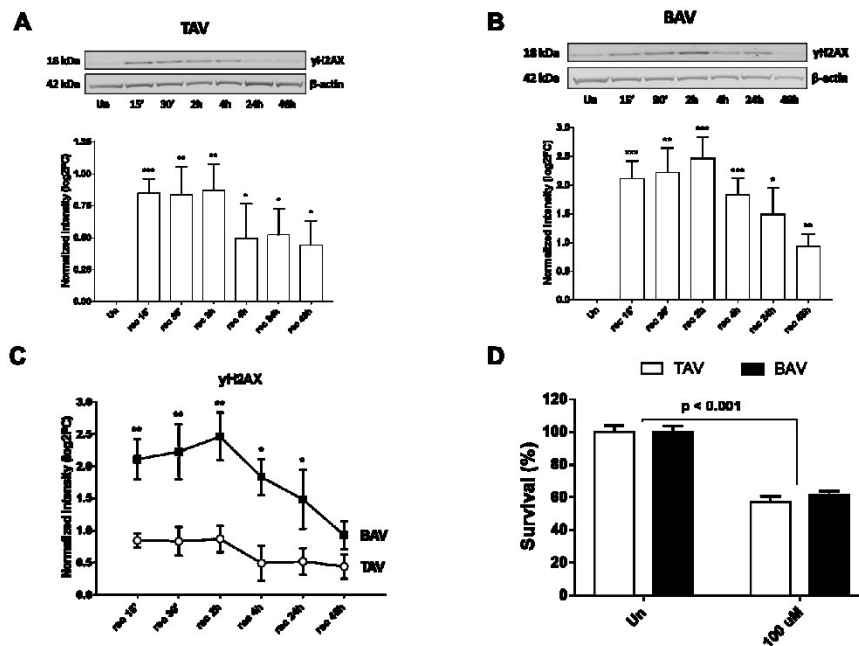


Figure 3.29. DNA Damage response activation. Representative Western blot images and relative quantification of phospho-histone 2AX (γ H2AX) in TAV ECs (n = 3) (A) and BAV ECs (n = 4) (B) treated for 1 h with 100 μ M H₂O₂ and then let recover for predetermined time points. B-actin was used as endogenous control. (C) Graph representing differential activation of γ H2AX in BAV and TAV ECs at predetermined time points of recovery after treatment. (D) Survival rate of BAV (n = 3) and TAV (n = 3) hVECs at 48 hours after an initial 1 hour treatment with H₂O₂ treatment.

3.5.4 Increased apoptosis of BAV hVECs

To evaluate the apoptotic signaling pathway, we detected the relative expression levels of 35 apoptosis-related proteins. The analysis, performed at basal levels, revealed that seven proteins were significantly over expressed in BAV ECs compared to TAV ECs ($p < 0.01$; **Supplemental Table 10**). In addition, we also noted that the phosphorylation levels of S46 and S392 of p53 were significantly higher in BAV ECs than TAV ECs ($p = 0.01$; **Supplemental Table 10**). The evaluation of the apoptotic marker annexin V confirmed a significant increment of the basal apoptotic process in BAV hVECs compared to TAV hVECs (11.0 ± 5.1 vs. $1.3 \pm 0.1\%$ of annexin V positive cells, respectively; $p < 0.001$) (**Figure 3.30A and B; C**). Since the single treatment with 100 μ M H₂O₂ resulted in comparable survival rate between BAV and TAV ECs (**Figure 3.29D**), we forced the system treating both hVECs groups chronically with 100 and 200 μ M H₂O₂ for three days. Both H₂O₂ treatments induced apoptosis in TAV hVECs as well as BAV hVECs (**Figure 3.30A and B**). At 100 μ M H₂O₂, BAV hVECs showed a significant increment in annexin V positive cells compared to TAV hVECs (25.9 ± 5.7 vs. $5.4 \pm 1.0\%$ of annexin V positive cells,

respectively; $p < .001$). At 200 μM H_2O_2 , we noticed a similar trend (BAV hVECs: 39.1 ± 6.8 ; TAV hVECs: $17.0 \pm 1.0\%$ of annexin V positive cells; $p < 0.001$; **Figure 3.30A and B**). Furthermore, the highest H_2O_2 concentration revealed that BAV hVECs had a significantly lower survival rate than TAV hVECs (53.3 ± 2.4 vs. 70.9 ± 2.4 ; $p < .001$; Fig. 7), indicating that BAV hVECs under high oxidative stress condition are more vulnerable than TAV hVECs.

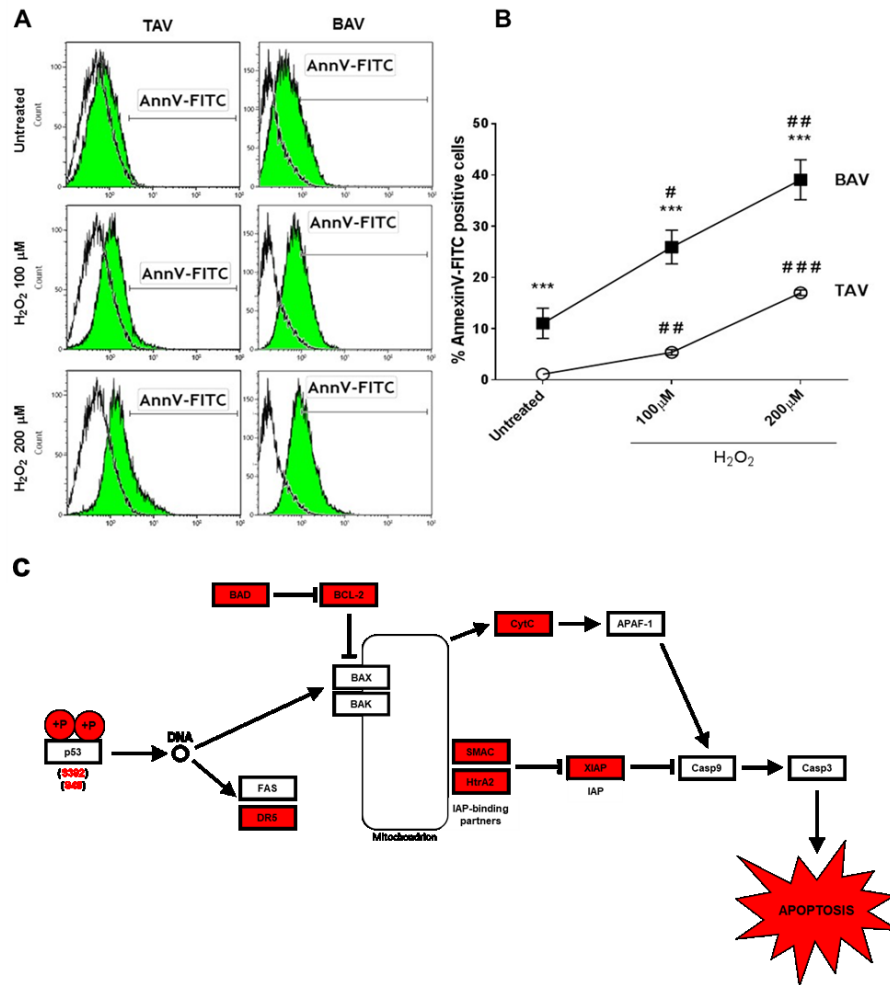


Figure 3.30. Apoptosis activation in BAV and TAV endothelial cells after treatment. (A) Representative flow cytometry analysis of annexin V in BAV and TAV hVECs in normal culture conditions and after 72 h of chronic treatment with 100 μM and 200 μM H_2O_2 . (B) Graph representing differential expression of annexin V in BAV ($n = 3$) and TAV ($n = 3$) hVECs in normal culture conditions and after 72 h of chronic treatment with 100 μM and 200 μM H_2O_2 . *** $p < 0.001$ BAV vs. TAV; # $p < .05$; ## $p < 0.01$; ### $p < 0.001$; Treated vs. Untreated. (C) Schematic intrinsic apoptotic pathway: proteins that resulted overexpressed in BAV compared to TAV ECs, at basal level, are depicted in red.

3.5.5 miR-328-3p directly regulate oxidative stress response in aortic valve hVECs

Among the eight miRNAs, differentially expressed between BAV and TAV hVECs, we focused on miR-328-3p since it targets oxidative stress related mRNAs (i.e. GPX3 and SRXN1). In order to investigate the putative functional relevance of this miRNA in the regulation of cellular response to oxidative stress and apoptosis, we transfected TAV and BAV hVECs with miR-328-3p mimic or inhibitor, respectively. We observed that GPX3 was down regulated in TAV transfected hVECs ($FC = -4.2 \pm 0.56$; $p < 0.01$) while up-regulated in BAV transfected hVECs ($FC = +0.51 \pm 0.1$; $p < 0.001$) compared to control groups. SRXN1 was significantly modulated only in TAV transfected hVECs than controls ($FC = -2.14 \pm 0.3$; $p < .001$) (**Figure 3.31A and B**). TAV hVECs transfected with mir-328-3p mimic, treated with 200 μ M H_2O_2 , showed a significant increment in annexin V positive cells as compared to the control group (45.31 ± 1.32 vs. $29.96 \pm 1.98\%$ of annexin V positive cells, respectively; $p < 0.001$) (Fig. 8C and E). BAV hVECs transfected with mir-328-3p inhibitor, treated with 200 μ M H_2O_2 , showed a significant decrease in annexin V positive cells than control group (20.32 ± 0.35 vs. $41.05 \pm 2.96\%$ of annexin V positive cells, respectively; $p < 0.001$) (**Figure 3.31D and E**).

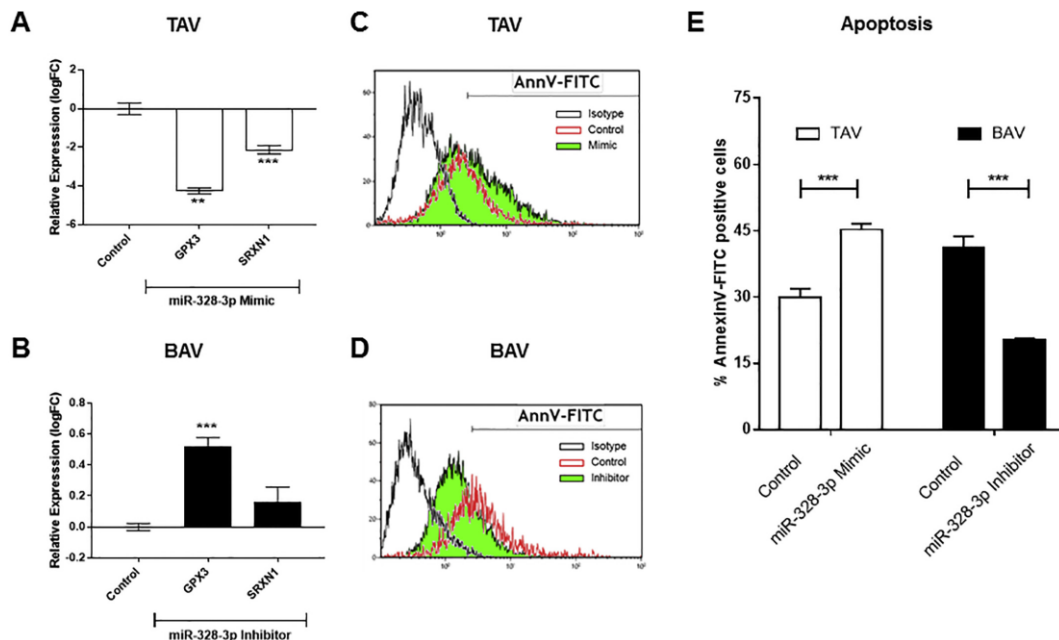


Figure 3.31. Hsa-miR-328-3p and oxidative stress response in aortic valve ECs. Quantitative PCR (qPCR) of glutathione peroxidase 3 (GPX3) and sulfiredoxin 1 (SRXN1) in TAV (n = 3) (A) and in BAV hVECs (n = 3) (B) after miR-328-3p mimic or inhibitor treatment, respectively. ** $p < 0.01$; *** $p < 0.001$ vs. Control. Representative flow cytometry analysis of annexin V in TAV (C) and BAV (D)

hVECs (D) in presence of miR-328-3p mimic or inhibitor, respectively, after 72 h of chronic treatment with 200 μ M H₂O₂. (E) Graph representing differential expression of annexin V in TAV (n = 3) and BAV hVECs (n = 3) in presence of miR-328-3p mimic or inhibitor, respectively, after 72 h of chronic treatment with 200 μ M. *** p < 0.001 vs. Control.

3.6 Players in aortic valve interstitial cell calcification identifiable as novel potential drug targets

3.6.1 Cyclophilin A inhibition reduce valve interstitial cells calcium deposition

3.6.1.1 Gene and protein expression levels of CyPA are elevated in AS leaflets

On the basis of the possible association between CyPA cell function and the cellular processes involved in AS, we checked the expression levels of CyPA transcript and protein comparing whole specimen extracts from aortic valves of insufficient (Ctrl) and AS patients. Both qPCR and Western blot assays provided evidence for an up-regulation of the CyPA transcript ($+5.6 \pm 0.9$ log₂ fold change, p < 0.0001; **Figure 3.32A**) and protein ($+29.0 \pm 8.6$ fold change, p = 0.03; **Figure 3.32B**) in AS compared with Ctrl specimens. These data suggest a considerable up-regulation of CyPA in AS valve tissue.

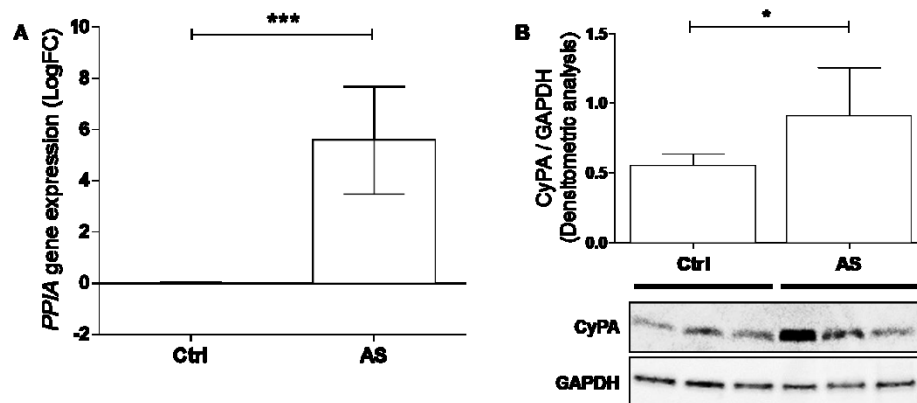


Figure 3.32. CyPA gene and protein expression levels are higher in valves of AS patients than Ctrl subjects. (A) CyPA gene expression in total RNA extracts from human insufficient (Ctrl) and stenotic (AS) aortic valve leaflets. qPCR analyses were performed in triplicate and data are shown as logarithmic fold change \pm SEM. n = 3. Student's t-test: ***p < 0.0001. (B) CyPA expression in total protein extracts

from human insufficient (Ctrl) and stenotic (AS) aortic valve leaflets. Western blot quantification data are shown as mean \pm SEM. n = 3. Student's t-test: *p < 0.05.

3.6.1.2 CyPA expression co-localizes with calcific lesions in AS specimens

In order to better characterize the CyPA expression levels in the aortic valve tissues, we performed histological evaluations on specimens from Ctrl and AS patients. The results of CyPA immunohistochemistry confirmed the significant up-regulation of CyPA in AS leaflets compared to Ctrl (15.6 ± 3.9 vs. 4.8 ± 1.2 , respectively, p = 0.03; **Figure 3.33A and B**). In addition, as shown in **Figure 3.33**, CyPA expression, in AS specimens, is evident in the same regions stained by Von Kossa, suggesting a co-localization between calcific and CyPA overexpression regions in AS leaflets. Altogether, these data confirm the CyPA overexpression in AS leaflets and add the information on CyPA and calcium co-localization, thus suggesting a potential role of CyPA in calcium deposition in AS specimens.

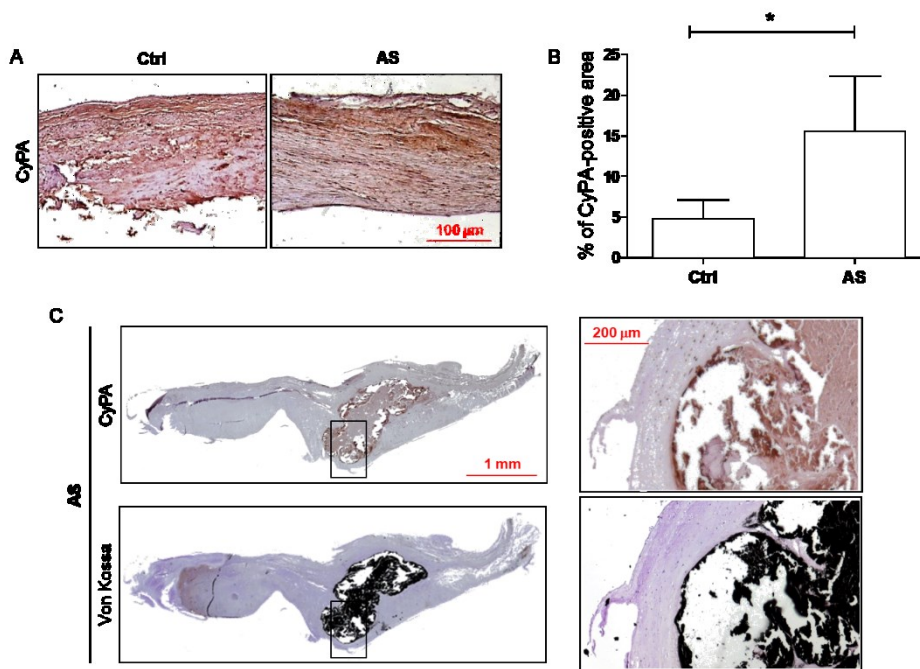


Figure 3.33. CyPA expression is increased in AS and is localized in calcified areas of damaged valve leaflets. (A) Representative images of immunohistochemistry for CyPA on human insufficient aortic valves, as control, (left panel. Ctrl) and stenotic aortic valves (right panel, AS). Magnification = 10 \times . Scale bar = 100 μ m. **(B)** Quantification of immunohistochemistry for CyPA has been shown as mean \pm SEM. n = 3. Student's t-test: *p < 0.05. **(C)** Representative images of immunohistochemistry for CyPA (upper panels) and Von Kossa staining performed on consecutive sections of AS leaflets (lower panels). Magnification = 2.5 \times . Scale bar = 1 mm. The images in the boxes depict the higher magnification (10X) of squared calcified area. Scale bar = 200 μ m

3.6.1.3 CyPA directly correlates with the *in vitro* valve interstitial cell calcification potential

The cell type residing in the inner, or interstitial, region of the aortic valve is called with the generic name of valve interstitial cells (VICs). Specifically, the majority of these cells are fibroblasts, which may differentiate into a number of other cell types in certain pathological conditions⁴. In the AS scenario, VICs switch into osteoblast-like cells, producing and depositing calcium crystals along with new extracellular matrix⁴. In order to confirm the detrimental contribution of VICs in AS and to study, in parallel, their specific involvement in producing/secreting CyPA, these cells were explanted from aortic valve leaflets of AS patients and cultured both in normal media (NM) and NM supplemented by inorganic phosphate (pro-calcifying media, PCM). The ELISA assay revealed a significant up-regulation of CyPA secretion by VICs in PCM compared to NM (30.3 ± 4.1 ng/ μ g of total protein vs. 11.1 ± 1.1 ng/ μ g, respectively, $p = 0.0002$; **Figure 3.34A**). In addition, as shown in **Figure 3.34B**, in PCM condition the secreted levels of CyPA and the amount of calcium deposition significantly correlated ($r^2 = 0.84$, $\rho = 0.92$, $p < 0.0001$). These data highlight the effects of inorganic phosphate in CyPA release by VICs and their positive correlation.

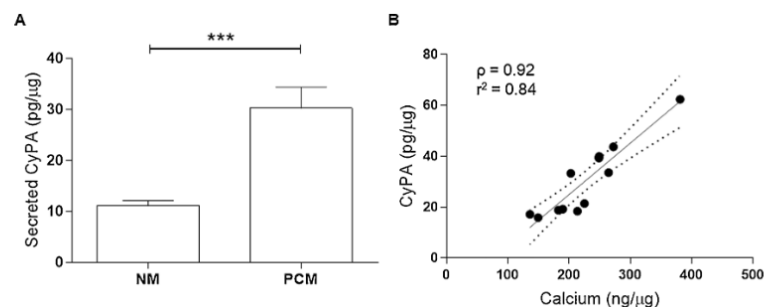


Figure 3.34 Pro-calcifying medium stimulates CyPA secretion by VICs and directly correlates with calcium deposition. (A) CyPA content in supernatant culture medium of VICs after 7 days of growth. ELISA data are expressed as mean \pm SEM. $n = 6$. Student's t-test: $*p < 0.05$. (B) Linear correlation between CyPA secreted levels and calcium content quantification in VIC cultures after 7 days of growth in PCM. Linear correlation evaluated by Pearson correlation has $\rho = 0.92$ with $r^2 = 0.84$ ($p < 0.0001$, 95% CI depicted in dashed lines).

3.6.1.4 Exogenous CyPA stimulates calcium deposition in VICs isolated by AS patients

To date, the ubiquitous localization of CyPA in intracellular compartments is well known¹⁰⁶. In addition, it has been reported that CyPA can be secreted in response to pathological stimuli and, more importantly, the secreted CyPA plays often a central and detrimental role in cardiovascular diseases^{108,114,147}. Thus, we evaluated in our in vitro model the direct effect of exogenous CyPA. VICs treated with increasing concentrations of CyPA (10 ng/mL, 100 ng/mL, and 1000 ng/mL), in NM and PCM, did not reveal any statistical difference in cell viability, underlining a weak CyPA cytotoxic effects on this cell type. Regarding calcification, VICs treated with increasing CyPA concentration showed a significant calcium deposition, starting at 100 ng/mL of CyPA in both NM and PCM (ANOVA $p = 0.0005$ and $p = 0.01$, respectively; **Figure 3.35**). In addition, we noticed a synergistic effect between exogenous CyPA and inorganic phosphate since the percentage of calcium caused by CyPA 100 ng/mL alone (e.g. in NM) was $4.3 \pm 0.6\%$ and the percentage of calcium caused by the combination of inorganic phosphate with CyPA 100 ng/mL (e.g. in PCM) was more than the sum of the single treatments ($158.4 \pm 31.0\%$). The same can be told by analyzing CyPA at 1000 ng/mL (alone $10.0 \pm 1.5\%$ and in combination $205.2 \pm 45.0\%$). These data highlight that exogenous CyPA, alone or in an osteogenic milieu, is able to promote calcium deposition of VIC isolated from AS patients.

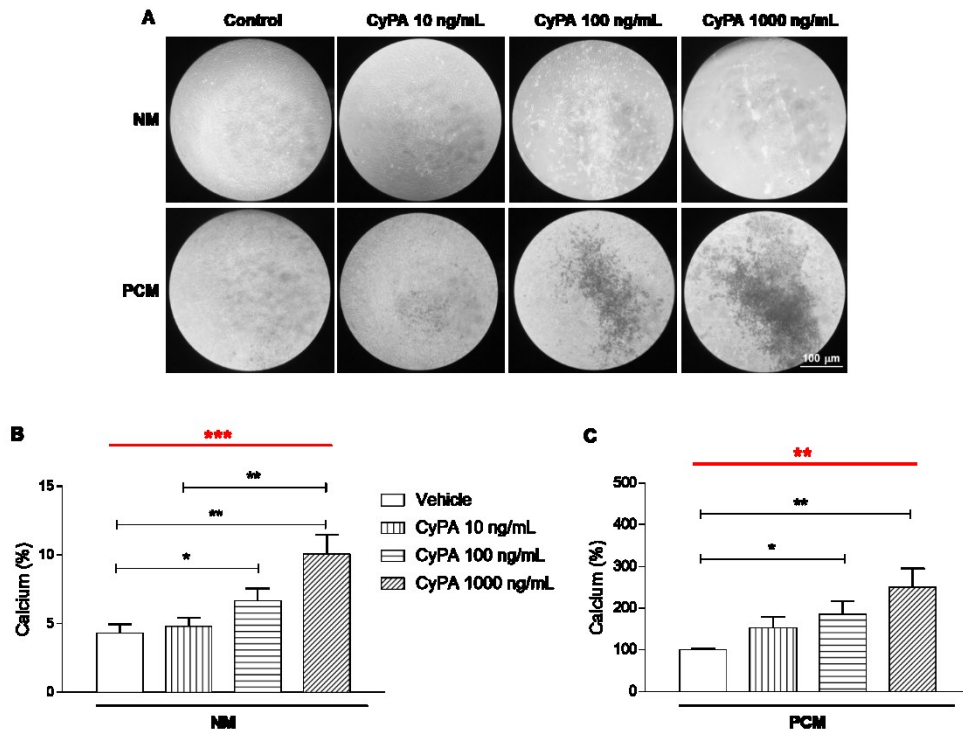


Figure 3.35. Exogenous CyPA induces VIC calcification in pro-calcifying medium. (A) Representative images in brightfield of AS patient-derived VICs and treated in vitro with increasing concentrations of CyPA (10, 100, and 1000 ng/mL). Magnification = 10 \times . Scale bar = 100 μ m. (B) Quantification of calcium content in VIC cultures after treatments with increasing CyPA concentrations (10, 100, and 1000 ng/mL). Data are shown as mean \pm SEM. n = 9. Two-way ANOVA: **p < 0.01, ***p < 0.001. Bonferroni post-test: *p < 0.05, **p < 0.01.

3.6.1.5 Exogenous CyPA inhibition reduces calcium deposition of AS patient-derived VIC

Finally, we evaluated whether CyPA effectively participates in the osteogenic differentiation and thus induces calcification by means of its molecular blockade, implementing an inhibitory compound called MM284 (**Figure 3.36A**). MM284 is a cyclosporine A analogue, impermeable to cell membranes, and able to selectively block exogenous CyPA¹⁴⁸. We treated VICs with the lowest effective exogenous CyPA concentration (100 ng/mL) in the presence of its inhibitor MM284 (250 ng/mL). We observed that CyPA inhibition mediated by MM284 led to a significant decrease of VIC calcium deposition compared to exogenous CyPA alone in both NM (1.7 \pm 0.3% vs. 6.6 \pm 0.9%, respectively, p = 0.0003) and PCM (58.0 \pm 7.9% vs. 185.4 \pm 31.0%, respectively, p = 0.003) with the addition of exogenous CyPA (**Figure 32B and C**). We also noticed a marked reduction of calcium deposits mediated by MM284, without the addition of exogenous CyPA, compared to the vehicle, in both NM (1.7 \pm

0.3% vs. $4.3 \pm 0.6\%$, respectively, $p = 0.004$) and PCM (26.2 ± 2.7 vs. 100 ± 3.8 , respectively, $p < 0.0001$). Taking all these evidence together, we report that MM284 markedly rescue CyPA-mediated calcium deposition on VICs and thus CyPA plays a critical detrimental role in isolated human stenotic aortic VICs.

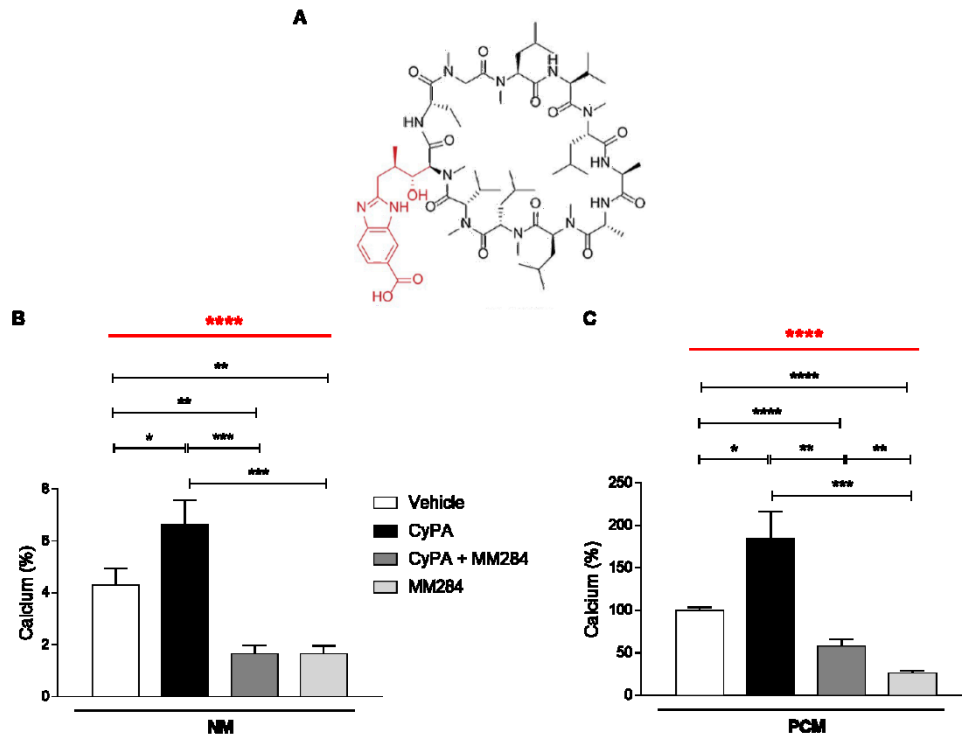


Figure 3.36. Pharmacological inhibition of CyPA reduces VIC calcification in pro-calcifying medium. (A) Molecular structure of cyclosporine A (CsA) analogue, namely MM284. The red box highlights the CsA modification that blocks the molecule cell permeability. (B) Quantification of calcium content in VIC cultures after treatments with 100 ng/mL CyPA, or 250 ng/mL MM284, or CyPA together with its inhibitor MM284. Data are shown as mean \pm SEM. $n = 9$. Two-way ANOVA: **** $p < 0.0001$. Bonferroni post-test: * $p < 0.05$, ** $p < 0.01$, *** $p < 0.001$, **** $p < 0.0001$.

3.6.2 PCSK9 in Calcific Aortic Valve Stenosis

3.6.2.1 Meta-analysis of the association between the PCSK9 R46L variant and CAVS

Figure 3.37A present the association between the PCSK9 R46L variant and CAVS in 1 published and 9 previously unpublished studies totaling 12,059 CAVS cases and 541,081 control patients. Carriers of the R46L variant had lower odds of CAVS compared with noncarriers (odds ratio: 0.80 [95% confidence interval: 0.70 to 0.91];

$p < 0.001$). A funnel plot of the resulting meta-analysis is presented in **Figure 3.37B**. The p value for heterogeneity was 0.418.

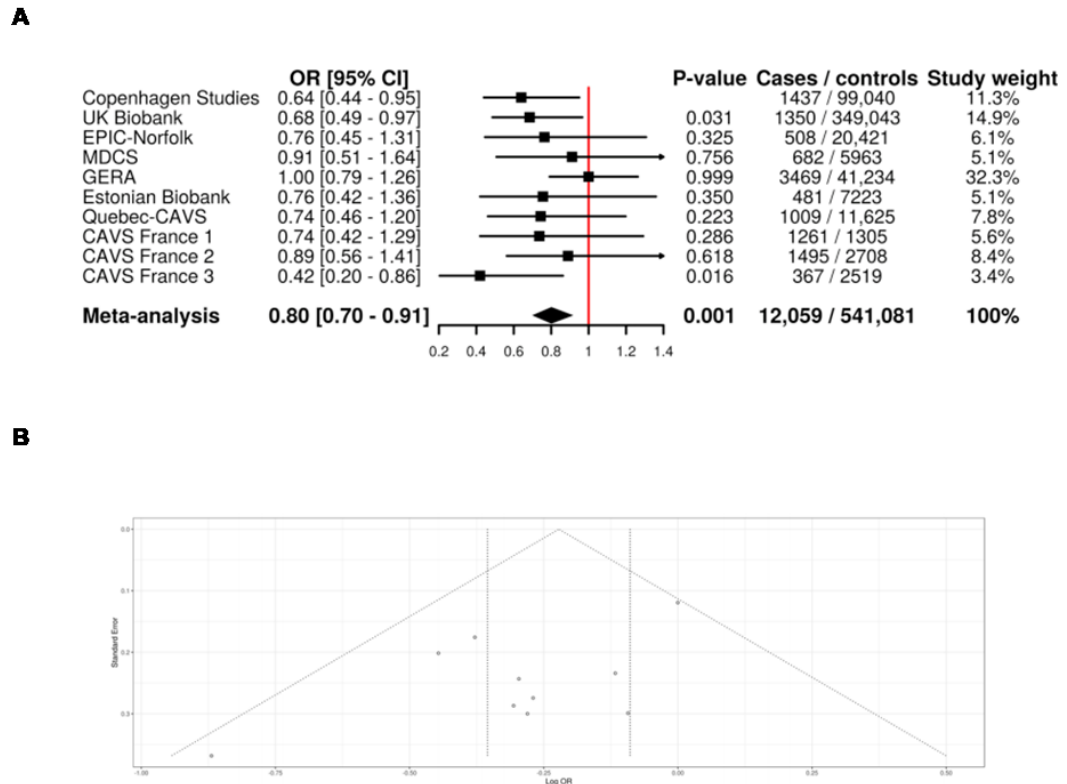


Figure 3.37 Association of the PCSK9 R46L variant with calcific aortic valve stenosis in a meta-analysis of 10 cohorts totaling 12,059 cases and 541,081 control subjects. (A) CAVS ¼ calcific aortic valve stenosis; CI ¼ confidence interval; EPIC ¼ European Prospective Investigation into Cancer and Nutrition; GERA ¼ Genetic Epidemiology Research on Aging study; MDCS ¼ Malmo Diet and Cancer Study; OR ¼ odds ratio. (B) Funnel plot of the PCSK9 R46L meta-analysis of calcific aortic valve stenosis.

3.6.2.2 PCSK9 expression and CAVS

Immunohisto-chemical analysis identified PCSK9 in both calcified and noncalcified leaflets. However, PCSK9 was highly abundant in calcified ones (fold change β 3.5 [IQR: β 1.7 to β 20.9]; p ¼ 0.009) compared with non-calcified leaflets (**Figure 3.38A, 3B, and 3E and Figures 3.39**). In healthy aortic valves, PCSK9 is detectable only in close proximity to cell nuclei, whereas in stenotic ones, PCSK9 is present also within the extracellular matrix (**Figures 3.38C and D and Figure 3.39**). Enzyme-linked immunosorbent assay confirmed that PCSK9 is overexpressed in calcified leaflets compared with healthy ones (315.8 [IQR: 216.4 to 547.9] vs. 2.3 [IQR: 0.0 to 88.1] pg of PCSK9/mg of total proteins, respectively; p ¼ 0.002) (**Figure 3.38F**).

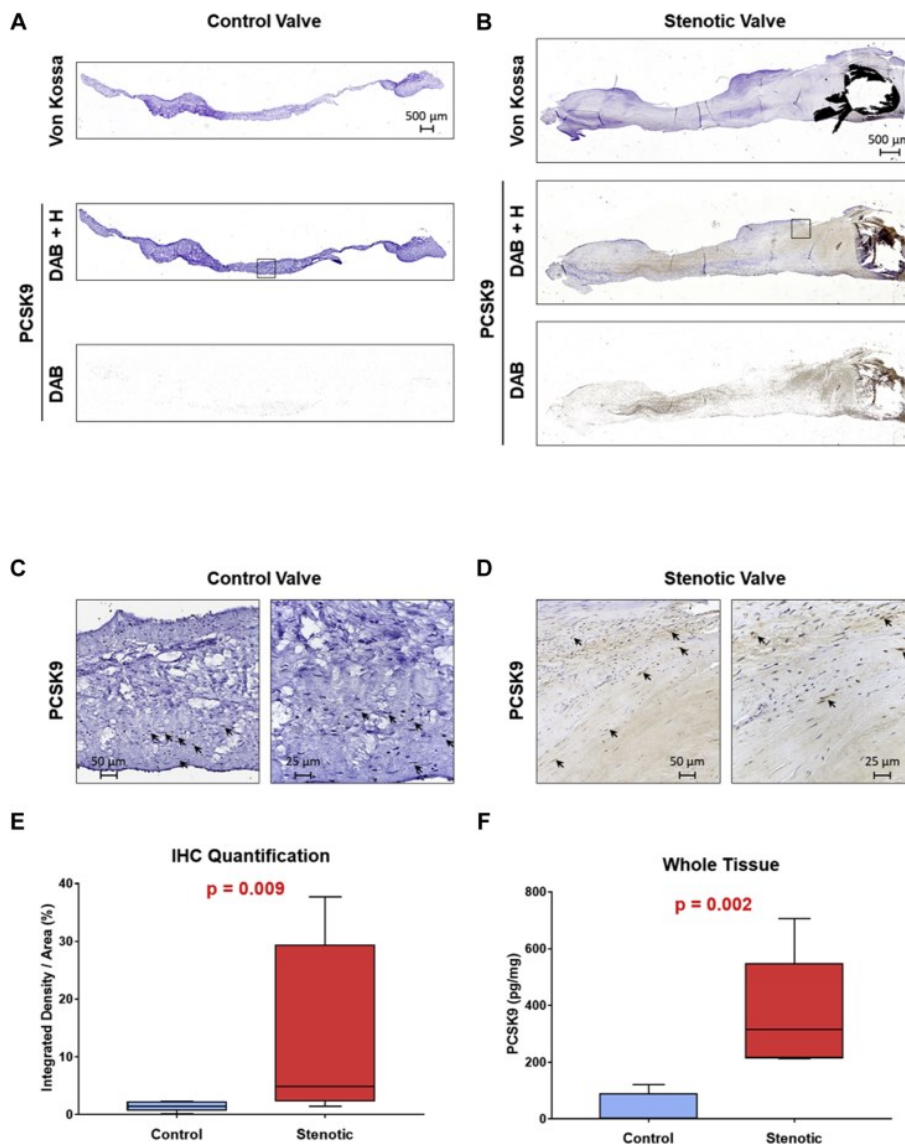


Figure 3.38. PCSK9 expression. (A) Representative explanted aortic valve leaflet with normal structure (control valve) and (B) representative calcified aortic valve leaflet (stenotic valve), both stained with Von Kossa to visualize calcium deposits (upper panels) and with anti-PCSK9 antibody (lower panels). PCSK9 immunohistochemical (IHC) staining is presented as 3,30 -diaminobenzidine (DAB) and hematoxylin (H) counter staining (DAB + H) and as deconvoluted image visualizing only the DAB staining. Panoramic images were taken with a 10x magnification. Black boxes indicate the higher magnification areas. (C and D) High magnification areas of aortic valve leaflets (20x left and 40x right). Arrows indicate representative PCSK9 expression in close proximity to cell nuclei. (E) Box and whisker plots represent DAB quantification by ImageJ with IHC Tool box plugin on normal (control; n = 6) and calcified (stenotic; n = 6) leaflets. (F) Box and whisker plots represent PCSK9 levels measured by enzyme-linked immunosorbent assay on control (n = 6) and stenotic (n = 6) whole tissue extracts

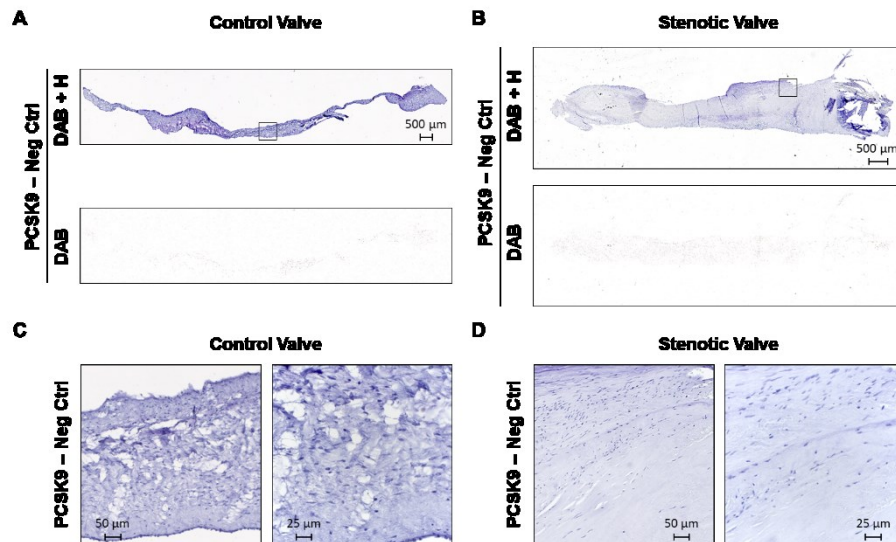


Figure 3.39. PCSK9 immunohistochemistry negative controls. (A) Representative explanted aortic valve leaflet with normal structure (control valve) and (B) representative calcified aortic valve leaflet (stenotic valve) negative immunohistochemistry controls. The negative controls are presented as 3,3'-Diaminobenzidine (DAB) and hematoxylin (H) counter staining (DAB + H) and as de-convoluted image visualizing only the DAB staining. Panoramic images were taken with a 10x magnification. Black boxes indicate the higher magnification areas. (C and D) High magnification area of aortic valve leaflets (20x left panels and 40x right panels).

3.6.2.3 PCSK9 secretion and VIC calcification

We sought to determine whether CAVS VICs could express PCSK9 under classic osteogenic stimulus. We treated human isolated VICs with osteogenic medium and then evaluated PCSK9 mRNA and secreted PCSK9 protein levels. PCSK9 transcript expression was induced by osteogenic medium treatment (log₂ fold change = +1.0 [IQR: +0.66 to +1.4]; p = 0.005) compared with VICs in normal medium (**Figure 3.40A**). As expected, osteogenic medium induced VIC calcification compared with normal medium (472.2 [IQR: 316.4 to 701.1] ng vs. 20.7 [IQR: 15.8 to 28.6] ng of calcium/mg of total proteins, respectively; p < 0.0001) (**Figure 3.40E**). In culture, VICs were able to secrete a detectable amount of PCSK9 into the medium. In particular, VICs treated with osteogenic medium secreted significantly higher PCSK9 levels compared with VICs in normal one (14.6 [IQR: 11.0 to 21.6] vs. 8.9 [IQR: 5.8 to 13.4] pg of PCSK9/mg of total proteins, respectively; p < 0.001) (**Figure 3.40B**). We also found a significant and positive correlation (Pearson's correlation coefficient $r_p = 0.91$; p < 0.0001) between the extent of calcification and the amount of secreted PCSK9 (**Figure 3.40C**). Finally, inhibition of extracellular PCSK9 was able to significantly reduce the calcium deposition both in normal medium (-6.3% [IQR: -

6.8% to -0.4%]; $p = 0.02$) and in osteogenic medium (-56.5% [IQR: -63.3% to -40.0%]; $p < 0.0001$) compared with their respective control medium (**Figure 37D**).

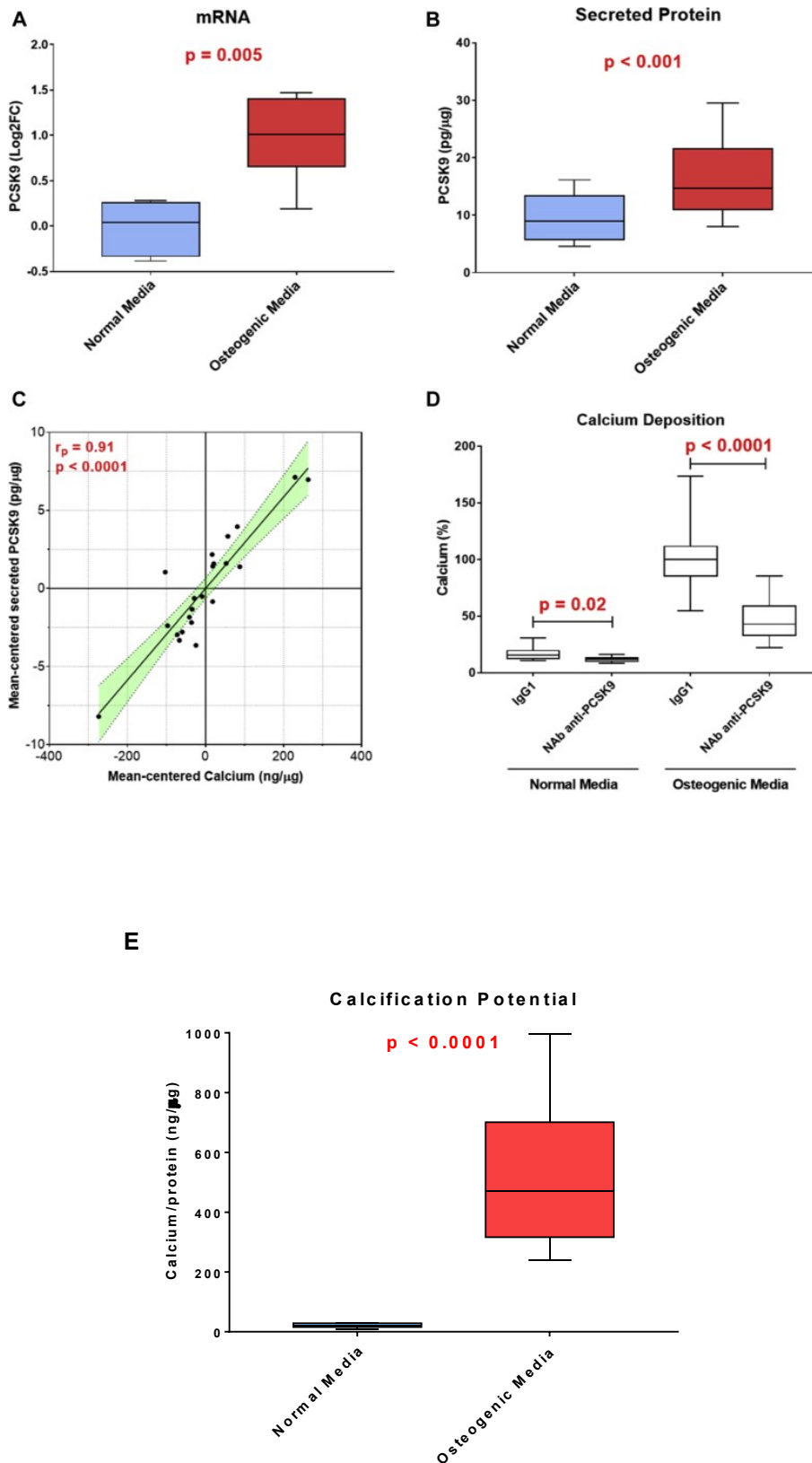


Figure 3.40. VIC' PSCK9 secretion and calcification. (A) Box and whisker plots represent PCSK9 transcript levels in valve interstitial cells (VIC) cultured for 7 days in normal or osteogenic media (n ¼ 6). RNA levels were normalized to GAPDH expression. (B) Box and whisker plots represent secreted PCSK9 levels from VICs cultured for 7 days in normal or osteogenic media (n ¼ 4). PCSK9 levels were normalized to total protein content. (C) Mean-centered correlation between secreted PCSK9 and calcium levels in VICs. The linear correlation between the 2 variables was performed with the Pearson correlation coefficient. (D) Bar graph shows the calcification potential, after 7 days, in normal and osteogenic media (n ¼ 3) of VICs treated with a neutralizing antibody anti-PCSK9 (NAb anti-PCSK9) or immunoglobulin G1 as control (IgG1). (E) Box and Whisker plots showing the calcium quantification of valve interstitial cells (VIC) cultured for 7 days in normal or osteogenic media (n = 4). Calcium levels were normalized to total protein content.

4. Discussion

4.1 Aortic valve sclerosis and prediction of short-term mortality in patients affected by coronary atherosclerosis

In this study, we show for the first time that AVSc is an independent predictor of short-term (90-day) mortality after isolated surgical myocardial revascularization. The presence of AVSc, as identified in the routine screening before CABG, increases the risk of postoperative short-term mortality of more than two folds, and AVSc significantly adds to the identification of patients at high-risk for short-term mortality compared to EuroSCORE II alone.

Being adjusted for propensity score, our findings suggest: first, that the differences observed are not due to a simple unbalance of confounding factors in the two groups and second that AVSc probably reflects a pathophysiological mechanism that it is not fully explained by factors included in the current version of ESII.

To date, few studies have attempted to define the role of AVSc as a predictor of postoperative short-term and/or long-term outcomes. Cai et al.¹⁴⁹ reported a significant association between the presence of AVSc and post-operative major adverse cardiac events (which also included cardiac death) in 185 renal transplant recipients followed-up for a mean of 60 months; in such study, however, the short-term mortality was not considered. By contrast, in another study, the prognostic implications of AVSc on both post-operative short-term (30-day) and long-term composite outcomes were tested in 1172 patients with peripheral arterial disease requiring vascular surgery¹⁵⁰. In multivariable regression analysis adjusted for age, gender, revised cardiac risk index, hypertension, hypercholesterolemia, and medication use, AVSc was not associated with either post-operative or long-term outcomes. According to these authors, the effect of AVSc was probably attenuated because their cohort was constituted by vascular surgery patients with extensive multi-vascular disease¹⁵⁰.

In the general population, AVSc is a rather common feature, with a prevalence ranging from 30 to 40%^{44,102,150} and AVSc has been associated with an increased risk of all-cause and CV mortality in many^{134,151-157} but not all¹⁵⁸ studies. Several authors have shown that the risk of dying from any-cause or for CV reasons in subjects with AVSc is significantly greater than in those without, even after adjustment for several risk factors^{134,152,159}. Other authors, however, have shown that such increased-risk is totally eliminated when analyses were adjusted for CV risk factors¹⁵⁸. AVSc, alone or included into cardiac calcium scores, also confers a greater risk of all-cause and CV

mortality in subjects with no history of CV disease¹⁵², in subjects with type 2 diabetes mellitus with or without history of myocardial infarction¹⁵⁴, and in patients hospitalized for overt or suspected CAD¹⁶⁰. A recent meta-analysis reported a low (but still present) risk of all-cause and CV mortality in patients with AVSc¹⁶¹. Coffey et al.¹⁵⁶ hypothesized that the relatively high baseline risk of patients included in the study has masked the additional risk due to AVSc. This hypothesis, however, was contrasted by the results of the Cardiovascular Health Study, an observational cohort study of 3782 elderly patients followed up for 5¹³⁴ or 6.6¹⁵³ years, where AVSc remained an independent predictor of both all-cause and CV mortality regardless the presence/absence of baseline CAD. Our data, documenting an increased risk of mortality in patients who underwent CABG, adds another piece of information to this controversy.

Despite all the evidence reported in the literature documenting AVSc as a risk-multiplier, its capacity to act additively or synergistically to ESII for prediction of short-term mortality after CABG has never been tested. Our findings, showing (a) that AVSc predicts short-term CV mortality independently from ESII and (b) that AVSc adds to the identification of high-risk patients compared to ESII, strongly endorse AVSc as a promising factor to be integrated with the approaches currently used for the recognition of patients who are at high-risk of complications after isolated CABG.

4.1.1 Clinical Relevance

The identification of new risk factors for peri- and post-operative mortality is a core issue for guaranteeing high-quality results in risk-scoring systems. Several studies have reported a progressive worsening of the ESII model performances when applied to follow-up longer than 30 days¹⁶². In particular for isolated CABG surgeries, a poor calibration of ESII, in both the highest and lowest risk-patient groups, was reported¹⁶³. To the best of our knowledge, our study is the first showing that AVSc could be combined with ESII to improve the identification of patients at high-risk of short-term mortality after CABG. Another point of relevance that deserves to be highlighted is that the detection of AVSc used for risk-prediction does not add any additional cost to usual clinical care, as the pre-operative echocardiography assessment is already mandatory in the evaluation of patients requiring cardiac surgery¹³⁹.

4.2 Aortic valve sclerosis and prediction of long-term mortality in patients affected by carotid atheromatous plaque requiring carotid endarterectomy

Our study, for the first to the best of our knowledge, revealed that patients who underwent CEA surgery have a high prevalence of AVSc. The age and renal function impairment, measured by eGFR, were independently associated with AVSc presence. The risk of death for all causes was increased in AVSc patients, and this was even stronger in AVSc patients with a mixed-fibrotic plaque. Finally, AVSc further adds to the prediction capability of all-cause mortality on top of eGFR. Taking together, our data suggest that the presence of AVSc combined with mildly impaired renal function may be used to better stratify the risk of patients undergoing CEA surgery.

The development of AVSc, as well as carotid atherosclerosis, share similar pathophysiological processes such as endothelial dysfunction, chronic inflammation, fibrosis, and calcification⁷⁷. Currently, the prevalence of AVSc in the general population is about 30% in subjects older than 65 years¹⁵⁶, while in patients with overt coronary atherosclerosis, AVSc reaches 50%¹⁶⁴. Of note, in our population, characterized by severe carotid atherosclerosis, the prevalence of AVSc exceeded 60%. Interestingly, the earliest manifestations of arterial injury, such as increased IMT and PVW as well as decreased FMD were found to be associated with AVSc¹⁶⁵. In addition, AVSc and IMT were shown to be predictors of cardiovascular events¹⁶⁵. At the same time, AVSc shows a significant association with the presence of atherosclerotic plaque and the degree of carotid artery stenosis, independently of CV clinical and echocardiographic risk factors¹⁶⁶. Even if we did not find any association between AVSc and the degree of carotid artery stenosis, the cumulative evidence indicates a continued correlation between AVSc and the carotid atherosclerosis process, from its sub-clinical form to the severe end-stage.

There are no doubts regarding the importance of better risk stratification of the symptomatic and asymptomatic patients who need carotid artery revascularization¹⁶⁷, given that the CEA is not a risk-free procedure, often associated with long-term outcomes such as the increased risk of ischemic stroke, cardiovascular events, and mortality^{168,169}. The risk of poor outcome after CEA depends on the baseline risk profile of the patients¹⁷⁰, and several different risk models and scores were aimed to investigate the predictors of morbidity and mortality after CEA¹⁷¹⁻¹⁷³. Our data

suggested that older age, low eGFR, and AVSc presence were associated with worst the 5 years survival. Age and chronic kidney disease (CKD) are well-proven independent risk predictors for poor outcomes or death after CEA^{172,174} and the correlation of AVSc prevalence with age is well-known¹⁶⁴. Nonetheless, there is no evidence in the literature on the relationship between impaired renal function and AVSc. However, patients with advanced aortic valve stenosis (AS) had an apparent association between kidney dysfunction and the faster AS progression¹⁷⁵. Moreover, the risk of AS development has been directly linked to eGFR levels¹⁷⁶. Our study adds to the current knowledge that preoperatively mildly impaired renal function is associated with AVSc (i.e., the earliest manifestation of CAVS) and their combination predicted all-cause mortality after CEA surgery.

In 1999, Otto et al.¹³⁴ discussed the association between AVSc and cardiovascular adverse clinical outcomes, suggesting that elderly patients had a 50% increased risk of death from cardiovascular causes. In addition, AVSc was defined as a potential cardiovascular risk marker in patients without the overt cardiovascular disease⁴⁴. The predictive ability of AVSc on short-term mortality in patients who underwent coronary artery revascularization was recently reported, suggesting that AVSc adds to a better risk assessment of these patients on top of EuroScore II¹⁷⁷. Furthermore, the results from a large meta-analysis of 31 studies, including 10,537 AVSc patients and 25,005 controls, showed the association of AVSc with CAD, stroke, and increased risk of cardiovascular mortality¹⁵⁷. However, there is currently no study available that focuses on the AVSc presence in patients requiring CEA. There is only one study, focused on patients with peripheral arterial disease undergoing vascular surgery, which showed no association between AVSc and long-term outcomes; however, only 21% of patients had carotid atherosclerosis that underwent CEA¹⁵⁰. In our study, we evaluated the association between AVSc and long-term all-cause mortality only in patients with carotid atherosclerosis requiring CEA and we found a 1.9-fold increase in mortality rate in patients with AVSc.

It has been shown that the composition of the plaque, in addition to the degree of stenosis¹⁷⁸, facilitates the pursuit of optimal management strategies and allows to determine patient negative outcomes after surgery¹⁷⁹. In particular, lipid-rich and low fibrotic plaques were associated with the worst prognosis after CEA surgery¹⁸⁰, long-term systemic cardiovascular outcomes¹⁸¹, and correlated with 5-year stroke risk prediction¹⁸². On the other hand, calcified plaques causing stenosis were found to be

more stable and were associated with less ischemic symptoms than is non-calcified ones¹⁷⁸. Indeed, a low plaque calcium score was found to be an independent predictor for recurrent stenosis at a 1-year follow-up after CEA¹⁷⁹, indicating possible protective properties of plaque calcification¹⁸³. To better understand the role of AVSc in the poor clinical outcomes in CEA patients, we stratified our study population by plaque type. Our results indicated that only mixed-fibrotic plaque was linked to long-term mortality with a 13 time increased risk in CEA patients with AVSc. Fibrosis is one of the main processes involved in the development of both atherosclerosis and AVSc, being associated with increased plaque vulnerability and AVSc progression^{183,184}. Unfortunately, the impact and contribution of these pathophysiological processes before and during the progression of both carotid atherosclerosis and AVSc are poorly studied¹⁸⁴. However, chronic systemic inflammation could be a key mechanism responsible for the worst outcome in patients with a mixed-fibrotic plaque and AVSc. Taking all these data together, our study suggests that aortic valve morphology, evaluated by echocardiography, could improve the risk stratification of patients with carotid atheromatous mixed-fibrotic plaque requiring CEA.

4.2.1 Clinical Relevance

Our findings may have relevant clinical implications since patients with AVSc may necessitate a deeper evaluation and a stricter cardiovascular follow-up compared to patients without signs of AVSc. Furthermore, we hypothesize that the early assessment of AVSc could add to the best medical treatment, including pharmacological treatment, risk factor control, and lifestyle coaching, allowing more accurate and personalized clinical monitoring as well as the management of patients with asymptomatic carotid stenosis even before reaching surgical criteria for CEA or endovascular intervention. That being said, further studies are needed to assess the clinical significance of AVSc regarding the cause of death and inter-current clinical events, such as non-fatal myocardial infarction and cerebrovascular events, in patients with carotid atherosclerosis who require CEA or endovascular intervention.

4.3 Enduring ROS emission causes aberrant protein S-glutathionylation transitioning human aortic valve cells from a sclerotic to a stenotic phenotype

Our study cements the view that escalating ROS emission in valve leaflets underscores the human CAVS involution from a sclerotic to a stenotic phenotype, a switch paralleled by a similar progressive increment in P-SSG deposition. Moreover, present findings suggest that borne as a compensatory system to face an excessive oxidative burden, P-SSG favors the switch of human VECs from an innate endothelial phenotype to a damaged one, paving, in turn, the way to calcium deposition. Relevant from a translational perspective, our study unearths that the antioxidant compound, N-acetyl-L-cysteine (NAC), effectively prevents P-SSG in VECs and their subsequent calcification (**Figure 8 d**).

Aortic stenosis (AS), the end-stage phase of calcific aortic valve stenosis (CAVS), is the third most common cardiovascular ailment after hypertension and coronary artery disease, being the most prevalent heart valve disorder in the western world^{29,185}. The AS prevalence is about 3% in the 65 years old population and above, increasing with advancing age³⁰: from 0.2% in the 50–59-year group to 9.8% in those aged 80–89 years¹⁸⁶. Despite severe AS is estimated to march up by 2.4-fold in year 2040 and likely escalating more than triple by 2060¹⁸⁶, no current effective pharmacological treatment for preventing or arresting CAVS progression is available at the moment; therefore, resting on surgical or transcatheter aortic valve replacement as the sole available options nowadays. CAVS remains a debilitating disease with a massive socioeconomic burden¹⁸⁷.

CAVS is a complex, active progressive disease characterized by a cascade of cellular events that initially cause fibrotic thickening (*i.e.*, AVSc), followed by the extensive calcification of the aortic valve leaflets (*i.e.*, AS). This involution entails several tissue/cellular alterations, such as endothelial dysfunction, inflammatory cell recruitment, and valve interstitial cell phenotypic switching in osteoblast-like phenotype^{37,188}. At least in part, these perturbations directly emanate from specific molecular processes, such as TGF- β signaling, bone morphogenetic protein signaling, wnt/ β -catenin signaling, notch signaling, MMPs, and ROS³⁷. Our data add to this scenario a significant feature: despite the upregulation of some non-enzymatic antioxidant systems, such as the glutathione one, ROS emission from human aortic

leaflets continues to grow with time, marking the transition from a sclerotic to a stenotic phenotype. Until now, however, very few studies attempted to connect altered valve cell redox conditions to CAVS final stage (*i.e.*, AS)^{80,92}. Nevertheless, in some instances, the strategy adopted to index ROS contribution was sub-optimal, as in the case of the use of dihydroethidium fluorescence to detect superoxide that is not so specific¹⁸⁹. While in other studies, ROS contribution was inferred by changes in superoxide dismutase expression^{80,91,92}. Paradoxically, no studies have delved into the glutathione system yet, *i.e.*, the primary non-enzymatic antioxidant system and reducing equivalents' providers in the cell^{190,191}. GSH is present in millimolar concentrations in eukaryotic cells' cytosol¹⁹¹ and, under normal conditions, the GSH/GSSG ratio ranges from 30:1 to 100:1¹⁹². During high ROS emission conditions, cells put up reversible S-glutathionylation to guard highly reactive cysteine residues from permanent oxidative modifications⁸⁸. Here, we performed, for the first time, a direct GSH/GSSG ratio assessment in human endothelial cells isolated from aortic valves at different stages of the disease, employing a state-of-art approach, such as LC-MS/MS, previously developed in our lab¹⁶⁴. Our studies in human valves reveal a progressive GSH/GSSG ratio increment, during CAVS disease, suggesting adaptive efforts to face the enduring oxidizing conditions occurring in stenotic valve cells. Furthermore, we proved the centrality of persistently elevated ROS emission in CAVS involution towards a stenotic phenotype using an *in vitro* approach. In this model, both induction and scavenging of P-SSG via de-glutathionylation are still at play. When removed from the *in situ* highly-oxidizing conditions occurring in the diseased human valve tissues and placed in a culture system where de-glutathionylation can intervene, human stenotic valve endothelial cells showcase protein S-glutathionylation levels superimposable to those found in control valves. These data suggest that *in situ* persistent P-SSG levels, in human stenotic cells, act as a "redoxstat"; at the same time, they testify the persistence of elevated ROS emission experienced by the valve tissue. In the end, P-SSG can ultimately serve to counter some ROS-mediated effects in valve cells. For instance, in the present case, it may explain why human stenotic cells display reduced levels of apoptosis compared to both controls and sclerotic cells. Notwithstanding, persistently elevated ROS and P-SSG levels in stenotic cells - the latter likely due to a reduced de-glutathionylation ability - seemingly factor in the morphological/functional switch of the endothelial phenotype. Ultimately, these alterations predispose human stenotic cells to calcium deposition. In aid of this

contention come data evaluating the expression levels of CD31 and MMP2. CD31 is a classic endothelial marker, and its loss is a possible consequence of an endothelial to mesenchymal transition¹⁹³. At the same time, here, we report upregulation of MMP2, a protein involved in matrix remodeling that is overexpressed whenever cells acquire invasive properties, thus the possibility of migrating towards the aortic valve's inner layers¹⁹⁴.

Present studies with NAC further corroborate the concept that unremitted ROS emission from valve cells favors CAVS progression towards stenosis. This exogenous thiol compound is an acetaminophen poisoning antidote¹⁹⁵, ROS scavenger, and reduced glutathione precursor¹⁹⁶. NAC impact has been tested in a plethora of cardiovascular disease models, highlighting its effectiveness in countering oxidative stress, attenuating fibrosis¹⁹⁷, ischemia-reperfusion injury¹⁹⁸, and apoptosis¹⁹⁹. NAC reduces systemic and myocardial oxidative stress when it comes to CAVS pathophysiology by restoring total myocardial glutathione, while attenuating myocardial fibrosis in an aortic stenosis rat model¹⁹⁷. Furthermore, it can also halt fibrosis during AS progression in mice with the genetic deletion of the low-density lipoprotein (LDL)²⁰⁰. However, these models are flawed by several limitations, including the different anatomical structures of the aortic valve of rodents *vs.* humans and the need to introduce dietary regimens or genetic interventions to induce valve calcification²⁰¹, all potential confounders. Present evidence showing that NAC prevents the modification of cysteines in the valve endothelial cells, their S-glutathionylation, and calcification attests the relevance of countering ROS progressive accumulation.

Several clinical trials tested NAC effectiveness in cardiovascular diseases, both as a short- and long-term treatment²⁰²⁻²⁰⁶. Tepel and colleagues, for instance, showed NAC-induced protection towards composite cardiovascular end-points, such as fatal and nonfatal myocardial infarction, cardiovascular disease death, need for coronary angioplasty, coronary bypass surgery, and coronary bypass surgery, and ischemic stroke, or peripheral vascular disease with amputation²⁰⁶. Interestingly, NAC attenuates *in vivo* oxidation of injected human LDL, eventually reducing atherosclerotic plaque formation²⁰⁴. Notably, oxidized LDL fuel CAVS progression through an osteogenic program²⁰⁷. Also, worth mentioning is that NAC, at intermediate dosages (1200 mg daily) and given chronically (12-24 months), shows no major side effects^{29,33}]. Besides its antioxidant properties, NAC can decrease the

gelatinolytic activity of MMPs, with effects that could be due to NAC's ability to scavenging ROS or direct interaction with gelatinases²⁰⁸. Thus, there is ample theoretical room for thinking that NAC, perhaps as an adjuvant, could contribute to preserve the valve endothelium preventing its progression towards a stenotic phenotype. However, this possibility remains to be tested. Consequently, NAC has been used here just as a proof of principle.

This study comes with some limitations; thus, aspects that warrant future, more in-depth investigation. First, here we evaluated P-SSG with a Western blot approach that revealed a single sharp band at the molecular weight of β -actin, as previously described by our group¹⁶⁴. In so doing, we could not detect P-SSG on other proteins, possibly due to the antibody's sensitivity. However, our data align with the literature where P-SSG causes structural and functional proteins' modifications^{87,89}. Besides, we did not delve into the endothelium/interstitium crosstalk. Indeed, for the present study, we aimed to unveil endothelial cell contribution (and of their transformation) to CAVS progression from a sclerotic to a stenotic phenotype. In essence, we are not naively saying that the present findings exhaust all possible mechanistic explanations, in this sense.

4.3.1 Conclusion

Our study demonstrates that unremitting ROS emission from endothelial cells, along with a P-SSG build-up, occurs and accounts, at least in part, for the morphological/functional changes occurring in the human aortic valves when they switch from sclerotic to stenotic, increasing the chance of calcification. Our *in vitro* data suggest that it is possible to de-activate this mechanism, leveraging on endogenous signaling or exogenous compounds able to blunt ROS emission and counter MMP expression/activity, as suggested herein by the use of NAC. In our view, two main complementary avenues should be pursued to arrest aortic valve disease progression. First, blunting ROS emission to reduce the need for P-SSG; then, preserving the endothelium integrity/function. In the end, both measures will conjure up to prevent the onset of maladaptive processes, ultimately paving the way to calcium deposition, and thus stenosis.

4.4 MiRNA profiling revealed enhanced susceptibility to oxidative stress of endothelial cells from bicuspid aortic valve

In this study, we show differences in the basal expression of several miRNAs between ECs isolated from bicuspid and tricuspid stenotic aortic valves. The functional pathway analyses highlighted a potential alteration of the hydrogen peroxide metabolism pathway, leading to excessive DNA damage, and of the intrinsic apoptotic signaling pathway. Indeed, experimental evidences confirmed that BAV ECs have an impairment to metabolize hydrogen peroxide leading to an increment in apoptosis. Finally, miR-328-3p over-expression was able to exacerbate oxidative stress damage in TAV ECs, while miR-328-3p inhibition was able to ameliorate oxidative stress damage in BAV ECs. This is, to our knowledge, the first experimental *in vitro* study showing that biological processes occurring at the endothelium level and involved in the initial stages of CAVS differ from bicuspid and tricuspid valves.

In the present study, eight miRNAs, involved in the regulation of cellular response to oxidative stress and DNA damage stimulus via p53 and of the intrinsic apoptotic signaling pathway, showed a different pattern of expression in ECs derived from BAV patients compared to ECs from TAV patients. There is accumulating evidence that dysregulation of miRNA expression patterns could alter valve tissue homeostasis leading to CAVS⁹⁵. Coffey et al.²⁰⁹ performed an integrated miRNA and mRNA analysis in CAVS patients confirming previous knowledge of the disease processes; however, distinction between bicuspid and tricuspid aortic valve anatomy was not evaluated since the study included only TAV patients. Furthermore, Martinez-Micaelo et al.⁹⁵, using an integrative bioinformatics approach, showed that circulating miRNA expression profile associated with secreted endothelial micro-particles differed between patients with bicuspid and tricuspid aortic valve anatomy. In this context, our data on miRNA expression levels in isolated ECs and differences between BAV and TAV suggest that dysregulated metabolism of reactive oxygen species leading to apoptosis might contribute to trigger aortic valve degeneration.

We evaluated the effect of oxidative stress susceptibility by assessing expression levels of anti-oxidant enzyme and the amount of DNA DSB after H₂O₂ treatment in ECs from BAV and TAV patients. GPX3 and SRXN1, both involved in the reduction of H₂O₂, were expressed at lower levels in BAV compared to TAV ECs. We also confirmed that BAV ECs had an impairment on these anti-oxidant enzymes since the amount of

DNA DSB were drastically increased in ECs from BAV than from TAV patients. A recent study evaluating smooth-muscle cells (SMC) derived from thoracic aortic aneurysm (TAA) with a BAV phenotype showed enhanced DNA damage compared to SMCs from TAA TAV²¹⁰. In addition, Miller et al.⁹² provided evidences that H₂O₂ levels were markedly elevated in calcified regions of stenotic aortic valves and this increment was due at least in part to reduction in expression and activity of antioxidant enzymes; however, no data are available on calcified BAV. Nevertheless, the presented data fits well with what it has been previously reported regarding the mechanism of BAV disease since the early event of abnormal oxidative stress resulted in a decrease of Notch1 function and an increase in Lrp5 expression which activates calcification processes involving VICs²¹¹.

Aberrant oxidative stress leads to DNA damage and consequently to apoptosis. We noticed that BAV ECs had a sustained apoptosis activation when compared to TAV ECs and this difference was exacerbated by oxidative stress stimulus leading to a reduced survival rate. In this regard, Algret et al.²¹² observed that BAV patients presented elevated circulating endothelial microparticles compared to TAV patients that were significantly reduced after aortic valve replacement, indicating a persistent and increased aortic valve endothelial damage in BAV patients. The authors concluded that this endothelial damage was due to endothelial destruction rather than apoptosis since the percentage of endothelial micro-particles expressing annexin V was comparable between the groups. However, the absolute value of annexin V positive endothelial micro-particles was twice in BAV compared to TAV patients, indicating that both mechanical destruction and apoptosis might concur in the observed aortic valve endothelial damage.

4.4.1 Conclusion

The present data showed molecular differences in oxidative stress susceptibility, DNA damage magnitude, and apoptosis induction between ECs derived from BAV and TAV patients. This could indicate that not only altered blood shear stress is involved in the endothelial damage occurring in BAV patients but also that biological factors such as aberrant oxidative stress leading to apoptosis concur to the degeneration of BAV.

4.5 Cyclophilin A inhibition as potential treatment of human aortic valve calcification

This study addressed for the first time, to our knowledge, a strong, direct, and detrimental *in vitro* involvement of CyPA in the modulation of the calcific process in patients affected by severe AS. Specifically, we discovered that i) in AS leaflets CyPA is overexpressed and co-localized with calcium deposits; ii) VICs isolated from AS leaflets were able to produce and release CyPA under pro-calcifying stimuli, in direct correlation with the amount of deposited calcium; iii) *in vitro* exogenous CyPA treatment led to an increased calcium deposition, while its direct inhibition strongly abolished the VIC calcification potential. This study highlights *in vitro* evidence on direct exacerbation of calcium deposition exerted by CyPA and, more importantly, shows an effective molecular strategy based on CyPA inhibition, suitable for further *in vivo* insights as a potential therapeutic approach for limiting detrimental calcification of AS leaflets. In such life-threatening condition as AS, the discovery of novel biological targets is not only a scientific imperative but also a crucial clinical need. Indeed, to date, the transcatheter (TAVR) or surgical aortic valve replacement (sAVR) are the only therapeutic options of choice for AS patients, because of several pharmacological drug inefficacy^{46,213,214}. More specifically, since similar molecular events, including the inflammatory process, are involved in the pathological development of both AS and atherosclerosis^{215,216} a number of studies focused on statin effects as a potential therapeutic drug to delay the aortic valve calcification progression. Although by literature have been suggested effects of statin treatment on VICs in down-regulating NF- κ B phosphorylation²¹⁷, the efficacy of statins on AS patients acquires controversial aspects. A number of clinical trials adopting statins with AS patents failed, since randomized controlled showed no difference between drug and placebo groups in terms of AS regression/prevention^{62,218-220}. As for atherosclerosis, also hypertension disease presents several contact points with AS. Both these pathologies are, in fact, age-related diseases and are, additionally, often coexistent for a long period of time before the start of treatment. Hypertensive disease, in terms of angiotensin II (AngII) over-expression and over-activity²²¹, plays per se a key role as primary pathological stimulus for the valve endothelial cell impairment⁴, which is the origin site of inflammatory cascade and reactive oxygen species production, both determining aortic valve calcification and AS²¹³. Similar to statins,

also anti-hypertensive drugs, and more specifically AngII receptor blockers, showed not encouraging results as potentially useful pharmacological compounds to prevent or limiting aortic valve calcification²¹³.

Supporting the hypothesis to investigate, and possibly discover, other biological actors able to provide future therapeutic targets, our results identified CyPA as an excellent candidate to cover this fundamental role. Among the protein family of cyclophilins, CyPA is the most represented member, with a wide spectrum of functions, in the nucleus and in the cytosol, as well as a secreted factor. Previous studies provided strong evidence on the dysfunctional ROS effects in an early asymptomatic stage of calcific aortic valve disease, as well as on CyPA secretion by cells exposed to AngII and ROS stimuli^{108,147,222,223}. Furthermore, several studies already have deeply investigated in vitro both the CyPA secretion after oxidative stress stimulus¹⁰⁸ and, viceversa, the CyPA-dependent increase in ROS production¹¹⁴. A detrimental role of CyPA over-expression has been reported in several cellular and molecular events (e.g. endothelial cell dysfunction), most of which involved in cardiovascular diseases^{108,109,116,224}. Interestingly, it has been already studied that CyPA in platelets during arterial thrombosis acts as an important calcium regulator, by activation of channels determining its entry from extracellular milieu²²⁵. All these features are strongly ascribable to our AS disease model, since our results confirm a strong gene and protein up-regulation of CyPA, which expression is localized exactly at the valve interstice, where the calcific lesion is massive. In addition, our results provided also a strong correlation between the in vitro CyPA release and calcium deposition by VICs, the cell type differentiating into osteoblast-like and thus responsible for calcific nodule formation in AS. Interestingly, CyPA was primarily identified as the immunosuppressive drug cyclosporine A (CsA) endogenous ligand^{226,227} and the CsA-CyPA complex prevents phosphoserine phosphatase reaction catalyzed by calcineurin²²⁸. In our pathological context, the inhibition of this enzymatic reaction is important for two complementing reasons. The first concerns the decreased levels of the calcineurin-mediated enzymatic reaction product, i.e. the inorganic phosphate²²⁸, responsible for in vitro calcification of VICs. The second reason regards the calcineurin inhibition, leading to the blockade of NFAT nuclear translocation, which prevents, in turn, the downstream production of pro-inflammatory mediators²²⁹. Altogether, these molecular events suggest the effectiveness in treating cells with CsA or non-immunosuppressive analogue molecules to beneficially regulate the

calcineurin-dependent pathway, and several studies, over the time, already reported this valuable effect^{230,231}. Finally, we provided in this study, for the first time, encouraging data on the effects of a CsA analogue (MM284) treatment on the reduction of VIC calcification potential after treatment. In detail, our results clearly showed the strong effectiveness of MM284 in limiting calcium deposition by extracellular CyPA inhibition and depicted the optimistic potential in opening new roads on novel pharmacological approaches targeted to AS, by shedding light on possible translational in vivo use of MM284. Mechanistic studies revealed that CyPA genetic deletion in several cardiovascular disease in vivo models reduced inflammation, oxidative stress, and extracellular matrix degradation¹⁰⁶. Furthermore, other pharmacological studies already provided evidence on CyPA inhibition beneficial role in different cardiovascular diseases, such as myocarditis²³², thrombi formation²³³, pro-fibrotic processes in thoracic aortic aneurysm²³⁴, as well as, more importantly, in vascular calcification¹¹³.

4.5.1 Conclusion

Our results demonstrate that i) CyPA levels are highly expressed in interstitial calcific nodules of AS leaflets, ii) VICs are responsible for CyPA up-regulation, especially in pro-calcifying conditions, iii) levels of secreted CyPA directly correlate with calcium deposition, iv) in vitro exogenous administration of CyPA amplifies the calcium deposition in pro-calcifying condition, and v) MM284 reduces pro-calcification effects of CyPA, by inhibiting its pathological function. Thus, our work defines, for the first time to our knowledge, the strong involvement of CyPA as exacerbating factor of pathological molecular events leading to AS development and opens to possible future therapeutic strategies to solve the unmet need of an etiological pharmacological treatment for AS patients.

4.6 Genetic and in vitro inhibition of PCSK9 and calcific aortic valve stenosis

Previous genetic association studies observed that carriers of genetic variants in PCSK9 associated with low LDL-C levels are at lower risk of a broad range of atherosclerotic cardiovascular diseases²³⁵. In this study, we confirmed that variants in PCSK9 associated with lower LDL-C levels are also associated with a lower risk of

CAVS, and for the first time to our knowledge, we demonstrated that PCSK9 is present in human aortic valves. The potential benefits of targeting PCSK9 for CAVS prevention were also supported by our in vitro experimental approach, showing that treating VICs with a neutralizing PCSK9 antibody reduced calcium accumulation in VICs under pro-osteogenic stimuli. In a previous report of 2,373 individuals included in a nested case-control design of the EPIC-Norfolk study, we have shown that carriers of the PCSK9R46L variant had lower levels of nuclear magnetic resonance spectroscopy-measured VLDL and LDL particle concentrations and lower Lp(a)²³⁶. In another study, Sliz et al.²³⁷ reported no impact of this variant on VLDL lipid measures. In our study, we found a significant association between PCSK9 variants and CAVS in the UK Biobank. However, given the relatively small number of CAVS cases in the UK Biobank (1,350), these results are not definitive, and additional studies are needed to confirm these findings and to determine whether the impact of reduced PCSK9 function is independent of the presence of concomitant CAD because approximately one-half of the patients with CAVS also have CAD. Our results confirm those of the Copenhagen cohorts¹³² and extend our previous observations that *Pcsk9*^{-/-} mice are less likely to develop aortic valve calcification than wild-type mice¹³³. Results of our previous study, confirmed by the present one, also suggest that there is a significant correlation between the amount of PCSK9 produced by VICs and the extent of VIC calcification¹³³.

4.6.1 Conclusion

We performed a large genetic association study as well as a series of experiments showing that variation in PCSK9 is linked with low cholesterol levels and protection against CAVS and that PCSK9 expression was higher in explanted aortic valves from patients with versus without CAVS. In human VICs, PCSK9 expression and secretion were induced by an exposure to a pro-osteogenic milieu and a PCSK9 neutralizing antibody reduced VIC calcium levels by more than 50%, thereby providing experimental support to our genetic findings. Although our results highlight the potential role of PCSK9 in the etiology of CAVS, the ultimate proof of causality and clinical benefit would be a clinical trial showing that PCSK9 inhibition is linked with a reduction in valvular outcomes. However, to our knowledge, no such trials are currently planned. An ongoing trial is currently testing the hypothesis that PCSK9 inhibition will reduce aortic valve macrocalcification (measured by computed

tomography) and microcalcification (measured by ¹⁸F-NaF positron-emission tomography/computed tomography) in patients with mild-to-moderate CAVS (PCSK9 Inhibitors in the Progression of Aortic Stenosis; NCT03051360). Interestingly, an exploratory analysis of the FOURIER trial recently revealed that PCSK9 inhibition with evolocumab could decrease CAVS incidence in patients with cardiovascular disease²³⁸.

5. Bibliography

- 1 Sacks, M. S., David Merryman, W. & Schmidt, D. E. On the biomechanics of heart valve function. *J Biomech* **42**, 1804-1824, doi:10.1016/j.jbiomech.2009.05.015 (2009).
- 2 Levin, A. R. *et al.* Intracardiac pressure-flow dynamics in isolated ventricular septal defects. *Circulation* **35**, 430-441, doi:10.1161/01.cir.35.3.430 (1967).
- 3 Anderson, R. H. Clinical anatomy of the aortic root. *Heart* **84**, 670-673, doi:10.1136/heart.84.6.670 (2000).
- 4 Perrucci, G. L. *et al.* Pathophysiology of Aortic Stenosis and Mitral Regurgitation. *Compr Physiol* **7**, 799-818, doi:10.1002/cphy.c160020 (2017).
- 5 Anderson, R. H. The surgical anatomy of the aortic root. *Multimed Man Cardiothorac Surg* **2007**, mmcts 2006 002527, doi:10.1510/mmcts.2006.002527 (2007).
- 6 Chen, J. H. & Simmons, C. A. Cell-matrix interactions in the pathobiology of calcific aortic valve disease: critical roles for matricellular, matricrine, and matrix mechanics cues. *Circ Res* **108**, 1510-1524, doi:10.1161/CIRCRESAHA.110.234237 (2011).
- 7 Stella, J. A. & Sacks, M. S. On the biaxial mechanical properties of the layers of the aortic valve leaflet. *J Biomech Eng* **129**, 757-766, doi:10.1115/1.2768111 (2007).
- 8 Mongkoldhumrongkul, N., Yacoub, M. H. & Chester, A. H. Valve Endothelial Cells - Not Just Any Old Endothelial Cells. *Curr Vasc Pharmacol* **14**, 146-154, doi:10.2174/1570161114666151202205504 (2016).
- 9 Tao, G., Kotick, J. D. & Lincoln, J. Heart valve development, maintenance, and disease: the role of endothelial cells. *Curr Top Dev Biol* **100**, 203-232, doi:10.1016/B978-0-12-387786-4.00006-3 (2012).
- 10 Butcher, J. T. & Nerem, R. M. Valvular endothelial cells and the mechanoregulation of valvular pathology. *Philos Trans R Soc Lond B Biol Sci* **362**, 1445-1457, doi:10.1098/rstb.2007.2127 (2007).
- 11 Farivar, R. S. *et al.* Transcriptional profiling and growth kinetics of endothelium reveals differences between cells derived from porcine aorta versus aortic valve. *Eur J Cardiothorac Surg* **24**, 527-534, doi:10.1016/s1010-7940(03)00408-1 (2003).
- 12 Deck, J. D. Endothelial cell orientation on aortic valve leaflets. *Cardiovasc Res* **20**, 760-767, doi:10.1093/cvr/20.10.760 (1986).

- 13 Simmons, C. A., Grant, G. R., Manduchi, E. & Davies, P. F. Spatial heterogeneity of endothelial phenotypes correlates with side-specific vulnerability to calcification in normal porcine aortic valves. *Circ Res* **96**, 792-799, doi:10.1161/01.RES.0000161998.92009.64 (2005).
- 14 Faure, E. *et al.* Side-dependent effect in the response of valve endothelial cells to bidirectional shear stress. *Int J Cardiol* **323**, 220-228, doi:10.1016/j.ijcard.2020.08.074 (2021).
- 15 Gendron, N. *et al.* Human Aortic Valve Interstitial Cells Display Proangiogenic Properties During Calcific Aortic Valve Disease. *Arterioscler Thromb Vasc Biol* **41**, 415-429, doi:10.1161/ATVBAHA.120.314287 (2021).
- 16 Lis, G. J. *et al.* Identification of CD34+/PGDFRalpha+ Valve Interstitial Cells (VICs) in Human Aortic Valves: Association of Their Abundance, Morphology and Spatial Organization with Early Calcific Remodeling. *Int J Mol Sci* **21**, doi:10.3390/ijms21176330 (2020).
- 17 Liu, A. C., Joag, V. R. & Gotlieb, A. I. The emerging role of valve interstitial cell phenotypes in regulating heart valve pathobiology. *Am J Pathol* **171**, 1407-1418, doi:10.2353/ajpath.2007.070251 (2007).
- 18 Rabkin-Aikawa, E., Farber, M., Aikawa, M. & Schoen, F. J. Dynamic and reversible changes of interstitial cell phenotype during remodeling of cardiac valves. *J Heart Valve Dis* **13**, 841-847 (2004).
- 19 Rabkin-Aikawa, E. *et al.* Clinical pulmonary autograft valves: pathologic evidence of adaptive remodeling in the aortic site. *J Thorac Cardiovasc Surg* **128**, 552-561, doi:10.1016/j.jtcvs.2004.04.016 (2004).
- 20 Chester, A. H. & Taylor, P. M. Molecular and functional characteristics of heart-valve interstitial cells. *Philos Trans R Soc Lond B Biol Sci* **362**, 1437-1443, doi:10.1098/rstb.2007.2126 (2007).
- 21 Ma, H., Killaars, A. R., DelRio, F. W., Yang, C. & Anseth, K. S. Myofibroblastic activation of valvular interstitial cells is modulated by spatial variations in matrix elasticity and its organization. *Biomaterials* **131**, 131-144, doi:10.1016/j.biomaterials.2017.03.040 (2017).
- 22 Rabkin, E. *et al.* Activated interstitial myofibroblasts express catabolic enzymes and mediate matrix remodeling in myxomatous heart valves. *Circulation* **104**, 2525-2532, doi:10.1161/hc4601.099489 (2001).

- 23 El-Hamamsy, I. *et al.* Endothelium-dependent regulation of the mechanical properties of aortic valve cusps. *J Am Coll Cardiol* **53**, 1448-1455, doi:10.1016/j.jacc.2008.11.056 (2009).
- 24 Chen, J. H., Chen, W. L., Sider, K. L., Yip, C. Y. & Simmons, C. A. beta-catenin mediates mechanically regulated, transforming growth factor-beta1-induced myofibroblast differentiation of aortic valve interstitial cells. *Arterioscler Thromb Vasc Biol* **31**, 590-597, doi:10.1161/ATVBAHA.110.220061 (2011).
- 25 Gould, S. T., Darling, N. J. & Anseth, K. S. Small peptide functionalized thiol-ene hydrogels as culture substrates for understanding valvular interstitial cell activation and de novo tissue deposition. *Acta Biomater* **8**, 3201-3209, doi:10.1016/j.actbio.2012.05.009 (2012).
- 26 Balachandran, K., Sucosky, P., Jo, H. & Yoganathan, A. P. Elevated cyclic stretch alters matrix remodeling in aortic valve cusps: implications for degenerative aortic valve disease. *Am J Physiol Heart Circ Physiol* **296**, H756-764, doi:10.1152/ajpheart.00900.2008 (2009).
- 27 Butcher, J. T. & Nerem, R. M. Valvular endothelial cells regulate the phenotype of interstitial cells in co-culture: effects of steady shear stress. *Tissue Eng* **12**, 905-915, doi:10.1089/ten.2006.12.905 (2006).
- 28 Peeters, F. *et al.* Calcific aortic valve stenosis: hard disease in the heart: A biomolecular approach towards diagnosis and treatment. *Eur Heart J* **39**, 2618-2624, doi:10.1093/eurheartj/ehx653 (2018).
- 29 Lindman, B. R. *et al.* Calcific aortic stenosis. *Nat Rev Dis Primers* **2**, 16006, doi:10.1038/nrdp.2016.6 (2016).
- 30 Pazianas, M. Calcific aortic stenosis. *N Engl J Med* **360**, 85; author reply 85-86, doi:10.1056/NEJMc082192 (2009).
- 31 O'Brien, K. D. Epidemiology and genetics of calcific aortic valve disease. *J Investig Med* **55**, 284-291, doi:10.2310/6650.2007.00010 (2007).
- 32 Otto, C. M. Calcific aortic valve disease: outflow obstruction is the end stage of a systemic disease process. *Eur Heart J* **30**, 1940-1942, doi:10.1093/eurheartj/ehp175 (2009).
- 33 Freeman, R. V. & Otto, C. M. Spectrum of calcific aortic valve disease: pathogenesis, disease progression, and treatment strategies. *Circulation* **111**, 3316-3326, doi:10.1161/CIRCULATIONAHA.104.486738 (2005).

- 34 Stewart, B. F. *et al.* Clinical factors associated with calcific aortic valve disease. Cardiovascular Health Study. *J Am Coll Cardiol* **29**, 630-634, doi:10.1016/s0735-1097(96)00563-3 (1997).
- 35 Bakaeen, F. G., Rosengart, T. K. & Carabello, B. A. Aortic Stenosis. *Ann Intern Med* **166**, ITC1-ITC16, doi:10.7326/AITC201701030 (2017).
- 36 Katz, R. *et al.* Relationship of metabolic syndrome with incident aortic valve calcium and aortic valve calcium progression: the Multi-Ethnic Study of Atherosclerosis (MESA). *Diabetes* **58**, 813-819, doi:10.2337/db08-1515 (2009).
- 37 Poggio, P. *et al.* MiRNA profiling revealed enhanced susceptibility to oxidative stress of endothelial cells from bicuspid aortic valve. *J Mol Cell Cardiol* **131**, 146-154, doi:10.1016/j.yjmcc.2019.04.024 (2019).
- 38 Siu, S. C. & Silversides, C. K. Bicuspid aortic valve disease. *J Am Coll Cardiol* **55**, 2789-2800, doi:10.1016/j.jacc.2009.12.068 (2010).
- 39 Ram, D. *et al.* Concepts of Bicuspid Aortic Valve Repair: A Review. *Ann Thorac Surg* **109**, 999-1006, doi:10.1016/j.athoracsur.2019.09.019 (2020).
- 40 Wallby, L., Janerot-Sjoberg, B., Steffensen, T. & Broqvist, M. T lymphocyte infiltration in non-rheumatic aortic stenosis: a comparative descriptive study between tricuspid and bicuspid aortic valves. *Heart* **88**, 348-351, doi:10.1136/heart.88.4.348 (2002).
- 41 Kanwar, A., Thaden, J. J. & Nkomo, V. T. Management of Patients With Aortic Valve Stenosis. *Mayo Clin Proc* **93**, 488-508, doi:10.1016/j.mayocp.2018.01.020 (2018).
- 42 Yousry, M. *et al.* Aortic valve type and calcification as assessed by transthoracic and transoesophageal echocardiography. *Clin Physiol Funct Imaging* **35**, 306-313, doi:10.1111/cpf.12166 (2015).
- 43 Baumgartner, H. *et al.* Recommendations on the Echocardiographic Assessment of Aortic Valve Stenosis: A Focused Update from the European Association of Cardiovascular Imaging and the American Society of Echocardiography. *J Am Soc Echocardiogr* **30**, 372-392, doi:10.1016/j.echo.2017.02.009 (2017).
- 44 Gharacholou, S. M., Karon, B. L., Shub, C. & Pellikka, P. A. Aortic valve sclerosis and clinical outcomes: moving toward a definition. *Am J Med* **124**, 103-110, doi:10.1016/j.amjmed.2010.10.012 (2011).

- 45 Agmon, Y. *et al.* Aortic valve sclerosis and aortic atherosclerosis: different manifestations of the same disease? Insights from a population-based study. *J Am Coll Cardiol* **38**, 827-834, doi:10.1016/s0735-1097(01)01422-x (2001).
- 46 Carabello, B. A. & Paulus, W. J. Aortic stenosis. *Lancet* **373**, 956-966, doi:10.1016/S0140-6736(09)60211-7 (2009).
- 47 Ross, J., Jr. & Braunwald, E. Aortic stenosis. *Circulation* **38**, 61-67, doi:10.1161/01.cir.38.1s5.v-61 (1968).
- 48 Pibarot, P. & Dumesnil, J. G. Prosthetic heart valves: selection of the optimal prosthesis and long-term management. *Circulation* **119**, 1034-1048, doi:10.1161/CIRCULATIONAHA.108.778886 (2009).
- 49 David, T. E. Surgical treatment of aortic valve disease. *Nat Rev Cardiol* **10**, 375-386, doi:10.1038/nrcardio.2013.72 (2013).
- 50 Ross, D. N. Replacement of aortic and mitral valves with a pulmonary autograft. *Lancet* **2**, 956-958, doi:10.1016/s0140-6736(67)90794-5 (1967).
- 51 Hwang, Y. M. *et al.* Conduction disturbance after isolated surgical aortic valve replacement in degenerative aortic stenosis. *J Thorac Cardiovasc Surg* **154**, 1556-1565 e1551, doi:10.1016/j.jtcvs.2017.05.101 (2017).
- 52 Montaigne, D. *et al.* Daytime variation of perioperative myocardial injury in cardiac surgery and its prevention by Rev-Erbalpha antagonism: a single-centre propensity-matched cohort study and a randomised study. *Lancet* **391**, 59-69, doi:10.1016/S0140-6736(17)32132-3 (2018).
- 53 Leon, M. B. *et al.* Transcatheter or Surgical Aortic-Valve Replacement in Intermediate-Risk Patients. *N Engl J Med* **374**, 1609-1620, doi:10.1056/NEJMoa1514616 (2016).
- 54 Auensen, A. *et al.* Morbidity outcomes after surgical aortic valve replacement. *Open Heart* **4**, e000588, doi:10.1136/openhrt-2017-000588 (2017).
- 55 Everett, R. J., Clavel, M. A., Pibarot, P. & Dweck, M. R. Timing of intervention in aortic stenosis: a review of current and future strategies. *Heart* **104**, 2067-2076, doi:10.1136/heartjnl-2017-312304 (2018).
- 56 Smith, C. R. *et al.* Transcatheter versus surgical aortic-valve replacement in high-risk patients. *N Engl J Med* **364**, 2187-2198, doi:10.1056/NEJMoa1103510 (2011).

- 57 Parolari, A. *et al.* Do statins improve outcomes and delay the progression of non-rheumatic calcific aortic stenosis? *Heart* **97**, 523-529, doi:10.1136/hrt.2010.215046 (2011).
- 58 Rajamannan, N. M., Subramaniam, M., Caira, F., Stock, S. R. & Spelsberg, T. C. Atorvastatin inhibits hypercholesterolemia-induced calcification in the aortic valves via the Lrp5 receptor pathway. *Circulation* **112**, 1229-234, doi:10.1161/01.CIRCULATIONAHA.104.524306 (2005).
- 59 Novaro, G. M. *et al.* Effect of hydroxymethylglutaryl coenzyme a reductase inhibitors on the progression of calcific aortic stenosis. *Circulation* **104**, 2205-2209, doi:10.1161/hc4301.098249 (2001).
- 60 Dichtl, W. *et al.* Prognosis and risk factors in patients with asymptomatic aortic stenosis and their modulation by atorvastatin (20 mg). *Am J Cardiol* **102**, 743-748, doi:10.1016/j.amjcard.2008.04.060 (2008).
- 61 Rossebo, A. B. *et al.* Intensive lipid lowering with simvastatin and ezetimibe in aortic stenosis. *N Engl J Med* **359**, 1343-1356, doi:10.1056/NEJMoa0804602 (2008).
- 62 Cowell, S. J. *et al.* A randomized trial of intensive lipid-lowering therapy in calcific aortic stenosis. *N Engl J Med* **352**, 2389-2397, doi:10.1056/NEJMoa043876 (2005).
- 63 Chan, K. L. *et al.* Effect of Lipid lowering with rosuvastatin on progression of aortic stenosis: results of the aortic stenosis progression observation: measuring effects of rosuvastatin (ASTRONOMER) trial. *Circulation* **121**, 306-314, doi:10.1161/CIRCULATIONAHA.109.900027 (2010).
- 64 Myasoedova, V. A. *et al.* Novel pharmacological targets for calcific aortic valve disease: Prevention and treatments. *Pharmacol Res* **136**, 74-82, doi:10.1016/j.phrs.2018.08.020 (2018).
- 65 Rassa, A. & Zahr, F. Hypertension and Aortic Stenosis: A Review. *Curr Hypertens Rev* **14**, 6-14, doi:10.2174/1573402114666180416161326 (2018).
- 66 Marquis-Gravel, G., Redfors, B., Leon, M. B. & Genereux, P. Medical Treatment of Aortic Stenosis. *Circulation* **134**, 1766-1784, doi:10.1161/CIRCULATIONAHA.116.023997 (2016).
- 67 Chen, S. *et al.* Impact of renin-angiotensin system inhibitors on clinical outcomes in patients with severe aortic stenosis undergoing transcatheter

- aortic valve replacement: an analysis of from the PARTNER 2 trial and registries. *Eur Heart J* **41**, 943-954, doi:10.1093/eurheartj/ehz769 (2020).
- 68 Rajamannan, N. M. & Otto, C. M. Targeted therapy to prevent progression of calcific aortic stenosis. *Circulation* **110**, 1180-1182, doi:10.1161/01.CIR.0000140722.85490.EA (2004).
- 69 Rosenhek, R. *et al.* Statins but not angiotensin-converting enzyme inhibitors delay progression of aortic stenosis. *Circulation* **110**, 1291-1295, doi:10.1161/01.CIR.0000140723.15274.53 (2004).
- 70 Ardehali, R., Leeper, N. J., Wilson, A. M. & Heidenreich, P. A. The effect of angiotensin-converting enzyme inhibitors and statins on the progression of aortic sclerosis and mortality. *J Heart Valve Dis* **21**, 337-343 (2012).
- 71 Nishimura, R. A. *et al.* 2014 AHA/ACC Guideline for the Management of Patients With Valvular Heart Disease: executive summary: a report of the American College of Cardiology/American Heart Association Task Force on Practice Guidelines. *Circulation* **129**, 2440-2492, doi:10.1161/CIR.0000000000000029 (2014).
- 72 Otto, C. M. *et al.* 2020 ACC/AHA Guideline for the Management of Patients With Valvular Heart Disease: Executive Summary: A Report of the American College of Cardiology/American Heart Association Joint Committee on Clinical Practice Guidelines. *Circulation* **143**, e35-e71, doi:10.1161/CIR.0000000000000932 (2021).
- 73 Ochiai, T. *et al.* Renin-angiotensin system blockade therapy after transcatheter aortic valve implantation. *Heart* **104**, 644-651, doi:10.1136/heartjnl-2017-311738 (2018).
- 74 Inohara, T. *et al.* Association of Renin-Angiotensin Inhibitor Treatment With Mortality and Heart Failure Readmission in Patients With Transcatheter Aortic Valve Replacement. *JAMA* **320**, 2231-2241, doi:10.1001/jama.2018.18077 (2018).
- 75 Lerman, D. A., Prasad, S. & Alotti, N. Calcific Aortic Valve Disease: Molecular Mechanisms and Therapeutic Approaches. *Eur Cardiol* **10**, 108-112, doi:10.15420/ecr.2015.10.2.108 (2015).
- 76 Espinosa-Diez, C. *et al.* Role of glutathione biosynthesis in endothelial dysfunction and fibrosis. *Redox Biol* **14**, 88-99, doi:10.1016/j.redox.2017.08.019 (2018).

- 77 Otto, C. M., Kuusisto, J., Reichenbach, D. D., Gown, A. M. & O'Brien, K. D. Characterization of the early lesion of 'degenerative' valvular aortic stenosis. Histological and immunohistochemical studies. *Circulation* **90**, 844-853, doi:10.1161/01.cir.90.2.844 (1994).
- 78 Olsson, M. *et al.* Accumulation of T lymphocytes and expression of interleukin-2 receptors in nonrheumatic stenotic aortic valves. *J Am Coll Cardiol* **23**, 1162-1170, doi:10.1016/0735-1097(94)90606-8 (1994).
- 79 O'Brien, K. D. *et al.* Apolipoproteins B, (a), and E accumulate in the morphologically early lesion of 'degenerative' valvular aortic stenosis. *Arterioscler Thromb Vasc Biol* **16**, 523-532, doi:10.1161/01.atv.16.4.523 (1996).
- 80 Farrar, E. J., Huntley, G. D. & Butcher, J. Endothelial-derived oxidative stress drives myofibroblastic activation and calcification of the aortic valve. *PLoS One* **10**, e0123257, doi:10.1371/journal.pone.0123257 (2015).
- 81 Bubb, K. J., Birgisdottir, A. B., Tang, O., Hansen, T. & Figtree, G. A. Redox modification of caveolar proteins in the cardiovascular system- role in cellular signalling and disease. *Free Radic Biol Med* **109**, 61-74, doi:10.1016/j.freeradbiomed.2017.02.012 (2017).
- 82 Elahi, M. M., Kong, Y. X. & Matata, B. M. Oxidative stress as a mediator of cardiovascular disease. *Oxid Med Cell Longev* **2**, 259-269, doi:10.4161/oxim.2.5.9441 (2009).
- 83 Birben, E., Sahiner, U. M., Sackesen, C., Erzurum, S. & Kalayci, O. Oxidative stress and antioxidant defense. *World Allergy Organ J* **5**, 9-19, doi:10.1097/WOX.0b013e3182439613 (2012).
- 84 Haenen, G. R. & Bast, A. Glutathione revisited: a better scavenger than previously thought. *Front Pharmacol* **5**, 260, doi:10.3389/fphar.2014.00260 (2014).
- 85 Asensi, M. *et al.* Ratio of reduced to oxidized glutathione as indicator of oxidative stress status and DNA damage. *Methods Enzymol* **299**, 267-276, doi:10.1016/s0076-6879(99)99026-2 (1999).
- 86 Emdin, M., Pompella, A. & Paolicchi, A. Gamma-glutamyltransferase, atherosclerosis, and cardiovascular disease: triggering oxidative stress within the plaque. *Circulation* **112**, 2078-2080, doi:10.1161/CIRCULATIONAHA.105.571919 (2005).

- 87 Giustarini, D., Rossi, R., Milzani, A., Colombo, R. & Dalle-Donne, I. S-glutathionylation: from redox regulation of protein functions to human diseases. *J Cell Mol Med* **8**, 201-212, doi:10.1111/j.1582-4934.2004.tb00275.x (2004).
- 88 Popov, D. Protein S-glutathionylation: from current basics to targeted modifications. *Arch Physiol Biochem* **120**, 123-130, doi:10.3109/13813455.2014.944544 (2014).
- 89 Ghezzi, P. Protein glutathionylation in health and disease. *Biochim Biophys Acta* **1830**, 3165-3172, doi:10.1016/j.bbagen.2013.02.009 (2013).
- 90 Pastore, A. & Piemonte, F. Protein glutathionylation in cardiovascular diseases. *Int J Mol Sci* **14**, 20845-20876, doi:10.3390/ijms141020845 (2013).
- 91 Branchetti, E. *et al.* Antioxidant enzymes reduce DNA damage and early activation of valvular interstitial cells in aortic valve sclerosis. *Arterioscler Thromb Vasc Biol* **33**, e66-74, doi:10.1161/ATVBAHA.112.300177 (2013).
- 92 Miller, J. D. *et al.* Dysregulation of antioxidant mechanisms contributes to increased oxidative stress in calcific aortic valvular stenosis in humans. *J Am Coll Cardiol* **52**, 843-850, doi:10.1016/j.jacc.2008.05.043 (2008).
- 93 Condorelli, G., Latronico, M. V. & Dorn, G. W., 2nd. microRNAs in heart disease: putative novel therapeutic targets? *Eur Heart J* **31**, 649-658, doi:10.1093/eurheartj/ehp573 (2010).
- 94 Songia, P. *et al.* Direct screening of plasma circulating microRNAs. *RNA Biol* **15**, 1268-1272, doi:10.1080/15476286.2018.1526538 (2018).
- 95 Martinez-Micaelo, N., Beltran-Debon, R., Aragonés, G., Faiges, M. & Alegret, J. M. MicroRNAs Clustered within the 14q32 Locus Are Associated with Endothelial Damage and Microparticle Secretion in Bicuspid Aortic Valve Disease. *Front Physiol* **8**, 648, doi:10.3389/fphys.2017.00648 (2017).
- 96 Kaikkonen, M. U., Lam, M. T. & Glass, C. K. Non-coding RNAs as regulators of gene expression and epigenetics. *Cardiovasc Res* **90**, 430-440, doi:10.1093/cvr/cvr097 (2011).
- 97 Bohmdorfer, G. & Wierzbicki, A. T. Control of Chromatin Structure by Long Noncoding RNA. *Trends Cell Biol* **25**, 623-632, doi:10.1016/j.tcb.2015.07.002 (2015).

- 98 Zhou, S. S. *et al.* miRNAs in cardiovascular diseases: potential biomarkers, therapeutic targets and challenges. *Acta Pharmacol Sin* **39**, 1073-1084, doi:10.1038/aps.2018.30 (2018).
- 99 Wojciechowska, A., Braniewska, A. & Kozar-Kaminska, K. MicroRNA in cardiovascular biology and disease. *Adv Clin Exp Med* **26**, 865-874, doi:10.17219/acem/62915 (2017).
- 100 Romaine, S. P., Tomaszewski, M., Condorelli, G. & Samani, N. J. MicroRNAs in cardiovascular disease: an introduction for clinicians. *Heart* **101**, 921-928, doi:10.1136/heartjnl-2013-305402 (2015).
- 101 Rutkovskiy, A. *et al.* Valve Interstitial Cells: The Key to Understanding the Pathophysiology of Heart Valve Calcification. *J Am Heart Assoc* **6**, doi:10.1161/JAHA.117.006339 (2017).
- 102 Poggio, P. *et al.* Osteopontin-CD44v6 interaction mediates calcium deposition via phospho-Akt in valve interstitial cells from patients with noncalcified aortic valve sclerosis. *Arterioscler Thromb Vasc Biol* **34**, 2086-2094, doi:10.1161/ATVBAHA.113.303017 (2014).
- 103 Osman, L., Chester, A. H., Amrani, M., Yacoub, M. H. & Smolenski, R. T. A novel role of extracellular nucleotides in valve calcification: a potential target for atorvastatin. *Circulation* **114**, 1566-572, doi:10.1161/CIRCULATIONAHA.105.001214 (2006).
- 104 Pawade, T. A., Newby, D. E. & Dweck, M. R. Calcification in Aortic Stenosis: The Skeleton Key. *J Am Coll Cardiol* **66**, 561-577, doi:10.1016/j.jacc.2015.05.066 (2015).
- 105 Wang, P. & Heitman, J. The cyclophilins. *Genome Biol* **6**, 226, doi:10.1186/gb-2005-6-7-226 (2005).
- 106 Nigro, P., Pompilio, G. & Capogrossi, M. C. Cyclophilin A: a key player for human disease. *Cell Death Dis* **4**, e888, doi:10.1038/cddis.2013.410 (2013).
- 107 Davis, T. L. *et al.* Structural and biochemical characterization of the human cyclophilin family of peptidyl-prolyl isomerases. *PLoS Biol* **8**, e1000439, doi:10.1371/journal.pbio.1000439 (2010).
- 108 Jin, Z. G. *et al.* Cyclophilin A is a secreted growth factor induced by oxidative stress. *Circ Res* **87**, 789-796, doi:10.1161/01.res.87.9.789 (2000).

- 109 Satoh, K. *et al.* Cyclophilin A mediates vascular remodeling by promoting inflammation and vascular smooth muscle cell proliferation. *Circulation* **117**, 3088-3098, doi:10.1161/CIRCULATIONAHA.107.756106 (2008).
- 110 Yurchenko, V. *et al.* Active site residues of cyclophilin A are crucial for its signaling activity via CD147. *J Biol Chem* **277**, 22959-22965, doi:10.1074/jbc.M201593200 (2002).
- 111 Shin, H. R. *et al.* Pin1-mediated Modification Prolongs the Nuclear Retention of beta-Catenin in Wnt3a-induced Osteoblast Differentiation. *J Biol Chem* **291**, 5555-5565, doi:10.1074/jbc.M115.698563 (2016).
- 112 Guo, M. *et al.* Cyclophilin A (CypA) Plays Dual Roles in Regulation of Bone Anabolism and Resorption. *Sci Rep* **6**, 22378, doi:10.1038/srep22378 (2016).
- 113 Tsuda, T. *et al.* Rho-associated protein kinase and cyclophilin a are involved in inorganic phosphate-induced calcification signaling in vascular smooth muscle cells. *J Pharmacol Sci* **142**, 109-115, doi:10.1016/j.jphs.2019.12.005 (2020).
- 114 Satoh, K. *et al.* Cyclophilin A enhances vascular oxidative stress and the development of angiotensin II-induced aortic aneurysms. *Nat Med* **15**, 649-656, doi:10.1038/nm.1958 (2009).
- 115 Prins, P. A. *et al.* Benzo[a]pyrene potentiates the pathogenesis of abdominal aortic aneurysms in apolipoprotein E knockout mice. *Cell Physiol Biochem* **29**, 121-130, doi:10.1159/000337593 (2012).
- 116 Nigro, P. *et al.* Cyclophilin A is an inflammatory mediator that promotes atherosclerosis in apolipoprotein E-deficient mice. *J Exp Med* **208**, 53-66, doi:10.1084/jem.20101174 (2011).
- 117 Seizer, P. *et al.* Disrupting the EMMPRIN (CD147)-cyclophilin A interaction reduces infarct size and preserves systolic function after myocardial ischemia and reperfusion. *Arterioscler Thromb Vasc Biol* **31**, 1377-1386, doi:10.1161/ATVBAHA.111.225771 (2011).
- 118 Yan, J. *et al.* The clinical implications of increased cyclophilin A levels in patients with acute coronary syndromes. *Clin Chim Acta* **413**, 691-695, doi:10.1016/j.cca.2011.12.009 (2012).
- 119 Satoh, K. *et al.* Plasma cyclophilin A is a novel biomarker for coronary artery disease. *Circ J* **77**, 447-455, doi:10.1253/circj.cj-12-0805 (2013).

- 120 Seidah, N. G. & Prat, A. The biology and therapeutic targeting of the proprotein convertases. *Nat Rev Drug Discov* **11**, 367-383, doi:10.1038/nrd3699 (2012).
- 121 Norata, G. D., Tibolla, G. & Catapano, A. L. PCSK9 inhibition for the treatment of hypercholesterolemia: promises and emerging challenges. *Vascul Pharmacol* **62**, 103-111, doi:10.1016/j.vph.2014.05.011 (2014).
- 122 Tibolla, G., Norata, G. D., Artali, R., Meneghetti, F. & Catapano, A. L. Proprotein convertase subtilisin/kexin type 9 (PCSK9): from structure-function relation to therapeutic inhibition. *Nutr Metab Cardiovasc Dis* **21**, 835-843, doi:10.1016/j.numecd.2011.06.002 (2011).
- 123 Wicinski, M., Zak, J., Malinowski, B., Popek, G. & Grzesk, G. PCSK9 signaling pathways and their potential importance in clinical practice. *EPMA J* **8**, 391-402, doi:10.1007/s13167-017-0106-6 (2017).
- 124 Poirier, S., Hamouda, H. A., Villeneuve, L., Demers, A. & Mayer, G. Trafficking Dynamics of PCSK9-Induced LDLR Degradation: Focus on Human PCSK9 Mutations and C-Terminal Domain. *PLoS One* **11**, e0157230, doi:10.1371/journal.pone.0157230 (2016).
- 125 Horton, J. D., Cohen, J. C. & Hobbs, H. H. PCSK9: a convertase that coordinates LDL catabolism. *J Lipid Res* **50 Suppl**, S172-177, doi:10.1194/jlr.R800091-JLR200 (2009).
- 126 Awan, Z., Baass, A. & Genest, J. Proprotein convertase subtilisin/kexin type 9 (PCSK9): lessons learned from patients with hypercholesterolemia. *Clin Chem* **60**, 1380-1389, doi:10.1373/clinchem.2014.225946 (2014).
- 127 Cariou, B. *et al.* PCSK9 dominant negative mutant results in increased LDL catabolic rate and familial hypobetalipoproteinemia. *Arterioscler Thromb Vasc Biol* **29**, 2191-2197, doi:10.1161/ATVBAHA.109.194191 (2009).
- 128 Pasta, A. *et al.* PCSK9 inhibitors for treating hypercholesterolemia. *Expert Opin Pharmacother* **21**, 353-363, doi:10.1080/14656566.2019.1702970 (2020).
- 129 Ray, K. K. *et al.* Effect of an siRNA Therapeutic Targeting PCSK9 on Atherogenic Lipoproteins: Prespecified Secondary End Points in ORION 1. *Circulation* **138**, 1304-1316, doi:10.1161/CIRCULATIONAHA.118.034710 (2018).

- 130 Zeitlinger, M. *et al.* A phase I study assessing the safety, tolerability, immunogenicity, and low-density lipoprotein cholesterol-lowering activity of immunotherapeutics targeting PCSK9. *Eur J Clin Pharmacol* **77**, 1473-1484, doi:10.1007/s00228-021-03149-2 (2021).
- 131 Wang, W. G. *et al.* Proprotein convertase subtilisin/kexin type 9 levels and aortic valve calcification: A prospective, cross sectional study. *J Int Med Res* **44**, 865-874, doi:10.1177/0300060516648030 (2016).
- 132 Langsted, A., Nordestgaard, B. G., Benn, M., Tybjaerg-Hansen, A. & Kamstrup, P. R. PCSK9 R46L Loss-of-Function Mutation Reduces Lipoprotein(a), LDL Cholesterol, and Risk of Aortic Valve Stenosis. *J Clin Endocrinol Metab* **101**, 3281-3287, doi:10.1210/jc.2016-1206 (2016).
- 133 Poggio, P. *et al.* PCSK9 Involvement in Aortic Valve Calcification. *J Am Coll Cardiol* **72**, 3225-3227, doi:10.1016/j.jacc.2018.09.063 (2018).
- 134 Otto, C. M., Lind, B. K., Kitzman, D. W., Gersh, B. J. & Siscovick, D. S. Association of aortic-valve sclerosis with cardiovascular mortality and morbidity in the elderly. *N Engl J Med* **341**, 142-147, doi:10.1056/NEJM199907153410302 (1999).
- 135 Chelko, S. P. *et al.* Exercise triggers CAPN1-mediated AIF truncation, inducing myocyte cell death in arrhythmogenic cardiomyopathy. *Sci Transl Med* **13**, doi:10.1126/scitranslmed.abf0891 (2021).
- 136 Shannon, P. *et al.* Cytoscape: a software environment for integrated models of biomolecular interaction networks. *Genome Res* **13**, 2498-2504, doi:10.1101/gr.1239303 (2003).
- 137 John, B. *et al.* Human MicroRNA targets. *PLoS Biol* **2**, e363, doi:10.1371/journal.pbio.0020363 (2004).
- 138 Betel, D., Koppal, A., Agius, P., Sander, C. & Leslie, C. Comprehensive modeling of microRNA targets predicts functional non-conserved and non-canonical sites. *Genome Biol* **11**, R90, doi:10.1186/gb-2010-11-8-r90 (2010).
- 139 Authors/Task Force, m. *et al.* 2014 ESC/EACTS Guidelines on myocardial revascularization: The Task Force on Myocardial Revascularization of the European Society of Cardiology (ESC) and the European Association for Cardio-Thoracic Surgery (EACTS) Developed with the special contribution of the European Association of Percutaneous Cardiovascular Interventions (EAPCI). *Eur Heart J* **35**, 2541-2619, doi:10.1093/eurheartj/ehu278 (2014).

- 140 Brott, T. G. *et al.* 2011
ASA/ACCF/AHA/AANN/AANS/ACR/ASNR/CNS/SAIP/SCAI/SIR/SNIS/S
VM/SVS guideline on the management of patients with extracranial carotid
and vertebral artery disease: a report of the American College of Cardiology
Foundation/American Heart Association Task Force on Practice Guidelines,
and the American Stroke Association, American Association of Neuroscience
Nurses, American Association of Neurological Surgeons, American College
of Radiology, American Society of Neuroradiology, Congress of
Neurological Surgeons, Society of Atherosclerosis Imaging and Prevention,
Society for Cardiovascular Angiography and Interventions, Society of
Interventional Radiology, Society of NeuroInterventional Surgery, Society
for Vascular Medicine, and Society for Vascular Surgery. *J Am Coll Cardiol*
57, e16-94, doi:10.1016/j.jacc.2010.11.006 (2011).
- 141 de Weert, T. T. *et al.* In vivo characterization and quantification of
atherosclerotic carotid plaque components with multidetector computed
tomography and histopathological correlation. *Arterioscler Thromb Vasc Biol*
26, 2366-2372, doi:10.1161/01.ATV.0000240518.90124.57 (2006).
- 142 Prasain, N. & Stevens, T. The actin cytoskeleton in endothelial cell
phenotypes. *Microvasc Res* **77**, 53-63, doi:10.1016/j.mvr.2008.09.012 (2009).
- 143 Eshaq, R. S. & Harris, N. R. Loss of Platelet Endothelial Cell Adhesion
Molecule-1 (PECAM-1) in the Diabetic Retina: Role of Matrix
Metalloproteinases. *Invest Ophthalmol Vis Sci* **60**, 748-760,
doi:10.1167/iovs.18-25068 (2019).
- 144 Otto, C. M. & Prendergast, B. Aortic-valve stenosis--from patients at risk to
severe valve obstruction. *N Engl J Med* **371**, 744-756,
doi:10.1056/NEJMra1313875 (2014).
- 145 Goto, S. *et al.* Standardization of Human Calcific Aortic Valve Disease in
vitro Modeling Reveals Passage-Dependent Calcification. *Front Cardiovasc*
Med **6**, 49, doi:10.3389/fcvm.2019.00049 (2019).
- 146 Bouquet, F., Muller, C. & Salles, B. The loss of gammaH2AX signal is a
marker of DNA double strand breaks repair only at low levels of DNA
damage. *Cell Cycle* **5**, 1116-1122, doi:10.4161/cc.5.10.2799 (2006).

- 147 Suzuki, J., Jin, Z. G., Meoli, D. F., Matoba, T. & Berk, B. C. Cyclophilin A is secreted by a vesicular pathway in vascular smooth muscle cells. *Circ Res* **98**, 811-817, doi:10.1161/01.RES.0000216405.85080.a6 (2006).
- 148 Malesevic, M. *et al.* Anti-inflammatory effects of extracellular cyclosporins are exclusively mediated by CD147. *J Med Chem* **56**, 7302-7311, doi:10.1021/jm4007577 (2013).
- 149 Cai, Q., Serrano, R., Kalyanasundaram, A. & Shirani, J. A preoperative echocardiographic predictive model for assessment of cardiovascular outcome after renal transplantation. *J Am Soc Echocardiogr* **23**, 560-566, doi:10.1016/j.echo.2010.03.008 (2010).
- 150 Valentijn, T. M. *et al.* Influence of aortic valve calcium on outcome in patients undergoing peripheral vascular surgery. *Am J Cardiol* **110**, 1195-1199, doi:10.1016/j.amjcard.2012.05.062 (2012).
- 151 Chandra, H. R. *et al.* Adverse outcome in aortic sclerosis is associated with coronary artery disease and inflammation. *J Am Coll Cardiol* **43**, 169-175, doi:10.1016/j.jacc.2003.08.036 (2004).
- 152 Volzke, H. *et al.* Heart valve sclerosis predicts all-cause and cardiovascular mortality. *Atherosclerosis* **209**, 606-610, doi:10.1016/j.atherosclerosis.2009.10.030 (2010).
- 153 Barasch, E., Gottdiener, J. S., Marino Larsen, E. K., Chaves, P. H. & Newman, A. B. Cardiovascular morbidity and mortality in community-dwelling elderly individuals with calcification of the fibrous skeleton of the base of the heart and aortosclerosis (The Cardiovascular Health Study). *Am J Cardiol* **97**, 1281-1286, doi:10.1016/j.amjcard.2005.11.065 (2006).
- 154 Rossi, A. *et al.* Aortic and mitral annular calcifications are predictive of all-cause and cardiovascular mortality in patients with type 2 diabetes. *Diabetes Care* **35**, 1781-1786, doi:10.2337/dc12-0134 (2012).
- 155 Taylor, H. A., Jr. *et al.* Relation of aortic valve sclerosis to risk of coronary heart disease in African-Americans. *Am J Cardiol* **95**, 401-404, doi:10.1016/j.amjcard.2004.09.043 (2005).
- 156 Coffey, S., Cox, B. & Williams, M. J. The prevalence, incidence, progression, and risks of aortic valve sclerosis: a systematic review and meta-analysis. *J Am Coll Cardiol* **63**, 2852-2861, doi:10.1016/j.jacc.2014.04.018 (2014).

- 157 Di Minno, M. N. D. *et al.* Cardiovascular morbidity and mortality in patients with aortic valve sclerosis: A systematic review and meta-analysis. *Int J Cardiol* **260**, 138-144, doi:10.1016/j.ijcard.2018.01.054 (2018).
- 158 da Rosa, E. M., Sant'anna, J. R., Oppermann, L. P. & Castro, I. Prognosis of aortic valve sclerosis in cardiovascular mortality of patients seen at the cardiology institute of Rio Grande do Sul. *Arq Bras Cardiol* **88**, 234-239, doi:10.1590/s0066-782x2007000200016 (2007).
- 159 Owens, D. S. *et al.* Aortic valve calcium independently predicts coronary and cardiovascular events in a primary prevention population. *JACC Cardiovasc Imaging* **5**, 619-625, doi:10.1016/j.jcmg.2011.12.023 (2012).
- 160 Corciu, A. I. *et al.* Cardiac calcification by transthoracic echocardiography in patients with known or suspected coronary artery disease. *Int J Cardiol* **142**, 288-295, doi:10.1016/j.ijcard.2009.01.021 (2010).
- 161 Pradelli, D. *et al.* Impact of aortic or mitral valve sclerosis and calcification on cardiovascular events and mortality: a meta-analysis. *Int J Cardiol* **170**, e51-55, doi:10.1016/j.ijcard.2013.10.081 (2013).
- 162 Barili, F. *et al.* The Impact of EuroSCORE II Risk Factors on Prediction of Long-Term Mortality. *Ann Thorac Surg* **102**, 1296-1303, doi:10.1016/j.athoracsur.2016.04.017 (2016).
- 163 Grant, S. W. *et al.* How does EuroSCORE II perform in UK cardiac surgery; an analysis of 23 740 patients from the Society for Cardiothoracic Surgery in Great Britain and Ireland National Database. *Heart* **98**, 1568-1572, doi:10.1136/heartjnl-2012-302483 (2012).
- 164 Valerio, V. *et al.* Impact of Oxidative Stress and Protein S-Glutathionylation in Aortic Valve Sclerosis Patients with Overt Atherosclerosis. *J Clin Med* **8**, doi:10.3390/jcm8040552 (2019).
- 165 Antonini-Canterin, F. *et al.* Relation of carotid intima-media thickness and aortic valve sclerosis (from the ISMIR study ["Ispessimento Medio Intimale e Rischio Cardiovascolare"] of the Italian Society of Cardiovascular Echography). *Am J Cardiol* **103**, 1556-1561, doi:10.1016/j.amjcard.2009.01.368 (2009).
- 166 Rossi, A. *et al.* Mitral and aortic valve sclerosis/calcification and carotid atherosclerosis: results from 1065 patients. *Heart Vessels* **29**, 776-783, doi:10.1007/s00380-013-0433-z (2014).

- 167 Burke, J. F., Morgenstern, L. B. & Hayward, R. A. Can risk modelling improve treatment decisions in asymptomatic carotid stenosis? *BMC Neurol* **19**, 295, doi:10.1186/s12883-019-1528-7 (2019).
- 168 Nam, H. J. *et al.* Long-Term Outcome After Carotid Endarterectomy in Patients with Ischemic Heart Disease. *World Neurosurg* **110**, e806-e814, doi:10.1016/j.wneu.2017.11.092 (2018).
- 169 Alves-Ferreira, J., Rocha-Neves, J., Dias-Neto, M. & Braga, S. F. Poor long-term outcomes after carotid endarterectomy: a retrospective analysis of two portuguese centers. *Scand Cardiovasc J* **53**, 266-273, doi:10.1080/14017431.2019.1638518 (2019).
- 170 van Lammeren, G. W. *et al.* Clinical prediction rule to estimate the absolute 3-year risk of major cardiovascular events after carotid endarterectomy. *Stroke* **43**, 1273-1278, doi:10.1161/STROKEAHA.111.647958 (2012).
- 171 Go, C. *et al.* Long-term clinical outcomes and cardiovascular events after carotid endarterectomy. *Ann Vasc Surg* **29**, 1265-1271, doi:10.1016/j.avsg.2015.03.031 (2015).
- 172 Qureshi, A. I., Chaudhry, S. A., Qureshi, M. H. & Suri, M. F. Rates and predictors of 5-year survival in a national cohort of asymptomatic elderly patients undergoing carotid revascularization. *Neurosurgery* **76**, 34-40; discussion 40-31, doi:10.1227/NEU.0000000000000551 (2015).
- 173 Dasenbrock, H. H. *et al.* Predictive Score of Adverse Events After Carotid Endarterectomy: The NSQIP Registry Carotid Endarterectomy Scale. *J Am Heart Assoc* **8**, e013412, doi:10.1161/JAHA.119.013412 (2019).
- 174 Klarin, D. *et al.* Perioperative and long-term impact of chronic kidney disease on carotid artery interventions. *J Vasc Surg* **64**, 1295-1302, doi:10.1016/j.jvs.2016.04.038 (2016).
- 175 Ersboll, M. *et al.* Predictors and progression of aortic stenosis in patients with preserved left ventricular ejection fraction. *Am J Cardiol* **115**, 86-92, doi:10.1016/j.amjcard.2014.09.049 (2015).
- 176 Vavilis, G. *et al.* Kidney Dysfunction and the Risk of Developing Aortic Stenosis. *J Am Coll Cardiol* **73**, 305-314, doi:10.1016/j.jacc.2018.10.068 (2019).

- 177 Poggio, P. *et al.* Aortic Valve Sclerosis Adds to Prediction of Short-Term Mortality in Patients with Documented Coronary Atherosclerosis. *J Clin Med* **8**, doi:10.3390/jcm8081172 (2019).
- 178 Nandalur, K. R., Baskurt, E., Hagspiel, K. D., Phillips, C. D. & Kramer, C. M. Calcified carotid atherosclerotic plaque is associated less with ischemic symptoms than is noncalcified plaque on MDCT. *AJR Am J Roentgenol* **184**, 295-298, doi:10.2214/ajr.184.1.01840295 (2005).
- 179 Katano, H., Mase, M., Nishikawa, Y., Yamada, H. & Yamada, K. Analysis of Recurrent Stenosis After Carotid Endarterectomy Featuring Primary Plaque Calcification. *Neurosurgery* **80**, 863-870, doi:10.1093/neuros/nyw119 (2017).
- 180 Takaya, N. *et al.* Association between carotid plaque characteristics and subsequent ischemic cerebrovascular events: a prospective assessment with MRI--initial results. *Stroke* **37**, 818-823, doi:10.1161/01.STR.0000204638.91099.91 (2006).
- 181 Sun, J. *et al.* Carotid Plaque Lipid Content and Fibrous Cap Status Predict Systemic CV Outcomes: The MRI Substudy in AIM-HIGH. *JACC Cardiovasc Imaging* **10**, 241-249, doi:10.1016/j.jcmg.2016.06.017 (2017).
- 182 Howard, D. P. *et al.* Symptomatic carotid atherosclerotic disease: correlations between plaque composition and ipsilateral stroke risk. *Stroke* **46**, 182-189, doi:10.1161/STROKEAHA.114.007221 (2015).
- 183 Lutgens, E. *et al.* Transforming growth factor-beta mediates balance between inflammation and fibrosis during plaque progression. *Arterioscler Thromb Vasc Biol* **22**, 975-982, doi:10.1161/01.atv.0000019729.39500.2f (2002).
- 184 Singh, S. & Torzewski, M. Fibroblasts and Their Pathological Functions in the Fibrosis of Aortic Valve Sclerosis and Atherosclerosis. *Biomolecules* **9**, doi:10.3390/biom9090472 (2019).
- 185 Rajamannan, N. M., Bonow, R. O. & Rahimtoola, S. H. Calcific aortic stenosis: an update. *Nat Clin Pract Cardiovasc Med* **4**, 254-262, doi:10.1038/ncpcardio0827 (2007).
- 186 Danielsen, R., Aspelund, T., Harris, T. B. & Gudnason, V. The prevalence of aortic stenosis in the elderly in Iceland and predictions for the coming decades: the AGES-Reykjavik study. *Int J Cardiol* **176**, 916-922, doi:10.1016/j.ijcard.2014.08.053 (2014).

- 187 Baumgartner, H. *et al.* 2017 ESC/EACTS Guidelines for the management of valvular heart disease. *Eur Heart J* **38**, 2739-2791, doi:10.1093/eurheartj/ehx391 (2017).
- 188 Liony, C. *et al.* [A case of primary osteosarcoma of the liver]. *Gastroenterol Clin Biol* **14**, 1003-1006 (1990).
- 189 Kalyanaraman, B. *et al.* Measuring reactive oxygen and nitrogen species with fluorescent probes: challenges and limitations. *Free Radic Biol Med* **52**, 1-6, doi:10.1016/j.freeradbiomed.2011.09.030 (2012).
- 190 Bajic, V. P. *et al.* Glutathione "Redox Homeostasis" and Its Relation to Cardiovascular Disease. *Oxid Med Cell Longev* **2019**, 5028181, doi:10.1155/2019/5028181 (2019).
- 191 Forman, H. J., Zhang, H. & Rinna, A. Glutathione: overview of its protective roles, measurement, and biosynthesis. *Mol Aspects Med* **30**, 1-12, doi:10.1016/j.mam.2008.08.006 (2009).
- 192 Hwang, C., Sinskey, A. J. & Lodish, H. F. Oxidized redox state of glutathione in the endoplasmic reticulum. *Science* **257**, 1496-1502, doi:10.1126/science.1523409 (1992).
- 193 Zeisberg, E. M., Potenta, S., Xie, L., Zeisberg, M. & Kalluri, R. Discovery of endothelial to mesenchymal transition as a source for carcinoma-associated fibroblasts. *Cancer Res* **67**, 10123-10128, doi:10.1158/0008-5472.CAN-07-3127 (2007).
- 194 Kumarswamy, R. *et al.* Transforming growth factor-beta-induced endothelial-to-mesenchymal transition is partly mediated by microRNA-21. *Arterioscler Thromb Vasc Biol* **32**, 361-369, doi:10.1161/ATVBAHA.111.234286 (2012).
- 195 Heard, K. J. Acetylcysteine for acetaminophen poisoning. *N Engl J Med* **359**, 285-292, doi:10.1056/NEJMct0708278 (2008).
- 196 Zafarullah, M., Li, W. Q., Sylvester, J. & Ahmad, M. Molecular mechanisms of N-acetylcysteine actions. *Cell Mol Life Sci* **60**, 6-20, doi:10.1007/s000180300001 (2003).
- 197 Reyes, D. R. A. *et al.* N-Acetylcysteine Influence on Oxidative Stress and Cardiac Remodeling in Rats During Transition from Compensated Left Ventricular Hypertrophy to Heart Failure. *Cell Physiol Biochem* **44**, 2310-2321, doi:10.1159/000486115 (2017).

- 198 Bartekova, M., Barancik, M., Ferenczyova, K. & Dhalla, N. S. Beneficial Effects of N-acetylcysteine and N-mercaptopyrionylglycine on Ischemia Reperfusion Injury in the Heart. *Curr Med Chem* **25**, 355-366, doi:10.2174/0929867324666170608111917 (2018).
- 199 Chaves Cayuela, N. *et al.* N-Acetylcysteine Reduced Ischemia and Reperfusion Damage Associated with Steatohepatitis in Mice. *Int J Mol Sci* **21**, doi:10.3390/ijms21114106 (2020).
- 200 Varshney, R. *et al.* Inactivation of platelet-derived TGF-beta1 attenuates aortic stenosis progression in a robust murine model. *Blood Adv* **3**, 777-788, doi:10.1182/bloodadvances.2018025817 (2019).
- 201 Sider, K. L., Blaser, M. C. & Simmons, C. A. Animal models of calcific aortic valve disease. *Int J Inflamm* **2011**, 364310, doi:10.4061/2011/364310 (2011).
- 202 Behr, J. *et al.* Lung function in idiopathic pulmonary fibrosis--extended analyses of the IFIGENIA trial. *Respir Res* **10**, 101, doi:10.1186/1465-9921-10-101 (2009).
- 203 Costa, D. L. C. *et al.* Randomized, Double-Blind, Placebo-Controlled Trial of N-Acetylcysteine Augmentation for Treatment-Resistant Obsessive-Compulsive Disorder. *J Clin Psychiatry* **78**, e766-e773, doi:10.4088/JCP.16m11101 (2017).
- 204 Cui, Y. *et al.* N-acetylcysteine inhibits in vivo oxidation of native low-density lipoprotein. *Sci Rep* **5**, 16339, doi:10.1038/srep16339 (2015).
- 205 Gupta, S. K., Kamendulis, L. M., Clauss, M. A. & Liu, Z. A randomized, placebo-controlled pilot trial of N-acetylcysteine on oxidative stress and endothelial function in HIV-infected older adults receiving antiretroviral treatment. *AIDS* **30**, 2389-2391, doi:10.1097/QAD.0000000000001222 (2016).
- 206 Tepel, M., van der Giet, M., Statz, M., Jankowski, J. & Zidek, W. The antioxidant acetylcysteine reduces cardiovascular events in patients with end-stage renal failure: a randomized, controlled trial. *Circulation* **107**, 992-995, doi:10.1161/01.cir.0000050628.11305.30 (2003).
- 207 Nsaibia, M. J. *et al.* OxLDL-derived lysophosphatidic acid promotes the progression of aortic valve stenosis through a LPAR1-RhoA-NF-kappaB pathway. *Cardiovasc Res* **113**, 1351-1363, doi:10.1093/cvr/cvx089 (2017).

- 208 Bavarsad Shahripour, R., Harrigan, M. R. & Alexandrov, A. V. N-acetylcysteine (NAC) in neurological disorders: mechanisms of action and therapeutic opportunities. *Brain Behav* **4**, 108-122, doi:10.1002/brb3.208 (2014).
- 209 Coffey, S. *et al.* Integrated microRNA and messenger RNA analysis in aortic stenosis. *Sci Rep* **6**, 36904, doi:10.1038/srep36904 (2016).
- 210 Blunder, S. *et al.* Targeted gene expression analyses and immunohistology suggest a pro-proliferative state in tricuspid aortic valve-, and senescence and viral infections in bicuspid aortic valve-associated thoracic aortic aneurysms. *Atherosclerosis* **271**, 111-119, doi:10.1016/j.atherosclerosis.2018.02.007 (2018).
- 211 Rajamannan, N. M. Bicuspid aortic valve disease: the role of oxidative stress in Lrp5 bone formation. *Cardiovasc Pathol* **20**, 168-176, doi:10.1016/j.carpath.2010.11.007 (2011).
- 212 Alegret, J. M., Martinez-Micaelo, N., Aragones, G. & Beltran-Debon, R. Circulating endothelial microparticles are elevated in bicuspid aortic valve disease and related to aortic dilation. *Int J Cardiol* **217**, 35-41, doi:10.1016/j.ijcard.2016.04.184 (2016).
- 213 Poggio, P. *et al.* Antihypertensive Treatments in Patients Affected by Aortic Valve Stenosis. *Curr Pharm Des* **23**, 1188-1194, doi:10.2174/1381612823666161123144534 (2017).
- 214 Duniyak, B. M. & Gestwicki, J. E. Peptidyl-Proline Isomerases (PPIases): Targets for Natural Products and Natural Product-Inspired Compounds. *J Med Chem* **59**, 9622-9644, doi:10.1021/acs.jmedchem.6b00411 (2016).
- 215 Kamath, A. R. & Pai, R. G. Risk factors for progression of calcific aortic stenosis and potential therapeutic targets. *Int J Angiol* **17**, 63-70, doi:10.1055/s-0031-1278283 (2008).
- 216 Palta, S., Pai, A. M., Gill, K. S. & Pai, R. G. New insights into the progression of aortic stenosis: implications for secondary prevention. *Circulation* **101**, 2497-2502, doi:10.1161/01.cir.101.21.2497 (2000).
- 217 Venardos, N. *et al.* Simvastatin reduces the TLR4-induced inflammatory response in human aortic valve interstitial cells. *J Surg Res* **230**, 101-109, doi:10.1016/j.jss.2018.04.054 (2018).

- 218 Norrington, K., Androulakis, E., Oikonomou, E., Vogiatzi, G. & Tousoulis, D. Statins in Aortic Stenosis. *Curr Pharm Des*, doi:10.2174/1381612823666170816113521 (2017).
- 219 Seo, J. H., Chun, K. J., Lee, B. K., Cho, B. R. & Ryu, D. R. Statins Have No Role in Preventing the Progression of Aortic Valve Sclerosis. *J Cardiovasc Imaging* **26**, 229-237, doi:10.4250/jcvi.2018.26.e27 (2018).
- 220 Capoulade, R. *et al.* Impact of metabolic syndrome on progression of aortic stenosis: influence of age and statin therapy. *J Am Coll Cardiol* **60**, 216-223, doi:10.1016/j.jacc.2012.03.052 (2012).
- 221 Fujisaka, T. *et al.* Angiotensin II promotes aortic valve thickening independent of elevated blood pressure in apolipoprotein-E deficient mice. *Atherosclerosis* **226**, 82-87, doi:10.1016/j.atherosclerosis.2012.10.055 (2013).
- 222 Seko, Y. *et al.* Hypoxia followed by reoxygenation induces secretion of cyclophilin A from cultured rat cardiac myocytes. *Biochem Biophys Res Commun* **317**, 162-168, doi:10.1016/j.bbrc.2004.03.021 (2004).
- 223 Sherry, B., Yarlett, N., Strupp, A. & Cerami, A. Identification of cyclophilin as a proinflammatory secretory product of lipopolysaccharide-activated macrophages. *Proc Natl Acad Sci U S A* **89**, 3511-3515, doi:10.1073/pnas.89.8.3511 (1992).
- 224 Satoh, K. *et al.* Cyclophilin A promotes cardiac hypertrophy in apolipoprotein E-deficient mice. *Arterioscler Thromb Vasc Biol* **31**, 1116-1123, doi:10.1161/ATVBAHA.110.214601 (2011).
- 225 Elvers, M. *et al.* Intracellular cyclophilin A is an important Ca(2+) regulator in platelets and critically involved in arterial thrombus formation. *Blood* **120**, 1317-1326, doi:10.1182/blood-2011-12-398438 (2012).
- 226 Handschumacher, R. E., Harding, M. W., Rice, J., Drugge, R. J. & Speicher, D. W. Cyclophilin: a specific cytosolic binding protein for cyclosporin A. *Science* **226**, 544-547, doi:10.1126/science.6238408 (1984).
- 227 Colgan, J., Asmal, M., Yu, B. & Luban, J. Cyclophilin A-deficient mice are resistant to immunosuppression by cyclosporine. *J Immunol* **174**, 6030-6038, doi:10.4049/jimmunol.174.10.6030 (2005).
- 228 Etzkorn, F. A., Chang, Z. Y., Stolz, L. A. & Walsh, C. T. Cyclophilin residues that affect noncompetitive inhibition of the protein serine

- phosphatase activity of calcineurin by the cyclophilin-cyclosporin A complex. *Biochemistry* **33**, 2380-2388, doi:10.1021/bi00175a005 (1994).
- 229 Liu, J. *et al.* Calcineurin is a common target of cyclophilin-cyclosporin A and FKBP-FK506 complexes. *Cell* **66**, 807-815, doi:10.1016/0092-8674(91)90124-h (1991).
- 230 Vasquez-Trincado, C. *et al.* Mitochondrial dynamics, mitophagy and cardiovascular disease. *J Physiol* **594**, 509-525, doi:10.1113/JP271301 (2016).
- 231 Waldmeier, P. C., Feldtrauer, J. J., Qian, T. & Lemasters, J. J. Inhibition of the mitochondrial permeability transition by the nonimmunosuppressive cyclosporin derivative NIM811. *Mol Pharmacol* **62**, 22-29, doi:10.1124/mol.62.1.22 (2002).
- 232 Heinzmann, D. *et al.* The Novel Extracellular Cyclophilin A (CyPA) - Inhibitor MM284 Reduces Myocardial Inflammation and Remodeling in a Mouse Model of Troponin I -Induced Myocarditis. *PLoS One* **10**, e0124606, doi:10.1371/journal.pone.0124606 (2015).
- 233 Seizer, P. *et al.* Extracellular cyclophilin A activates platelets via EMMPRIN (CD147) and PI3K/Akt signaling, which promotes platelet adhesion and thrombus formation in vitro and in vivo. *Arterioscler Thromb Vasc Biol* **35**, 655-663, doi:10.1161/ATVBAHA.114.305112 (2015).
- 234 Perrucci, G. L. *et al.* Cyclophilin A/EMMPRIN Axis Is Involved in Pro-Fibrotic Processes Associated with Thoracic Aortic Aneurysm of Marfan Syndrome Patients. *Cells* **9**, doi:10.3390/cells9010154 (2020).
- 235 Rao, A. S. *et al.* Large-Scale Phenome-Wide Association Study of PCSK9 Variants Demonstrates Protection Against Ischemic Stroke. *Circ Genom Precis Med* **11**, e002162, doi:10.1161/CIRCGEN.118.002162 (2018).
- 236 Verbeek, R. *et al.* Carriers of the PCSK9 R46L Variant Are Characterized by an Antiatherogenic Lipoprotein Profile Assessed by Nuclear Magnetic Resonance Spectroscopy-Brief Report. *Arterioscler Thromb Vasc Biol* **37**, 43-48, doi:10.1161/ATVBAHA.116.307995 (2017).
- 237 Sliz, E. *et al.* Metabolomic consequences of genetic inhibition of PCSK9 compared with statin treatment. *Circulation* **138**, 2499-2512, doi:10.1161/CIRCULATIONAHA.118.034942 (2018).

238 Bergmark, B. A. *et al.* An Exploratory Analysis of Proprotein Convertase Subtilisin/Kexin Type 9 Inhibition and Aortic Stenosis in the FOURIER Trial. *JAMA Cardiol* **5**, 709-713, doi:10.1001/jamacardio.2020.0728 (2020).

6. Appendix

Supplemental Table 5. Baseline characteristics of the patients undergoing CEA, stratified accordingly to normal aortic valve morphology (No-AVSc) and aortic valve sclerosis (AVSc) and divided by plaque type.

Variables	No-AVSc			AVSc					
	Soft (n=72)	Calcified (n=38)	Mixed/ fibrotic (n=83)	Soft (n=104)	Calcified (n=83)	Mixed/ fibrotic (n=161)	Soft plaque p-Value	Calcified plaque p-Value	Mixed/ fibrotic p-Value
Age, years	68.3±8.4	68.6±8.6	66.8±8.0	71.9±6.1	73.4±6.5	72.3±6.9	0.004	0.002	<0.001
Male sex, n (%)	44(61)	22(58)	48(58)	69(66)	44(53)	106(66)	0.524	0.696	0.263
Diabetes, n (%)	17(24)	12(32)	32(39)	30(29)	12(14)	38(24)	0.491	0.047	0.02
Hypertension, n (%)	49(68)	30(79)	64(77)	84(81)	66(80)	130(81)	0.425	1.000	0.508
Dyslipidaemia, n (%)	56(78)	27(71)	67(81)	76(73)	61(73)	118(73)	0.596	0.827	0.211
Current Smoking, n (%)	9(13)	7(18)	21(25)	10(10)	17(20)	26(16)	0.624	1.000	0.090
Ex-Smokers, n (%)	21(29)	11(29)	24(29)	43(41)	30(36)	60(37)	0.113	0.536	0.204
Body mass index, kg/m ²	25.7± 2.9	24.9±3.8	25.7±4.0	26.3±3.3	25.4±3.9	26.1±3.1	0.205	0.520	0.418
eGFR, mL/min/1.73m ²	70.7±19.0	72.9±15.4	72.9±20.0	69.9±17.6	68.1±18.1	66.0±16.7	0.778	0.133	0.009
Previous MI, n (%)	11(15)	6(16)	12(14)	15(14)	8(10)	15(9)	1.000	0.365	0.006
Previous CVE, n (%)	22(31)	8(21)	19(23)	28(27)	13(16)	35(22)	0.614	0.309	0.871

CA Stenosis Severity, (%)	80.4±8.6	78.0±7.3	78.2±6.9	80.2±8.1	80.6±7.7	79.8±8.7	0.906	0.078	0.124
LVEF, n (%)	61.6±6.9	61.5±6.7	62.3±6.5	63.5±7.6	61.1±9.8	61.8±7.7	0.096	0.829	0.648
NYHA, n (%)									
I	26(36)	12(32)	32(39)	32(31)	17(20)	61(38)	0.515	0.250	1.000
II	31(43)	20(53)	34(41)	51(49)	46(55)	68(42)	0.447	0.438	0.891
III	3(4)	0	0	3(3)	1(1)	7(4)	0.689	-	-
IV	0	0	1(1)	0	0	0	-	-	-

AVSc: aortic valve sclerosis; eGFR: estimated glomerular filtration rate; CA: carotid artery; CVE: cerebrovascular event; LVEF: left ventricular ejection fraction; MI: myocardial infarction; NYHA: New York Heart Association

Supplemental Table 6. Multivariate analysis of AVSc prevalence in CEA patients with different plaque types.

Variables	Soft plaque p-Value	Calcified plaque p-Value	Mixed/fibrotic plaque p-Value
Age, years	0.004	0.003	< 0.001
Diabetes, n (%)	-	0.081	0.061
eGFR, mL/min/1.73m²	-	-	0.793
Previous MI, n (%)	-	-	0.798

AVSc: aortic valve sclerosis; eGFR: estimated glomerular filtration rate; MI: myocardial infarction.

Supplemental Table 7. Baseline characteristics of alive and death patients divided by plaque type.

Variables	Alive			Dead			Soft plaque p-Value	Calcific plaque p-Value	Mixed/fibrotic p-Value
	Soft (n=153)	Calcific (n=97)	Mixed/fibrotic (n=218)	Soft (n=23)	Calcific (n=23)	Mixed/fibrotic (n=27)			
Age, years	69.4±7.1	71.3±7.5	70.1±7.9	76.8±5.5	74.4±6.8	73.0±6.0	<0.001	0.077	0.066
Male sex, n (%)	94(61)	52(54)	134(62)	19(83)	13(57)	21(78)	0.048	0.801	0.097
Diabetes, n (%)	39(26)	22(23)	67(31)	9(39)	3(13)	7(26)	0.171	0.306	0.608
Hypertension, n (%)	116(76)	81(84)	171(78)	17(74)	15(65)	23(85)	0.843	0.049	0.415
Dyslipidaemia, n (%)	114(75)	75(77)	165(76)	18(78)	13(57)	20(74)	0.698	0.043	0.854
Smoking, n (%)	68(44)	50(52)	116(53)	15(65)	14(61)	15(56)	0.063	0.420	0.818
Body mass index, kg/m ²	26.0±3.1	25.6±3.8	26.1±3.4	26.6±3.3	23.7±3.7	25.2±3.7	0.402	0.037	0.208
eGFR, mL/min/1.73m ²	71.5±17.9	72.0±16.1	69.5±18.3	61.6±17.5	59.2±19.5	59.0±14.3	0.014	0.002	0.002
Previous MI, n (%)	20(13)	11(11)	24(11)	6(26)	2(8)	4(15)	0.101	0.714	0.558
Previous CVE, n (%)	43(28)	15(16)	48(22)	7(30)	6(26)	6(22)	0.817	0.228	0.981
CA Stenosis Severity, (%)	80.4±8.6	79.5±7.8	79.1±8.0	79.3±6.0	81.6±6.8	81.6±9.4	0.564	0.603	0.134
LVEF, n (%)	63.2±6.8	62.4±8.3	62.3±6.7	59.3±10.0	57.0±10.2	58.7±10.5	0.086	0.008	0.090
AVSc, n (%)	89(58)	65(67)	136(62)	15(65)	18(78)	25(93)	0.522	0.294	0.002
NYHA, n (%)									

I	56(37)	23(24)	86(39)	2(9)	6(26)	7(26)	0.008	0.811	0.172
II	69(45)	51(53)	87(40)	13(57)	14(61)	16(59)	0.306	0.473	0.055
III	3(2)	1(1)	5(2)	3(13)	0(0)	2(7)	0.006	-	0.132
IV	0	0	1(1)	0	0	0	-	-	-

AVSc: aortic valve sclerosis; eGFR: estimated glomerular filtration rate; CA: carotid artery; CVE: cerebrovascular event; LVEF: left ventricular ejection fraction; MI: myocardial infarction; NYHA: New York Heart Association.

All the p-Values represent the significance of the difference in clinical characteristics between alive and dead patients for the soft plaque group, calcified plaque group, and mixed/fibrotic plaque group, respectively.

Supplemental Table 8. Patient's Characteristics.

Variable	CABG (n = 29)	CABG + AVSc (n = 29)	P value
Age, years	62.2 ± 6.2	65.2 ± 8.4	0.133
Male sex, n (%)	29 (100)	29 (100)	1.000
Diabetes, n (%)	7 (24)	5 (17)	0.525
Hypertension, n (%)	17 (59)	22 (76)	0.168
Dyslipidemia, n (%)	22 (76)	19 (65.5)	0.396
Current Smoking, n (%)	3 (10)	7 (24)	0.171
Ex-Smokers, n (%)	15 (52)	13 (45)	0.607
Body mass index, kg/m²	26.7 ± 2.9	27.8 ± 3.6	0.156
Creatinine, mg/dL	0.91 ± 0.12	0.94 ± 0.17	0.411
C-reactive protein, mg/L	2.61 ± 2.56	2.73 ± 2.14	0.853
<i>New York Heart Association (NYHA) class</i>			
I	10 (34)	11 (38)	1.000
II	16 (56)	12 (41)	0.593
III	3 (10)	6 (21)	0.470
IV	-	-	-
3-Vessels coronary disease, n (%)	20 (69)	19 (65.5)	0.784
Logistic EuroSCORE	1.93 ± 1.79	2.68 ± 2.14	0.160
<i>Echocardiography</i>			
Left ventricle ejection fraction, n (%)	61.3 ± 10.1	57.9 ± 10.1	0.210
LV hypertrophy index, mm	0.35 ± 0.13	0.41 ± 0.12	0.134
Max. aortic velocity, m/s	0.99 ± 0.54	1.23 ± 0.59	0.100
Max. aortic gradient, mmHg	5.14 ± 3.16	7.55 ± 6.79	0.090
<i>Therapies</i>			
Antiplatelets, n (%)	21 (72)	18 (62)	0.410
Angiotensin receptor blockers, n (%)	5 (17)	6 (21)	0.743
Converting enzyme inhibitors, n (%)	8 (28)	11 (38)	0.410
Calcium channel blockers, n (%)	9 (31)	9 (31)	1.000
Beta-blockers, n (%)	19 (65.5)	19 (65.5)	1.000
Nitrates, n (%)	6 (21)	10 (34.5)	0.248
Statins, n (%)	18 (62)	19 (65.5)	0.789

The values are presented as number of patients (n) with percentage in brackets and mean ± standard error.

Supplemental Table 9. Undetermined genes involved in hydrogen peroxide metabolism in TAV and BAV ECs.

Gene ID	Name	Ct
ALOX12	Arachidonate 12- Lipoxygenase, 12S Type	Undetermined
DUOX1	Dual Oxidase 1	Undetermined
DUOX2	Dual Oxidase 2	Undetermined
EPX	Eosinophil Peroxidase	Undetermined
GPX2	Glutathione Peroxidase 2	Undetermined
GPX5	Glutathione Peroxidase 5	Undetermined
GPX6	Glutathione Peroxidase 6	Undetermined
LPO	Lactoperoxidase	Undetermined
MPO	Myeloperoxidase	Undetermined
TPO	Thyroid Peroxidase	Undetermined

Supplemental Table 10. Evaluation of apoptotic pathway.

Intrinsic Apoptotic Pathway	BAV	TAV	Diff	SE	p value	Adj p value
Bad	1447	1072	374.8	59.55	6.2E-07	9.3E-06
Cytochrome c	3480	2183	1297	292.9	1.2E-04	4.9E-04
Bcl-2	551.6	411.6	140	36.66	7.5E-04	2.2E-03
Survivin	748.1	512.4	235.6	70.36	2.2E-03	5.8E-03
SMAC/Diablo	5014	3682	1332	410.7	2.9E-03	6.8E-03
HTRA2/Omi	1664	1247	417.4	133.6	3.9E-03	7.8E-03
XIAP	688.1	483.6	204.5	65.8	4.1E-03	7.8E-03
Phospho-p53 (S392)	468.2	376.8	91.44	31.27	6.5E-03	1.0E-02
Phospho-p53 (S46)	543.1	453.2	89.88	31.01	6.9E-03	1.0E-02

BAV: Bicuspid Aortic Valve; TAV: Tricuspid Aortic Valve; Diff: difference; SE: Standard Error